SPECTRALLY EFFICIENT MULTICARRIER SYSTEMS FOR FIBER-OPTIC TRANSMISSION

By

Yuanyuan Zhang

Submitted to the graduate degree program in the Department of Electrical Engineering and Computer Science and the Graduate Faculty of the University of Kansas in partial fulfillment of the requirements for the degree of Doctor of Philosophy.

_____

Chairperson Rongqing Hui

_____

Victor Frost

_____

Christopher Allen

_____

Erik Perrins

_____

Hui Zhao

Date Defended: Jan. 25th, 2012

The Dissertation Committee for Yuanyuan Zhang

certifies that this is the approved version of the following dissertation:

SPECTRALLY EFFICIENT MULTICARRIER SYSTEMS FOR FIBER-OPTIC TRANSMISSION

_____

Chairperson Rongqing Hui

Date approved: Jan. 25th, 2012

Abstract

The purpose of this research is to provide a comprehensive study of spectrally efficient multicarrier systems for fiber-optic transmission. Multicarrier optical systems partition a high-data rate digital signal in a wavelength channel into multiple subcarriers. The data rate on each subcarrier can be sufficiently low and thus, the tolerance to transmission impairments can be significantly improved. Although different modulation and detection techniques are used, all the multicarrier systems investigated in this dissertation achieve a high spectral efficiency of 1 Baud/s/Hz.

Orthogonal frequency-division multiplexing (OFDM) and Nyquist wavelength-division multiplexing (Nyquist-WDM) are the two basic approaches to achieve the 1 Baud/s/Hz spectral efficiency. OFDM allows spectral overlap of adjacent subcarriers and crosstalk elimination by integration at the receiver; Nyquist-WDM limits the spectral spreading of each subcarrier channel to the symbol rate per subcarrier to avoid spectral overlap. In terms of detection method, both direct detection and coherent detection can be applied in multicarrier systems.

This dissertation focuses on the use of three high spectral efficiency optical multicarrier systems. In the theoretical and experimental investigation of a 11.1Gb/s FFT-based OFDM system, a simple dual-drive Mach-Zehnder modulator (MZM) was employed in the transmitter and direct detection in the receiver, which provided an OFDM system implementation with reduced complexity. The data was transmitted through 675km uncompensated standard single-mode fiber (SMF). Next, a 22.2Gb/s digital subcarrier multiplexing based (DSCM-based) OFDM system was used in

conjunction with 10 subcarrier channels using QPSK modulation. In this system, an IQ modulator was utilized in the transmitter and coherent detection in the receiver. By using coherent detection, the receiver was able to dynamically select the desired subcarrier channels for detection without changing the system configuration. The present research also explored a 22.2Gb/s 10 subcarrier Nyquist-WDM system with coherent detection, compared its system performance with OFDM systems, and subsequently examined the impact of filter roll-off factor.

Finally, a systemic comparison of the three proposed multicarrier systems was performed in terms of their transmission performance and system flexibility. The design tradeoffs were analyzed for different applications and summarized principles for the modern multicarrier fiber-optic system design.

Acknowledgements

Firstly, I would like to express my sincere gratitude to my advisor, Dr. Rongqing Hui, for his support, patience, and encouragement throughout my academic program. Throughout the course of my Ph.D. studies, he has taught me numerous lessons and has provided many insights on academic research. His expert guidance and valuable suggestions were essential to the completion of this dissertation. I appreciate all his contributions of time, ideas, and funding to make my Ph.D. experience productive and stimulating.

My thanks also go out to other members of my committee. Thank you to Dr. Christopher Allen, Dr. Victor Frost, Dr. Erik Perrins, and Dr. Hui Zhao for serving on my dissertation committee and giving me invaluable suggestions throughout my research. Also, I want to thank Dr. Maurice O'Sullivan for his valuable suggestions on my research, and for reviewing my papers.

Finally, I would like to thank my family for their patience, support, and encouragement throughout my Ph.D. studies. This dissertation is dedicated to them. I also would like to thank my friends who helped and encouraged me in the past few years.

Table of Contents

1. Introduction 1

1.1 Fiber-optic communication systems 1

1.2 Band-limited channels 4

1.3 Orthogonal frequency-division multiplexing (OFDM) 7

1.4 Implementation of modern optical multicarrier systems 14

1.5 Summary of the dissertation 19

2. Optical multicarrier systems 22

2.1 Transmission equations of optical multicarrier systems 22

2.2 Impact of filter shape 29

2.3 Impact of chromatic dispersion 37

2.4 Impact of fiber nonlinearity 39

2.5 Conclusion 42

3. FFT-based optical OFDM system 43

3.1 Principle of operation 45

3.2 Experimental setup 53

3.3 Results and discussion 55

3.4 Conclusion 68

4. DSCM-based optical OFDM system 70

4.1 Principle of operation 72

4.2 Experimental setup 74

4.3 Results and discussion 78

4.4 Conclusion 93

5. Nyquist-WDM system 95

5.1 Principle of operation 95

5.2 Experimental setup 97

5.3 Results and discussion 98

5.4 Conclusion 104

6. Conclusion and future work 105

References 108

1. Introduction

1.1 Fiber-optic communication systems

In 1970, a team of researchers at Corning successfully fabricated optical fibers using fused-silica with a loss of less than 20dB/km at 633nm wavelength, which was the most significant step toward the practical application of fiber-optic communications [1]. Subsequently, fiber-optic communication systems have revolutionized the telecommunication industry and have played a major role in the advent of the so-called "Information Age" [2].

In comparison with twisted pair and coaxial cable, optical fiber has the advantages of wide bandwidth, low loss, and high tolerance to electromagnetic interference. The first commercial fiber-optic communication system was developed by General Telephone and Electronics (GTE) on April 22, 1977. The popularity of this fiber-optic communication with telecommunication companies was accelerated by the success of wavelength-division multiplexing (WDM) and optical amplifier. By using WDM, signals modulated on different wavelengths of light could be transmitted in a single fiber, which greatly expanded the transmission bandwidth and reduced the cost of the transmission system. Furthermore, the implementation of optical amplifiers greatly reduced the requirement of optical-to-electrical (OE) and electrical-to-optical (EO) conversion in long distance transmission systems, which enabled the accommodation of different technologies without changing the backbone network. These two breakthroughs revealed the transmission power of fiber-optics, which therefore resulted in the doubling of system capacity every six months starting in 1992 until a bit rate of 10 Tb/s was

reached by 2001 [2]. As a result, optical fiber has largely replaced copper wire communications in core networks.

Early on, commercial WDM systems started with up to eight channels on wavelengths in C-Band (1530nm to 1565 nm), with the data rate of each wavelength channel typically lower than 10Gb/s. The continuous demand for higher network capacity and the availability of erbium-doped fiber amplifier (EDFA) and Raman amplifier extended the concept of WDM into dense-WDM (DWDM). The DWDM system utilizes the C-Band and L-Band (1565nm to 1625 nm) with denser channel spacing, and typically uses 40 channels at 100 GHz spacing or 80 channels with 50 GHz spacing. Some technologies are capable of making the channel spacing as low as 25 GHz, which allow the number of channels carried in a single fiber to dramatically increase. A 64-Tb/s (640×107-Gb/s) PDM-36QAM transmission over 320km using both pre- and post-transmission digital equalization has even been reported [3].

It is clear that fiber-optics changed the telecommunication industry, with the change coming closer to meeting the needs of end users. Due to high installation and operation expenses, fiber-optic transmission was not applied to the distribution network until 2000. Since 2000, the prices of fiber-optic systems have dropped significantly, and researches on the utilization of fiber into access networks have gained extensive attention. Research indicates that an all-fiber network is in the near future.

In order to connect the lower bandwidth end users to the core network, researchers have adopted the structure of WDM into passive optical network (PON), known as WDM-PON. The channel capacity in the existing DWDM system is still much larger than the need of each end user. To make the best compromise between the

efficiency of optical and electrical components, a finer wavelength division is needed. Also within the core network, transmitting high speed information through multiple lower-speed channels reduces inter-symbol interference and simplifies equalization circuits at the receiver, which therefore reduces the cost of the system. Under these motivations, multicarrier systems are proposed. Multicarrier optical systems partition a high-data rate digital signal in a wavelength channel into multiple subcarriers. Here, the data rate on each subcarrier has the potential to be sufficiently low and thus, the tolerance to transmission degradations such as chromatic dispersion and polarization mode dispersion could be significantly improved.

Today's rapid growth of high data rate internet applications is increasing the demand for bandwidth. The once regarded unlimited bandwidth in optical fiber is no longer true. Thus, the focus of the next generation fiber-optic communication system will likely be the extension of the usable bandwidth of fiber and an increase in the bandwidth efficiency (also called spectral efficiency). Spectral efficiency is defined by the data-rate carried by each hertz of optical bandwidth. In the past decade, many techniques on band-limited channels in electrical and wireless transmission have been adopted to fiber-optic transmission. The developments of analog-to-digital converters (ADCs) and digital-to-analog converters (DACs) have helped to facilitate this practice. Theoretical analysis of narrowing the spectral bandwidth of a modulated optical channel has been outlined in the literature [4]. Experimental systems utilizing optical [5] or digital filters [6] to limit the effective bandwidth also have been reported.

Aforementioned, high spectral efficiency is a fundamental requirement for the next generation fiber-optic networks. The means to achieve this goal have become a

central focus of research. Higher spectral efficiency in a multicarrier system can be achieved from two directions, by either shrinking the spectral bandwidth of each subcarrier or allowing spectral overlap of adjacent subcarriers. The general introductions of theory and technologies adopted in these two approaches are outlined in section 1.2 and section 1.3.

1.2 Band-limited channels

If the frequency response of a channel is nonzero only within a certain frequency window, this channel is referred to as a band-limited channel. Frequency components outside the boundary are removed after passing through the channel. Band-limited channels are primarily the result of the desire to transmit multiple independent signals in the same medium, by partitioning the total bandwidth into multiple spectral bands. As in wireless systems, FM radio is often broadcast in the 87.5 MHz - 108 MHz range [7]. The available bandwidth of optical fiber is limited by the wavelength-dependent loss in fiber, and from Fig. 1.2.1 we can see that the fiber attenuation has been reduced significantly by advanced fabrication technologies in modern fibers. Among the three transmission windows, the lowest loss window is around 1550nm, including the C-band and L-band, which is the most frequently selected window by many commercial systems. Some systems also exploit another window, S-band (1460nm to 1530 nm), in order to extend the total transmission bandwidth.

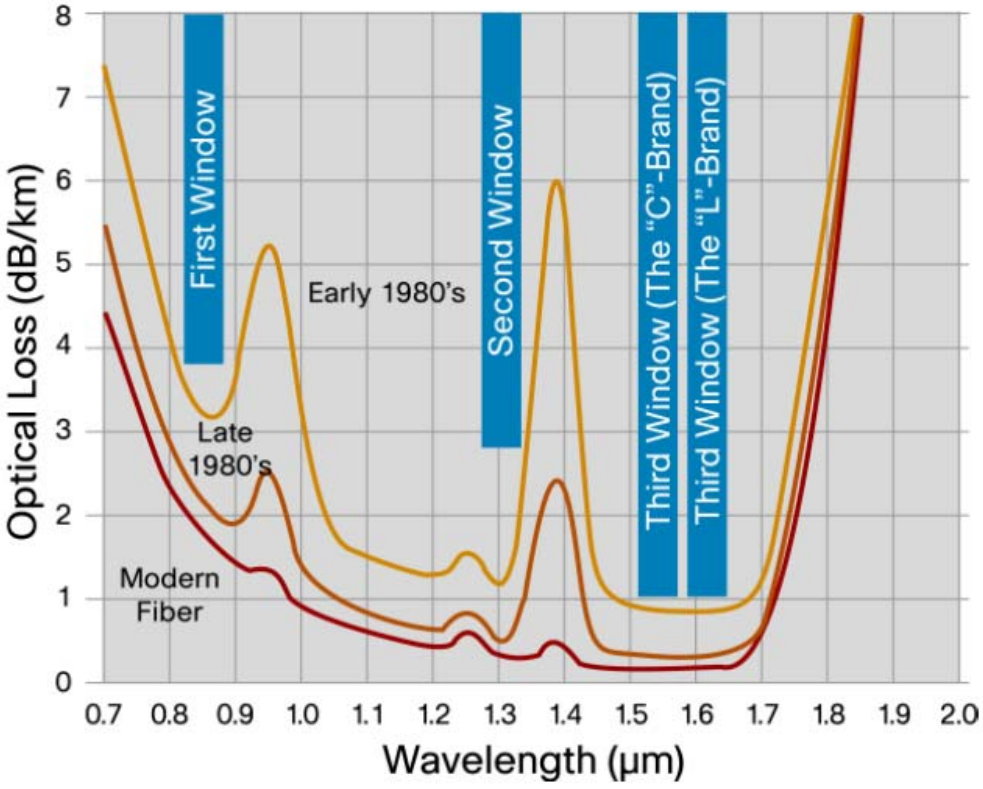

Fig. 1.2.1 Attenuation versus wavelength and transmission windows (REF [8])

The spectrum of a given signal cannot be compressed unlimitedly without introducing waveform distortion. The theoretical maximum symbol rate that can be accommodated by a certain available bandwidth was predicted by Harry Nyquist [9]. A channel with a baseband bandwidth of B Hz can transmit a symbol rate of 2B Hz without intersymbol interference (ISI). In other words, a signal with 2B Hz symbol rate requires a minimum of B Hz baseband bandwidth. If the signal is transmitted through a channel with bandwidth narrower than this Nyquist limit, ISI is introduced to deteriorate the transmission performance.

The spectrum of a modulated signal is determined by the pulse shape. Therefore, a pulse shaping filter can be used to limit the effective bandwidth. This reduces inter-channel crosstalk in a multi-carrier system, and also keeps the ISI in control at the same time. The ideal pulse shaping filter is the Sinc filter, its impulse response is a Sinc function in the time domain, and its frequency response is a rectangular function. Fig. 1.2.2 indicates that the impulse response of a Sinc pulse with a baseband bandwidth B will have zero crossings at integer multiples of 1/(2B) in the time domain, which are the sampling points of other symbols of the 2B Hz pulse train. Thus, no ISI will be introduced. But the Sinc filter is idealized and cannot be physically realized because of the finite time response of realistic electronic components. In digital communication, boxcar filter, raised cosine filter and Nyquist filter are often used to approximate the Sinc filter.

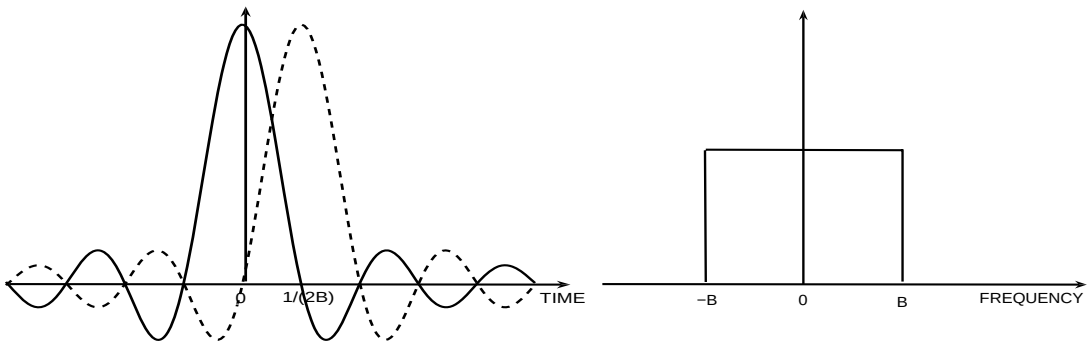

(a) (b)

Fig. 1.2.2 Sinc function (a) Impulse response and (b) Frequency response

1.3 Orthogonal frequency-division multiplexing (OFDM)

OFDM is a multicarrier transmission system with mutually orthogonal subcarriers. The orthogonality among subcarriers is ensured by the special pulse shaping filter and channel spacing in OFDM systems. In an OFDM system, the pulse shaping filter is the boxcar filter, thus the channel spacing must be integer multiples of the symbol rate. As previously mentioned in Section 1.2, the boxcar filter is the counterpart of the Sinc filter, but with a rectangular shape in time domain and Sinc function shape in frequency domain. Its flat impulse response in symbol period ensures the cancellation of the inter-channel crosstalk. Because the spectral bandwidth of an ideal boxcar filter has to be infinite, it is not widely applied in traditional digital communications. However, OFDM system partitions the total signal into a large number of subcarriers, with a relatively low data rate on each subcarrier, so that it is virtually unaffected by the practical bandwidth limitation of the receiver.

To demonstrate the crosstalk cancellation in OFDM, consider an FDM system with N carriers in which the input symbol duration is T, and the symbol duration on each carrier is NT which we will denote by T_{fdm}. During one FDM symbol interval the FDM signal can be expressed as follows:

$$x_{fdm}(t) = \sum_{k=0}^{N-1} A_k \cos(2\pi(f_c + k\Delta f)t + \phi_k) \tag{1.3.1}$$

A_k is the user symbol on the k_{th} subcarrier;

f_c is the optical carrier frequency;

Δf is the separation between subcarriers, k_{th} subcarrier frequency is $f_k = f_c + k\Delta f$;

ϕ_k is a random static phase offset of the k_{th} subcarrier.

We can recover symbol on the j_{th} subcarrier by demodulating the FDM signal with a phase coherent local carrier as:

$$\begin{aligned}
&\frac{1}{T_{fdm}}\int_{T_{fdm}} x_{fdm}(t)\cos[2\pi(f_c + j\Delta f)t + \phi_j]dt \\
&\quad = \frac{1}{T_{fdm}}\int_{T_{fdm}} \sum_{k=0}^{N-1} A_k \cos[2\pi(f_c + k\Delta f)t + \phi_k]\cos[2\pi(f_c + j\Delta f)t + \phi_j]dt \\
&\quad = \frac{1}{T_{fdm}}\int_{T_{fdm}} A_j \cos[2\pi(f_c + j\Delta f)t + \phi_j)\cos[2\pi(f_c + j\Delta f)t + \phi_j]dt \\
&\qquad + \frac{1}{T_{fdm}}\int_{T_{fdm}} \sum_{k\neq j}^{N-1} A_k \cos[2\pi(f_c + k\Delta f)t + \phi_k]\cos[2\pi(f_c + j\Delta f)t + \phi_j]dt
\end{aligned} \tag{1.3.2}$$

Here, the first term in Eq. (1.3.2) is the desired symbol output, and the second term is the cross-talk term between the carriers. The first term can be expressed as:

$$\begin{aligned}
&\frac{1}{T_{fdm}}\int_{T_{fdm}} A_j \cos[(2\pi(f_c + j\Delta f)t + \phi_j]\cos[(2\pi(f_c + j\Delta f)t + \phi_j]dt \\
&\quad = \frac{1}{T_{fdm}}\int_{T_{odm}} A_j \frac{1}{2}dt + \frac{1}{T_{ofdm}}\int_{T_{ofdm}} A_j \cos[2\pi(2f_c + 2j\Delta f)t + 2\phi_j)dt \\
&\quad \approx \frac{A_j}{2} \quad if \quad 2f_cT_{fdm} >> 1
\end{aligned} \tag{1.3.3}$$

The cross talk term can be rewritten as:

$$\begin{aligned}
&\frac{1}{T_{fdm}}\int_{T_{fdm}} \sum_{k\neq j}^{N-1} A_k \cos[2\pi(f_c + k\Delta f)t + \phi_k]\cos[2\pi(f_c + j\Delta f)t + \phi_j]dt \\
&\approx \frac{1}{2}\sum_{k\neq j}^{N-1} A_k \frac{1}{T_{fdm}}\int_{ofdm} \cos(2\pi(k-j)\Delta f)t + \phi_k - \phi_j)dt \quad if \quad 2f_cT_{fdm} >> 1
\end{aligned} \tag{1.3.4}$$

From Eq. (1.3.4) we obtain the orthogonality condition for eliminating cross-talk in an FDM system as follows:

$$\frac{1}{T_{fdm}}\int_{T_{fdm}} \cos(2\pi(k-j)\Delta f)t + \phi_k - \phi_j)dt \ = 0 \tag{1.3.5}$$

For arbitrary values of ϕ_j and ϕ_k, the above condition is satisfied for a minimum frequency separation of the following:

$$\Delta f_{\min} = 1/T_{fdm} \tag{1.3.6}$$

In other words, the minimum frequency separation for orthogonality is the inverse of the subcarrier symbol time. In the case of OFDM, it will be denoted by T_{ofdm}. For purposes of notational clarity we define the orthogonality condition as:

$$\Delta f_{\min} = 1/T_{fodm}; T_{ofdm} = NT \tag{1.3.7}$$

The conceptual implementation of OFDM modulator is given in Fig. 1.3.1 (a), which requires N analog mixers (N as the number of channels). When N is too large, the analog implementation may not be practical because of the overwhelming complexity. The OFDM demodulator can also be implemented in conceptual form using analog mixers followed by matched filters as shown in Fig. 1.3.1 (b).

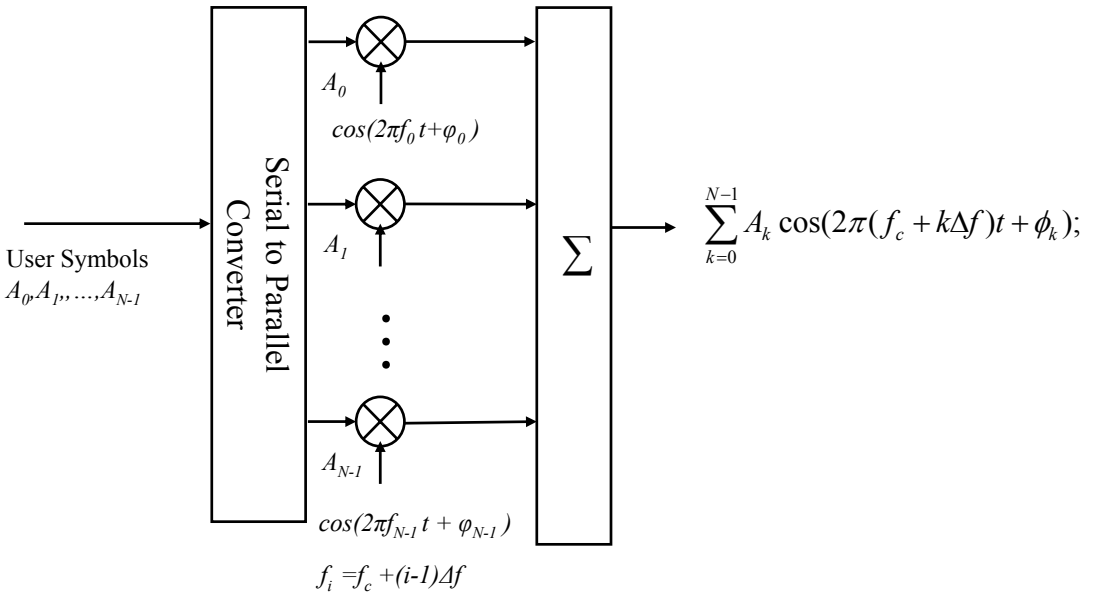

(a)

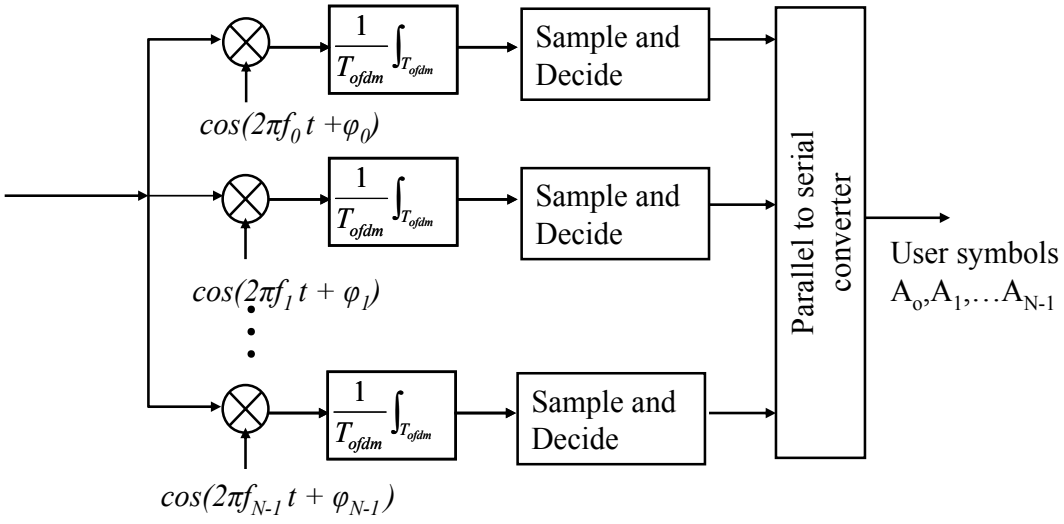

(b)

Fig. 1.3.1 Conceptual block diagrams of OFDM system: (a) Modulator; (b) Demodulator.

With the rapid progress of high-speed digital electronic circuits including ADC and DAC in the recent years, the use of OFDM for high-speed optical transmission systems became possible, in which multiple subcarriers are created in digital domain. In several research studies, IFFT and FFT are used for the generation of OFDM signals [10]. In the FFT-based optical OFDM, which is also referred to as digital-OFDM, the subcarriers are generated by electronic IFFT in the transmitter and then uploaded onto an optical carrier by an external electro-optic modulator. At the receiver, the matched filter is then realized by electronic FFT.

According to Eq. (1.3.1), the bandpass OFDM signal can be expressed as:

$$x_{BP}(t) = \sum_{k=0}^{N-1} A_k \cos(2\pi(f_c + k\Delta f)t + \theta_k); \quad 0 < t < T_{ofdm}; \quad \Delta f = 1/T_{ofdm} \tag{1.3.8}$$

Where $A_k e^{j\theta_k} = \widetilde{X}_k = \text{Complex QPSK/QAM symbol on the kth carrier}$, to simplify the analysis, the random phase offset of each subcarrier is set to zero. Eq. (1.3.8) can be expressed as:

$$x_{BP}(t) = \text{Re}\{\exp(j2\pi f_c t)\sum_{k=0}^{N-1} X_k \exp(j2\pi k\Delta f t)\} \tag{1.3.9}$$

Where $\sum_{k=0}^{N-1} \widetilde{X}_k \exp(j2\pi k\Delta f t)$ is defined as the complex lowpass equivalent representation of the OFDM signal:

$$\widetilde{x}_{LP}(t) = \sum_{k=0}^{N-1} \widetilde{X}_k \exp(j2\pi k\Delta f t) \tag{1.3.10}$$

When the lowpass equivalent OFDM signal is sampled at the Nyquist rate of $f_s = N\Delta f$, then the sampled version can be expressed with the following equation:

$$\begin{aligned} \widetilde{x}_{LP}(nT_s) &= \sum_{k=0}^{N-1} \widetilde{X}_k \exp(j2\pi k\Delta f nT_s) = \sum_{k=0}^{N-1} \widetilde{X}_k \exp(j2\pi kn/N) \\ &= IFFT\{\widetilde{X}_0, \widetilde{X}_{1,}....., \widetilde{X}_{N-1}\} \end{aligned} \tag{1.3.11}$$

Eq. (1.3.11) shows that the time domain samples of the lowpass equivalent version of the OFDM signal can be generated by taking the Inverse Fourier Transform (IFT) of the input symbol sequence. It is also clear that the input symbols can be recovered from the OFDM samples by the Fourier Transform operator as follows:

$$\begin{aligned} \widetilde{X}(k) &= \frac{1}{N}\sum_{n=0}^{N-1} \widetilde{x}(nT_s)\exp(j2\pi k\Delta f n/N) \\ &= FT\ of\quad \{\widetilde{x}(0), \widetilde{x}(1),...\widetilde{x}(N-1)\} \end{aligned} \tag{1.3.12}$$

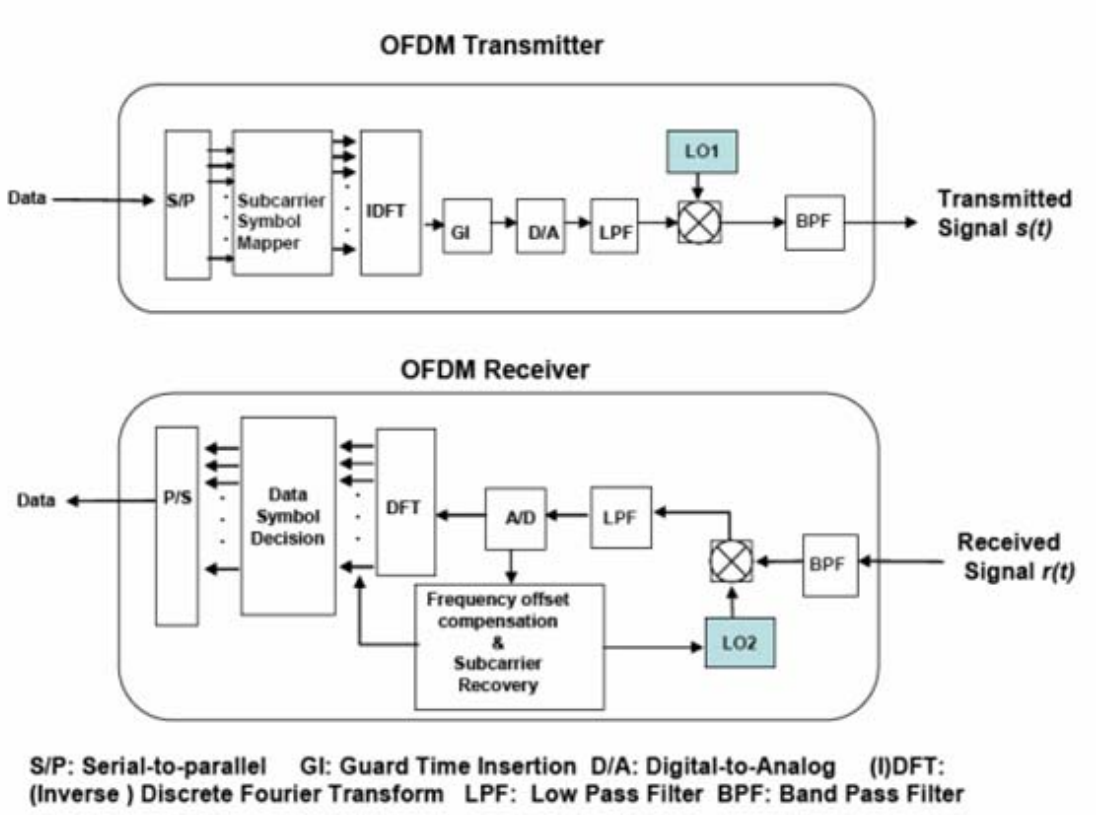

Fig. 1.3.2 OFDM system block diagram. (REF [10])

The block diagram of the signal processing stages in OFDM systems are described in Fig. 1.3.2. Because of the orthogonality between subcarrier channels and the elimination of an extra frequency guard band between them, OFDM provides improved spectral efficiency compared to conventional subcarrier multiplexed (SCM) systems based on the analog domain. In addition, other digital signal processing techniques can be applied to reduced inter-symbol interference through digital equalization, and pre- or post- digital compensations. As a well-studied digital modulation method, OFDM supports various advanced electrical and optical modulation formats, and utilizes various

digital signal processing algorithms to achieve high spectral efficiency and excellent system performance for high-speed optical transmission.

1.4 Implementation of modern optical multicarrier systems

In a traditional WDM system, banks of independent lasers are used to generate optical carriers that each contains a different wavelength. If the channel spacing is not wide enough, incoherent interference occurs when beat signals arise from adjacent channels that fall within the receiver bandwidth. This process is noise-like, if the relative phase of the two channels is random. This is the case when independent lasers are used for each channel, unless strong optical pre-filtering is used in the transmitter. Unlike traditional WDM systems, optical multicarrier systems have relatively stable optical phase difference between adjacent channels, so that the phase of the interference signal is deterministic. This can be removed at the receiver with proper signal processing. This interference control may be achieved by replacing the typical bank of free-running lasers in a conventional WDM system with one or more coherent comb sources [11], or by generating the subcarriers digitally before optical modulation [12].

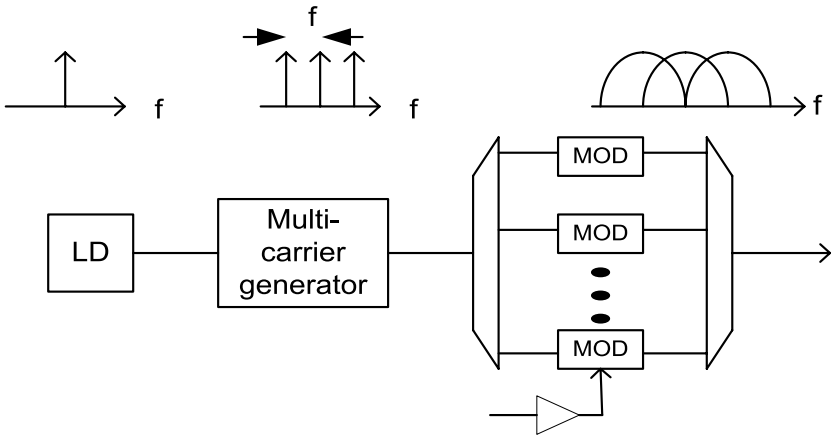

Fig. 1.4.1 Coherent optical multicarrier generator

The transmitter setup using a coherent multicarrier generator is shown in Fig. 1.4.1. Here, the CW light-wave coming out of the laser diode first goes through a multicarrier generator to obtain mutually coherent subcarriers. Next, an optical demultiplexer is used to separate the subcarriers. After that, each subcarrier is modulated with an independent optical modulator. The modulated subcarriers are finally combined by a multiplexer for transmission.

A typical implementation of a multicarrier generator is illustrated in Fig. 1.4.2, also referred to as comb generator. The comb generator consists of a CW laser and two consecutive Mach-Zehnder modulators (MZM) driven by a high frequency sinusoidal wave. The first MZM works as an intensity modulator while the second MZM is configured as a phase modulator. The frequency of the sine wave determines the frequency spacing of the generated comb carriers. By carefully adjusting the modulation indices of the DC bias of the IM modulator and the relative phase delay between the signals driving the two modulators, a group of flattened coherent subcarriers are generated. In this type of setup, each optical subcarrier must be modulated by an independent electro-optic modulator for data encoding. This setup may become impractical when there are a large number of optical subcarriers. In these instances, several electro-optic external modulators would be required, which would therefore increase the system cost.

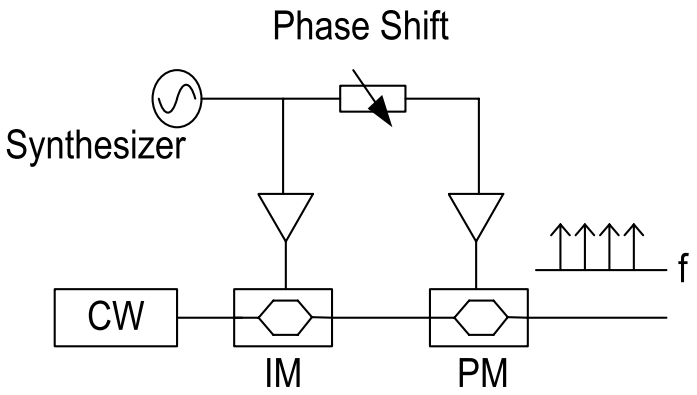

Fig. 1.4.2 Configuration of comb generator

Another way of generating multiple mutually coherent subcarriers is to utilize digital electronic circuits. The transmitter configuration is shown in Fig. 1.4.3, where data is directly modulated onto different subcarriers and aggregated in digital domain. The digital signal is then converted into analog domain through DACs, and subsequently used to drive an electro-optic modulator. In this case, only a single electro-optic modulator is used for the composite signal, which contains multiple subcarriers. However, the bandwidth of the modulator has to be wide enough to accommodate all the subcarrier channels. In order to have the ability to modulate both the intensity and the phase of the optical signal simultaneously, a pair of independent DACs is needed to drive the two electrodes of an electro-optic modulator. This modulator could be either an IQ modulator or a dual drive MZM, depending on the modulation technique applied on each subcarrier channel.

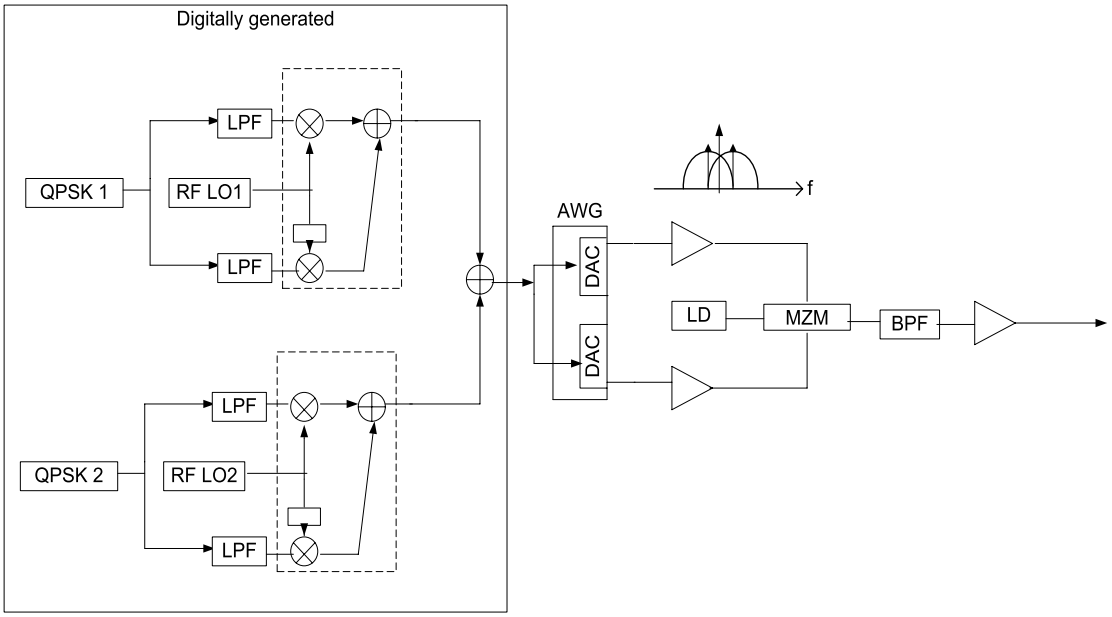

Fig. 1.4.3 Digital multicarrier transmitter

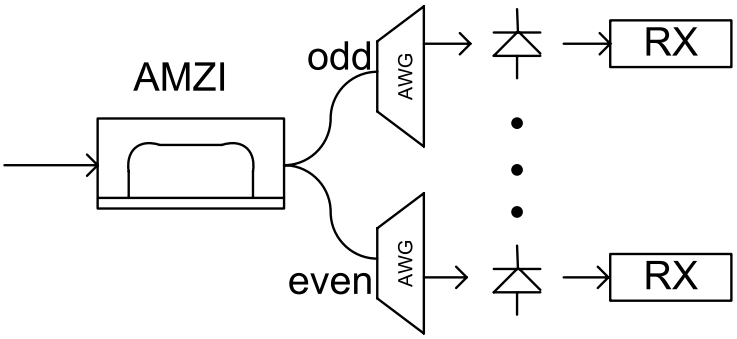

Fig. 1.4.4 Configuration of direct detection

The detection method of multicarrier systems can be either direct detection or coherent detection. Fig. 1.4.4 illustrates the configuration of a direct detection setup. Because the frequency spacing between subcarrier channels is very narrow and a typical demulplexer is not fine enough to separate them, the received optical signal usually passes through an asymmetric Mach-Zehnder interferometer. This serves as a frequency

interleaver to separate the odd and even channels. Demultiplexers with large channel counts, such as AWGs, are then used to further separate the channels. This receiver can perform the function of matched filters under the condition that the phases of all the subcarriers are precisely controlled. The phase control can be done by shifting the phase of adjacent carriers by $\pi/2$, so that interference between them can be eliminated by the receiver [13]. Because the interference from adjacent channels has the largest influence on the signal, it is important that the phase control of the optical carriers obtain crosstalk-free channel extraction. After the channel separation, each individual subcarrier channel can then be detected by a separate photodiode.

In the case of complex modulation in which data is carried both by the optical intensity and by the optical phase, coherent detection will have to be used at the receiver. The configuration of a coherent detection receiver is shown in Fig. 1.4.5. With coherent detection, the optical field is detected and the optical spectrum is linearly mapped onto the electrical domain. Subsequently, subcarrier separation can be performed digitally, in conjunction with other data recovery functions such as dispersion compensation, equalization and carrier recovery.

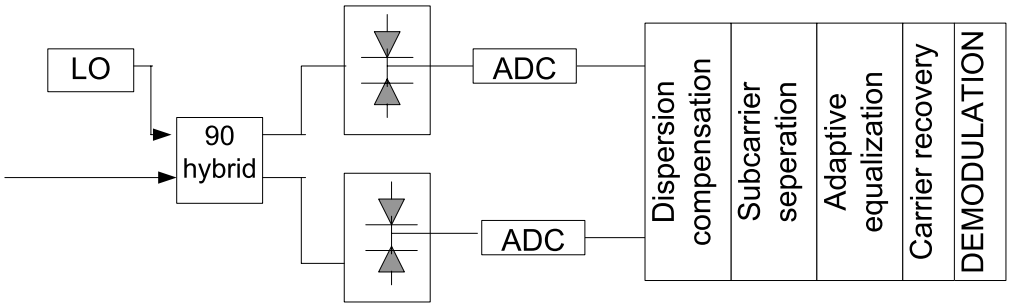

Fig. 1.4.5 Configuration of coherent detection

1.5 Summary of the dissertation

To improve performance tolerance to transmission impairments such as chromatic dispersion and PMD, optical multicarrier systems were first introduced around 2002 [14]. Here, a high speed data channel was partitioned into multiple low data rate subcarrier channels. In early works such as these, subcarriers were multiplexed and demultiplexed in RF domain using analog devices, with a spectral guardband required between subcarrier channels to minimize the crosstalk between them. As a result of the fast advance of digital electronics such as DAC/ADC and DSP, high spectral efficiency multicarrier systems were introduced into optical communication, which allowed a spectral efficiency of 1 bit/s/Hz with binary modulation and can be further increased by multilevel modulation formats.

Both direct detection and coherent can be used at the receiver of modern optical multicarrier systems. Direct detection utilizes only 50% of the available bandwidth to avoid the impact of inter-mixing between subcarrier channels. This topic will be expanded upon in the next section. Coherent detection, on the other hand, has better spectral efficiency and channel selection flexibility. In comparison to multicarrier systems in wireless communication, several different issues have to be taken into consideration for its application in high-speed optical communication. For example, phase noise of laser diode and chromatic dispersion in the fiber will impact signal equalization and carrier recovery. Furthermore, amplified spontaneous emission noise from optical amplifiers and nonlinearity of optical fibers will introduce signal degradation and crosstalk. Thus, advanced DSP algorithm to improve data recovery in

optical coherent detection is arguably one of the hottest current topics in the communication research and development communities.

A detailed analysis of optical field evolution along the optical transmission system, which consists of the concatenation of various optical and electronic functional components, can provide a clear understanding of the operation and degradation mechanisms of components and their subsequent impact on the system performance. To this end, Chapter 2 will provide the necessary analytical equations that describe every section of the system, as well as their influence on the overall system performance.

As demonstrated in section 1.3 and 1.4, OFDM and pulse shaping filtering are two approaches to achieve high spectral efficiency in modern multicarrier systems. For OFDM systems, IFFT/FFT and digital subcarrier multiplexing (DSCM) are two ways to distribute data onto the subcarriers.

In FFT-based OFDM, the data stream is first mapped into a 2-D array. An IFFT is then performed such that each column of the data array becomes a subcarrier channel. In this way an OFDM symbol is usually partitioned into different subcarriers [15]. At the receiver, an FFT process is used to convert the 2-D data array back into frequency domain and the original digital signal is reconstructed through parallel to serial conversion. An FFT-based OFDM system is demonstrated in Chapter 3, in which direct detection was utilized at the receiver. For the first time, the present research demonstrates a compatible single-side modulation was implemented to achieve the same spectral efficiency as coherent detection. The system with 11.1 Gb/s data rate was tested through a 675km SMF transmission, and the impacts of chromatic dispersion, nonlinearity and modulator bias are discussed and analyzed in subsequent chapters.

In DSCM-based OFDM, subcarrier channels are digitally generated and linearly up-converted to an optical carrier by an electro-optic IQ modulator. This allows a higher degree of flexibility in bandwidth allocation and scalability in data rate granularity, while maintaining high bandwidth efficiency. The receiver with coherent detection has the flexibility to dynamically select a different number of DSCM channels in the detection without the need to change system configuration. The bandwidth requirement in the receiver can be reduced if only a subset of subcarrier channels is to be detected instead of the entire OFDM frame. A DSCM-based OFDM system is demonstrated in Chapter 4, with an accompanying exploration of the impacts of DSCM channel spacing and time mismatch between subcarrier channels.

The use of a pulse shaping filter to limit the spectrum of the modulated signal is the alternate way to achieve high spectral efficiency. By limiting the bandwidth of each channel to the symbol rate, 1 baud/s/Hz spectral efficiency could be achieved without overlapping adjacent channels. Various optical or digital electronic filters have been adopted in research papers [5, 6]. In Chapter 5, a Nyquist-WDM system is demonstrated, in which a pair of Nyquist filters were used for pulse shaping and channel selection at the transmitter and receiver. This chapter also includes an investigation of the transmission performance of this system.

Lastly, in Chapter 6 includes a summarization of the dissertation, and provides guidelines for the modern multicarrier system design in different transmission environments.

2. Optical multicarrier systems

To increase the system capacity and to make more efficient use of the available bandwidth in optical fiber transmission, the frequency spacing between DWDM channels has been continuously reduced in recent decades. Furthermore, multilevel modulation formats for the transceivers and long fiber spans between optical amplifiers in the transmission line require high optical powers per channel to satisfy signal-to noise ratio (SNR) requirements. The high per-channel optical power in the fiber and the narrow spacing between channels give rise to ISI within each subcarrier, as well as to inter-channel crosstalk between subcarriers. The unique transmission characteristics of optical fiber that include linear and nonlinear impairments also influence the performance of optical multicarrier systems. Thus, this chapter presents the theoretical analysis based on fundamental physical mechanisms of optical multicarrier systems. Additionally, numerical simulations will be used to analyze the performance limits introduced by various impairments.

2.1 Transmission equations of optical multicarrier systems

To obtain a system level perspective on the optical field evolution of a multicarrier system in fiber-optic transmission, it is first necessary to build a model that includes all sources of signal distortion from the transmitter all the way to the receiver through the transmission fiber. The causes of distortion on the received signal waveform can be pulse shaping filtering, chromatic dispersion (CD), polarization mode dispersion (PMD), or fiber nonlinearity. And at the receiver, we can classify the distortion into two categories, namely ISI and inter-channel crosstalk.

Because optical waveform changes with time and the impairments introduced by optical fiber accumulate over the transmission distance, optical filed can be defined as a two dimensional variable as a function of both time and distance. In a multicarrier system, each subcarrier channel is assigned a unique sub-wavelength. The interplay between different sub-wavelength channels is also an important issue in the analysis. For convenience, the definitions of variables used in the model are listed below:

z: distance along the optical fiber;

t: time frame of the optical signal;

k: the number of sub-wavelength channel;

m: the number of symbol.

First, we define $E_k(z,t)$ as the optical field of the k_{th} subcarrier. The optical signal coming out of the multi-carrier laser source at z=0 can be written as follows.

$$E_k(0,t) = \sqrt{P_k}\,\exp(j\omega_k t + \varphi_k) \tag{2.1.1}$$

Here, P_k is the average power, ω_k and φ_k are the frequency and initial phase of the k_{th} subcarrier channel. Next, an information symbol $A_{k,m}$ is encoded onto the optical carrier through an electro-optic modulator, where $A_{k,m}$ denotes the m_{th} symbol on the k_{th} channel. $A_{k,m}$ can be real or complex depending on the modulation method.

$$E_k(0,t) = \sum_{m=-\infty}^{\infty} \sqrt{P_k}\,A_{k,m}\exp(j\omega_k t + \varphi_k) \tag{2.1.2}$$

After modulation, P_k becomes the peak optical power of the k_{th} channel, and the spectral bandwidth of each subcarrier channel is determined by the speed of modulation. In order to make full use of the limited optical bandwidth, the spectrum of each subcarrier channel can be made narrower through pulse shaping with a band limiting

filter. Both digital and analog filters can be used. Adding the filter impulse response $I_k(t)$ to Eq. (2.1.2), we have:

$$E_k(0,t) = \left[\sum_{m=-\infty}^{\infty} \sqrt{P_k} A_{k,m} \exp(j\omega_k t + \varphi_k) \right] * I_k(t) \tag{2.1.3}$$

Here, * denotes convolution. It is then possible to add all the subcarriers together to obtain the total optical field at the transmitter output:

$$E(0,t) = \sum_{k=1}^{J} \left[\sum_{m=-\infty}^{\infty} \sqrt{P_k} A_{k,m} \exp(j\omega_k t + \varphi_k) \right] * I_k(t) \tag{2.1.4}$$

This optical signal will be launched into optical fiber for transmission. $H_{channel}(z,t)$ is used to denote the total impulse response of the transmission fiber, which includes chromatic dispersion, PMD and fiber nonlinearity. At the receiver, a matched filter is added to select the channel of interest, which is defined as $Q_k(t)$. The fiber attenuation coefficient α is also included in Eq. (2.1.5). Thus, the q_{th} channel at the receiver after channel selection can be expressed as follows.

$$E_q(z,t) = \left\{ \sum_{k=1}^{J} \left[\sum_{m=-\infty}^{\infty} \sqrt{P_k} \exp(-\alpha z) A_{k,m} \exp(j\omega_k t + \varphi_k) \right] * I_k(t) \right\} * H_{channel}(z,t) * Q_q(t) \tag{2.1.5}$$

Eq. (2.1.5) fully represents the evolution of the optical field of a multicarrier system through fiber-optic transmission. To make it concise, it is possible to combine the pulse shaping filter, channel impulse response and receiver filter to one impulse response $H(t)$ which is defined as,

$$H(z,t) = IFFT\left[FFT(I(t)) \cdot FFT(H_{channel}(z,t)) \cdot FFT(Q(t))\right] \tag{2.1.6}$$

According to the central wavelength of the pulse shaping filter and receiver matched filter, we can define the subscript of $H(t)$ such that,

$$H_{q,q}(z,t) = IFFT\left[FFT(I_q(t)) \cdot FFT(H_{channel}(z,t)) \cdot FFT(Q_q(t))\right]$$

$$H_{k,q}(z,t) = IFFT\left[FFT(I_k(t)) \cdot FFT(H_{channel}(z,t)) \cdot FFT(Q_q(t))\right]$$

In these equations, $H_{q,q}(z,t)$ represents the selection of the desired q_{th} channel, whereas $H_{k,q}(z,t)$ represents the crosstalk from the k_{th} channel. Taking the multi-channel effect $H(t)$ into Eq. (2.1.5), the electrical field of the selected q_{th} channel is therefore,

$$E_q(z,t) = \sum_{k=1}^{J} \sum_{m=-\infty}^{\infty} \sqrt{P_k} \exp(-\alpha z) A_{k,m} \exp(j\omega_k mT + \varphi_k) H_{k,q}(z, t - mT) \tag{2.1.7}$$

Where T is the symbol period, decompose Eq. (2.1.7) into the channel of interest and crosstalk from other channels,

$$\begin{aligned} E_q(z,t) &= \sum_{m=-\infty}^{\infty} \sqrt{P_q} \exp(-\alpha z) A_{q,m} \exp(\varphi_q) H_{q,q}(z, t - mT) \\ &+ \sum_{k \neq q} \sum_{m=-\infty}^{\infty} \sqrt{P_k} \exp(-\alpha z) A_{k,m} \exp[j(\omega_k - \omega_n)mT + \varphi_k - \varphi_n] H_{k,q}(z, t - mT) \end{aligned} \tag{2.1.8}$$

In Eq. (2.1.8), the first term on the right-hand side (RHS) represents the channel of interest including the impact of ISI, and the second term on the RHS is the crosstalk from all other channels.

In digital transmission, the analog signals that reach the receiver need to be digitized and sampled for symbol decision and data recovery. Furthermore, because the symbol decision is made only based on finite sampling points made at the optimum phase within each symbol, Eq. (2.1.8) was sampled at a sampling rate equal to the symbol rate. By setting $t=nT$, we have the following:

$$\begin{aligned} E_q(z,nT) &= \sum_{m=-\infty}^{\infty} \sqrt{P_q} \exp(-\alpha z) A_{q,m} \exp(\varphi_q) H_{q,q}(z, nT - mT) \\ &+ \sum_{k \neq q} \sum_{m=-\infty}^{\infty} \sqrt{P_k} \exp(-\alpha z) A_{k,m} \exp[j(\omega_k - \omega_n)mT + \varphi_k - \varphi_n] H_{k,q}(z, nT - mT) \end{aligned} \tag{2.1.9}$$

After sampling the received signal, it is then possible to further decompose the first term on the RHS of Eq. (2.1.9) into signal of interest and ISI.

$$\begin{aligned} E_q(z,nT) &= \sqrt{P_q}\exp(-\alpha z)A_{q,m}\exp(\varphi_q)H_{q,q}(z,0) \\ &+ \sum_{m\neq n}\sqrt{P_q}\exp(-\alpha z)A_{q,m}\exp(\varphi_q)H_{q,q}(z,nT-mT) \\ &+ \sum_{k\neq q}\sum_{m=-\infty}^{\infty}\sqrt{P_k}\exp(-\alpha z)A_{k,m}\exp[j(\omega_k-\omega_n)mT+\varphi_k-\varphi_n]H_{k,q}(z,nT-mT) \end{aligned} \tag{2.1.10}$$

The three terms in Eq. (2.1.10) clearly represent the signal (first term on the RHS), ISI (second term on the RHS) and crosstalk (third term on the RHS), which determine the quality of the performance of sampling and symbol decision.

Next, in order to compare the magnitudes of ISI and crosstalk comparing to the signal of interest which demonstrate their impacts in the sampling and decision, the signal to crosstalk power ratio (SCPR) and signal to ISI power ratio (SIPR) is defined as:

$$SCPR = \frac{\left|\sqrt{P_q}\exp(-\alpha z)A_{q,m}\exp(\varphi_q)H_{q,q}(z,0)\right|^2}{\left|\sum_{k\neq q}\sum_{m=-\infty}^{\infty}\sqrt{P_k}\exp(-\alpha z)A_{k,m}\exp[j(\omega_k-\omega_n)mT+\varphi_k-\varphi_n]H_{k,q}(z,nT-mT)\right|^2} \tag{2.1.11}$$

$$SIPR = \frac{\left|\sqrt{P_q}\exp(-\alpha z)A_{q,m}\exp(\varphi_q)H_{q,q}(z,0)\right|^2}{\left|\sum_{m\neq n}\sqrt{P_q}\exp(-\alpha z)A_{q,m}\exp(\varphi_q)H_{q,q}(z,nT-mT)\right|^2} \tag{2.1.12}$$

To simplify the analysis, it is assumed that the input average powers in all the subcarrier channels are equal; the channel spacing is integer multiples of the symbol rate; and the receiver filter is matched to the pulse shaping filter in the transmitter to minimize noise impact. These ideal conditions can be summarized as:

$P_1 = P_2 = \ldots = P_J$;

$\omega_k - \omega_q = 2\pi p / T$, where p is an integer;

$Q_k(t) = I_k(t)$;

$H_{channel}(z,t)$=1.

Because the average modulus of $A_{k,m}$ on each subcarrier channel is the same, the parameter dependence on the data pattern $A_{k,m}$ in Eq. (2.1.11) can be eliminated. Thus, the SCPR and SIPR can be simplified into the following:

$$SCPR = \frac{\left|Q_q(0)\right|^4}{\left|\sum_{k\neq q}\sum_{m=-\infty}^{\infty} H_{k,q}(z, nT - mT)\right|^2} \tag{2.1.13}$$

$$SIPR = \frac{\left|Q_q(0)\right|^4}{\left|\sum_{m\neq n} H_{q,q}(z, nT - mT)\right|^2} \tag{2.1.14}$$

In order to find the general rules of SCPR and SIPR in the ideal situation, the SCPR and SIPR were calculated as a function of filter bandwidth/symbol rate in a system with 10 subcarrier channels using a Sinc filter on each channel. The results are plotted in Fig. 2.1.1 and Fig. 2.1.2 in which the filter bandwidth was the variable. Because of the ideal situation, ISI is small when the filter bandwidth is much larger than the symbol rate. Oppositely, crosstalk is small when the filter bandwidth is much smaller than the symbol rate so different ranges were chosen for the horizontal axis.

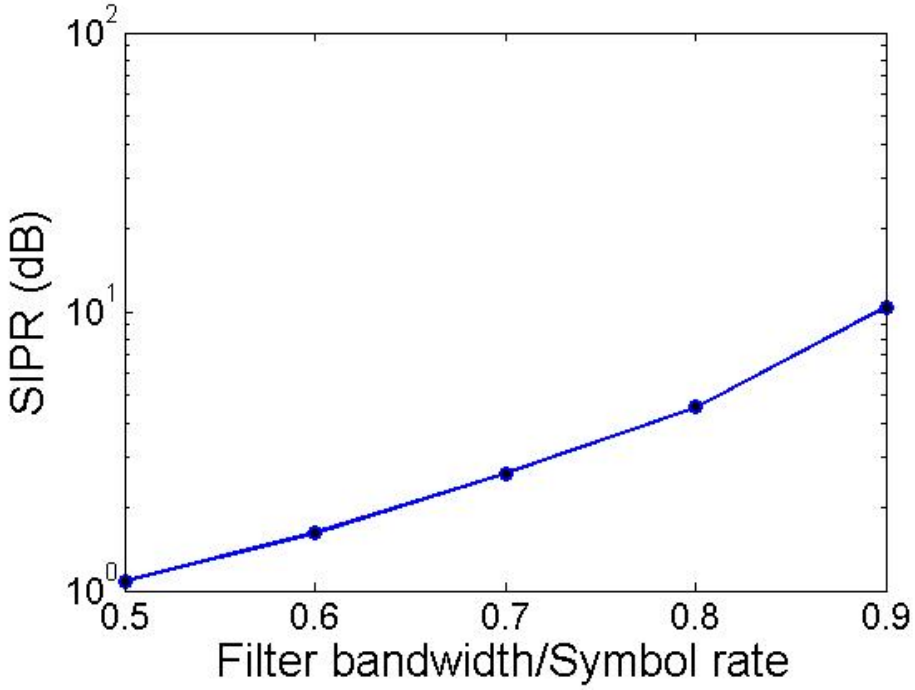

Fig. 2.1.1 Inter-symbol interference as the function of the filter bandwidth

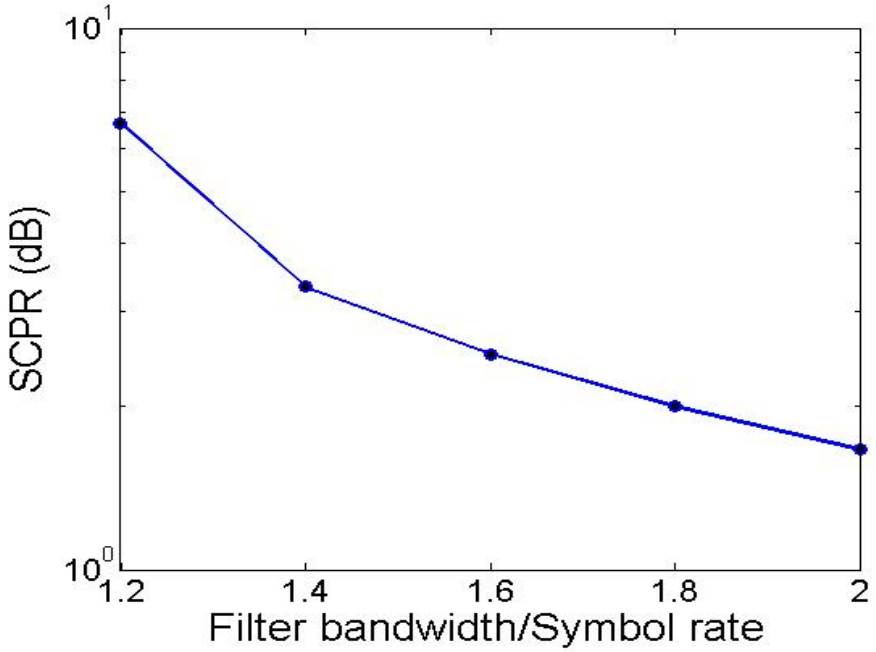

Fig. 2.1.2 Inter-channel crosstalk as the function of the filter bandwidth

From the plot, it is evident that normalized ISI represented by SIPR increases with the filter bandwidth. On the other hand, normalized inter-channel crosstalk represented by SCPR has a stronger impact when the filter bandwidth is smaller than the symbol rate, which is in agreement with Nyquist theorem.

The above results are for ideal filters in the transmitter and receiver and ideal transmission channel. However, in the real systems, the transfer function of the channel is unknown at the receiver. It is therefore only possible to make the matched filter at the receiver equal to the pulse shaping filter at the transmitter. With this in mind, the following is true;

$$Q_k(t) = I_k(t)$$

When designing the matched filters at the receiver, it is therefore important to consider degradation introduced through channel transmission impairments. In the following sections, the impacts of filter shape are discussed, as well an examination of transmission impairments caused by chromatic dispersion (CD) and fiber nonlinearity. Finally, in section 2.6 we will summarize the dominant factors for different data rates and transmission lengths.

2.2 Impact of filter shape

As previously discussed, in order to make full use of the available optical bandwidth, the spectrum of each channel has to be confined and the width has to be as narrow as possible. Pulse shaping filters are widely used for this purpose. Boxcar, raised cosine, and Nyquist are the most common filters used in digital communication for pulse shaping. In this section, a theoretical investigation of the general properties and impact in multicarrier optical systems is examined in great detail.

First, the impulse response of a boxcar filter is:

$$f(t)=\begin{cases}1 & |t|\le\dfrac{T}{2}\\ 0 & |t|>\dfrac{T}{2}\end{cases} \tag{2.2.1}$$

From Fig. 2.2.1(a), it is evident that the boxcar filter does not introduce ISI because the energy in one symbol does not leak into other symbols. But, the frequency response of boxcar filters shown in Fig. 2.2.1(b) indicates that the spectrum of one channel may overlap with other channels, so crosstalk may be introduced.

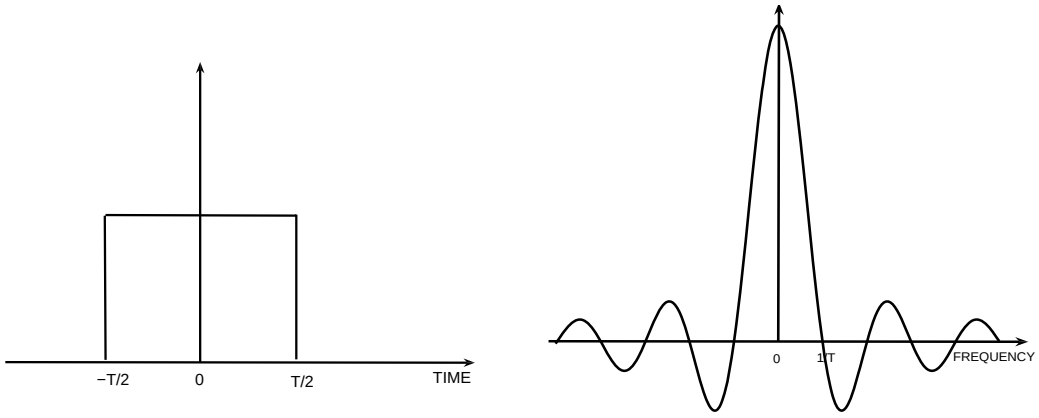

(a) (b)

Fig. 2.2.1 Boxcar filter: (a) impulse response; (b) frequency response.

However, when the channel spacing equals to the symbol rate, which is the situation in OFDM systems, the crosstalk can be removed by integration in the receiver.

Another widely used pulse shaping filter in digital communication is square-root raised cosine (SRRC) filter. Its impulse response can be written as:

$$h(t) = \frac{\sin\left(\pi \frac{t}{T}(1-\beta)\right) + 4\beta \frac{t}{T}\cos\left(\pi \frac{t}{T}(1+\beta)\right)}{\pi \frac{t}{T}\left(1-\left(4\beta \frac{t}{T}\right)^2\right)} \qquad (2.2.2)$$

In Eq. (2.2.2), β is the roll-off factor. SRRC filters can be used at both the transmitter and the receiver to minimize the impact of noise. The concatenation of transmitter and receiver SRRC filters is equivalent to a raised cosine filter. Thus, its impulse response and frequency response with different roll-off factors are described in Fig. 2.2.2.

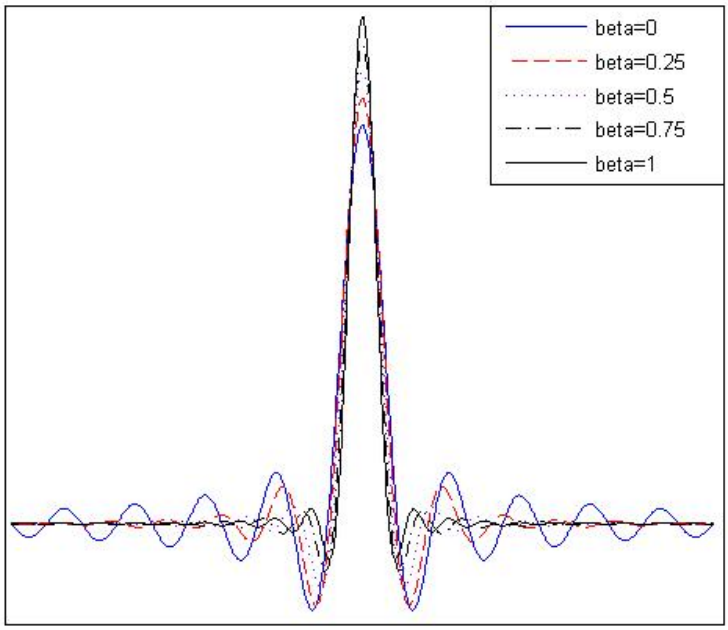

(a)

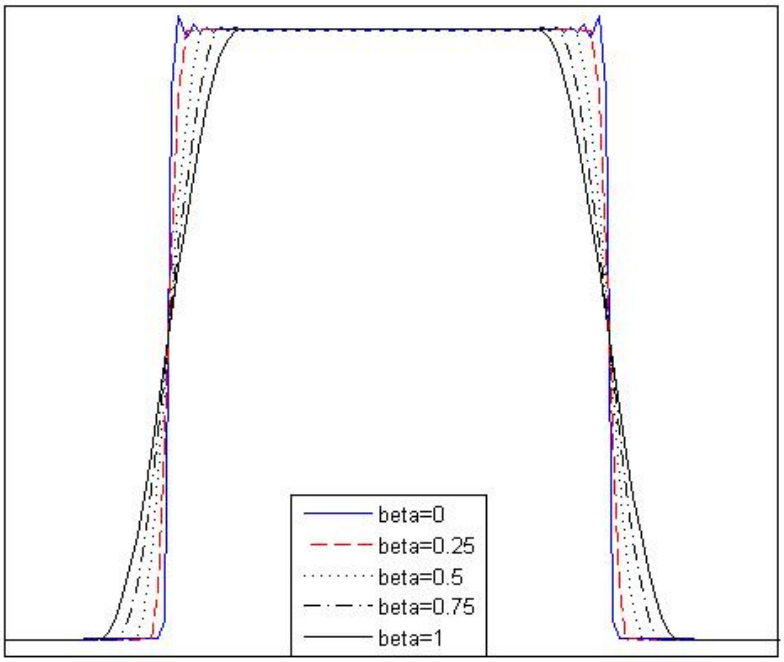

(b)

Fig. 2.2.2 SRRC filter: (a) impulse response; (b) frequency response.

Nyquist filter is another commonly used filter in communication systems. The major purpose of applying a Nyquist filter in the transmitter is to shape the pulse and limit the bandwidth of the channel. On the other hand, the purpose of the filter in the receiver is to perform channel selection and noise reduction. Therefore, different forms of Nyquist filters are usually used in the transmitter and the receiver. The typical transfer function of a Nyquist filter in the transmitter is:

$$H_T(f)=\begin{cases}\dfrac{\pi fT}{\sin(\pi fT)}; & |f|\le\dfrac{1-\beta}{2T};\quad 0\le\beta\le 1\\ \dfrac{\pi fT}{\sin(\pi fT)}\cos\left\{\dfrac{\pi T}{2\beta}\left(|f|-\dfrac{1-\beta}{2T}\right)\right\}; & \dfrac{1-\beta}{2T}\le|f|\le\dfrac{1+\beta}{2T}\\ 0; & |f|\ge\dfrac{1+\beta}{2T}\end{cases} \tag{2.2.3}$$

Fig. 2.2.3 shows the transfer function of the transmitter Nyquist filter with different roll-off factor β values.

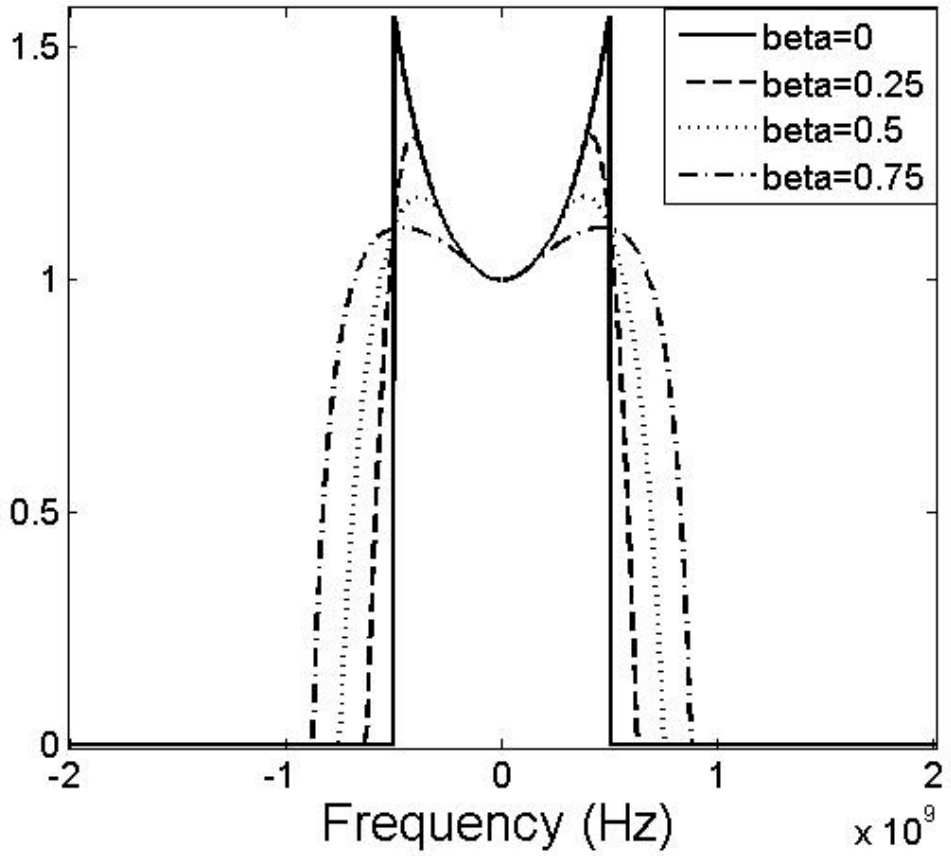

Fig. 2.2.3 The transfer function of the transmitter side Nyquist filter

The transfer function of a Nyquist filter in the receiver is usually expressed as:

$$H_R(f)=\begin{cases}1 & |f|\le\dfrac{1-\beta}{2T};\ \ 0\le\beta\le 1\\ \cos\left\{\dfrac{\pi T}{2\beta}\left(|f|-\dfrac{1-\beta}{2T}\right)\right\} & \dfrac{1-\beta}{2T}\le|f|\le\dfrac{1+\beta}{2T}\\ 0 & |f|\ge\dfrac{1+\beta}{2T}\end{cases} \tag{2.2.4}$$

The receiver Nyquist filter transfer function is plotted in Fig. 2.2.4 with different roll-off factor β values.

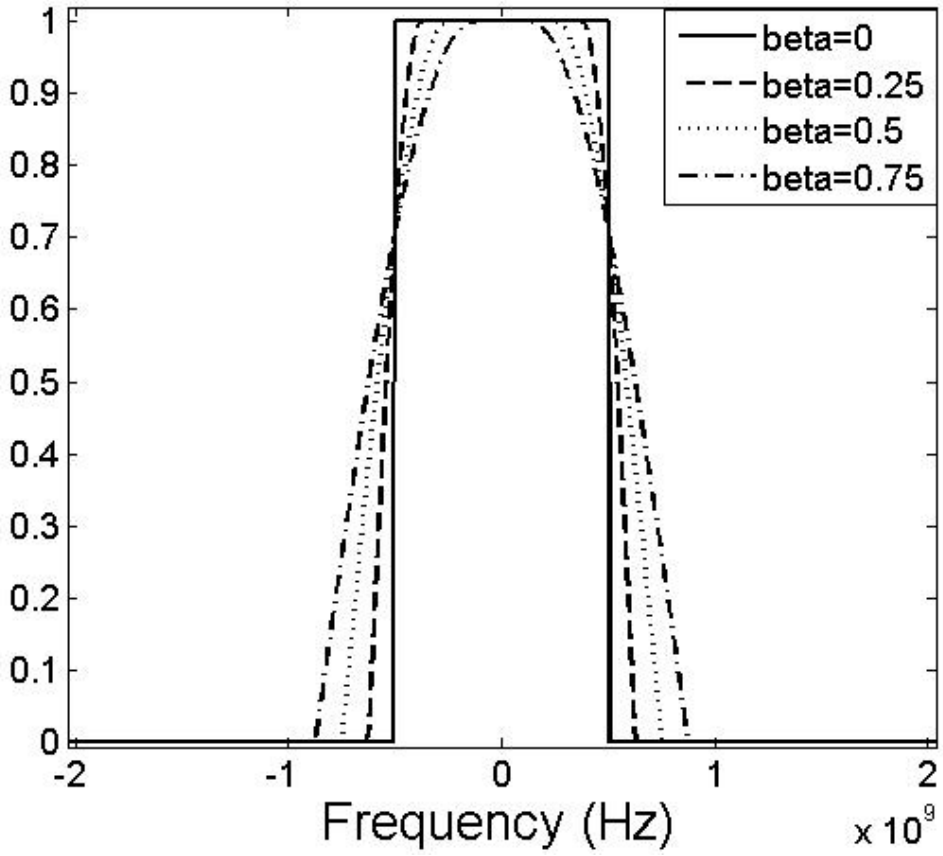

Fig. 2.2.4 The transfer function of the receiver side Nyquist filter

In digital communication, a pair of filters is used in the transmission line, which is located at the transmitter and receiver respectively. The filter in transmitter is for the pulse shaping, which controls the spectral bandwidth of the modulated signal; the filter in receiver is for the noise elimination which filters out the out of band noise. To avoid ISI, the product of the two filters has to meet the Nyquist criterion. Furthermore, to minimize the noise impact, the shape of the two filters should be similar. So, although the ultimate goal is the pulse shaping for band-limited channel, it is important to consider both the transmitter and the receiver.

This section introduced three widely used filters, boxcar filter, raised cosine filter and Nyquist filter. Abovementioned, boxcar filter has a rectangular impulse response and infinite frequency transfer function. As a result, it can only be used for extremely low data rate channels for which the system bandwidth is much larger (more than 100 times) than that of each channel. Additionally, because of the steep edge of the impulse response, boxcar filters can only be realized in digital domain. OFDM system is an example of boxcar filter application in digital communication. A raised cosine filter is an approximation of the ideal Sinc filter, but because it has a smooth edge in frequency domain, which makes it realizable by electronic or optical materials. Because of the nonideal shape of raised cosine filter, it introduced both ISI and crosstalk to multicarrier systems, but it is still widely used for the easy realization. Nyquist filter is another approximation of Sinc filter, but it has a different shape for the transmitter and receiver. The concave top in the transmitter can compensate for the convex shape of the modulated signal, which gives the output of the transmitter a rectangular spectral shape, thus ensuring the zero ISI.

The roll-off factor of pulse shaping filters has a great influence on the transmission performance of multicarrier systems. In order to see the impact quantitatively, the numerical simulation of a multicarrier system with 10 subcarrier channels using Nyquist filter is calculated. The channel spacing between subcarrier channels is 1GHz, the data rate on each subcarrier channel is 1Gb/s using binary modulation, and the optical signal to noise ratio (OSNR) at the receiver is set to 10dB.

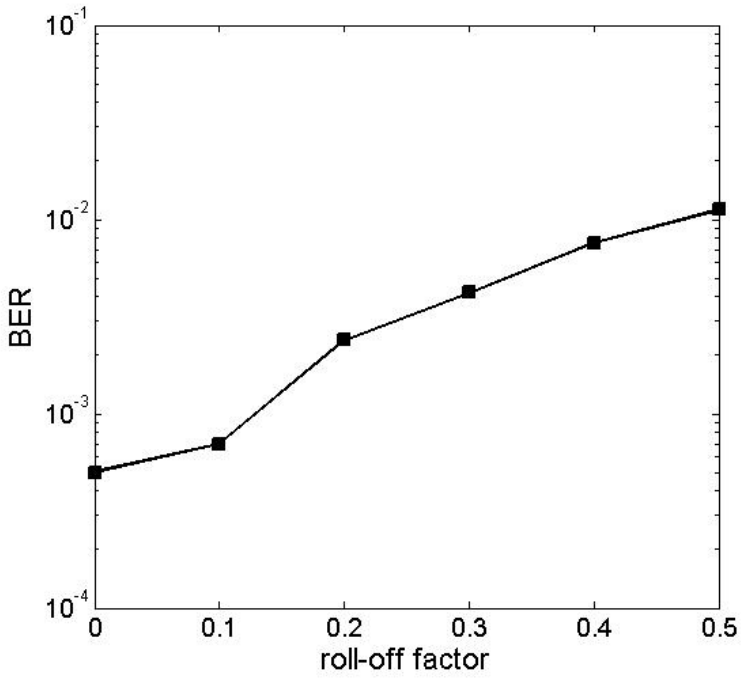

Fig. 2.2.5 BER vs. filter roll-off factor in a multicarrier system

The bit error rate (BER) with different filter roll-off factors in a back-to back transmission is calculated in Fig. 2.2.5, The plot indicates that the BER increases rapidly with a roll-off factor greater than 0.1. In order to obtain zero inter-channel crosstalk, zero roll-off is required. Because of the response time of electronic and optical components,

the zero roll-off Nyquist filter cannot be realized by electrical or optical filters with current techniques. To solve this problem, digital filters that are capable of producing steep edges in frequency domain are widely used in modern optical multicarrier systems.

2.3 Impact of chromatic dispersion

When optical signal propagates along an optical fiber, different frequency components within the optical signal propagate at slightly different speeds. This frequency-dependency of propagation speed is commonly known as the chromatic dispersion (CD). In high data rate systems, the influence of CD may be significant because the transmitted signal occupies a wide optical bandwidth. Meanwhile, the system tolerance to chromatic dispersion is reduced at a high data-rate because the temporal length of each bit is short. In traditional 10Gb/s and 40Gb/s optical systems, dispersion compensation is commonly used. Here, CD in the transmission fiber is compensated by a dispersion compensator, which contains the opposite sign of chromatic dispersion as the transmission fiber. Popular dispersion compensators include dispersion compensating fibers (DCFs) and passive optical components, such as fiber Bragg gratings (FBG). In recent years, the rapid advance of digital electronic circuits enabled high speed digital-signal processing has allowed the dispersion compensation to be accomplished in the electrical domain. Additionally, advanced optical and electrical modulation formats have made electrical-domain CD compensation realistic and more efficient.

Theoretically, chromatic dispersion can be treated as a frequency chirp added to the optical signal. The transfer function of a dispersive component such as an optical fiber can be expressed as:

$$H_{CD}(z,\omega) = \exp(j\frac{1}{2}\beta_2\omega^2 z) \tag{2.3.1}$$

In Eq. (2.3.1), β_2 is the group delay dispersion parameter. The frequency chirp makes pulse broadening after transmission, which is described in Fig. 2.3.1. In the plot, a Gaussian pulse is transmitter through a single mode fiber (SMF). *T* stands for the pulse width and T_0 as the initial pulse width, with z representing the transmission distance and $L_D = \frac{T_0^2}{|\beta_2|}$ defined as the CD length.

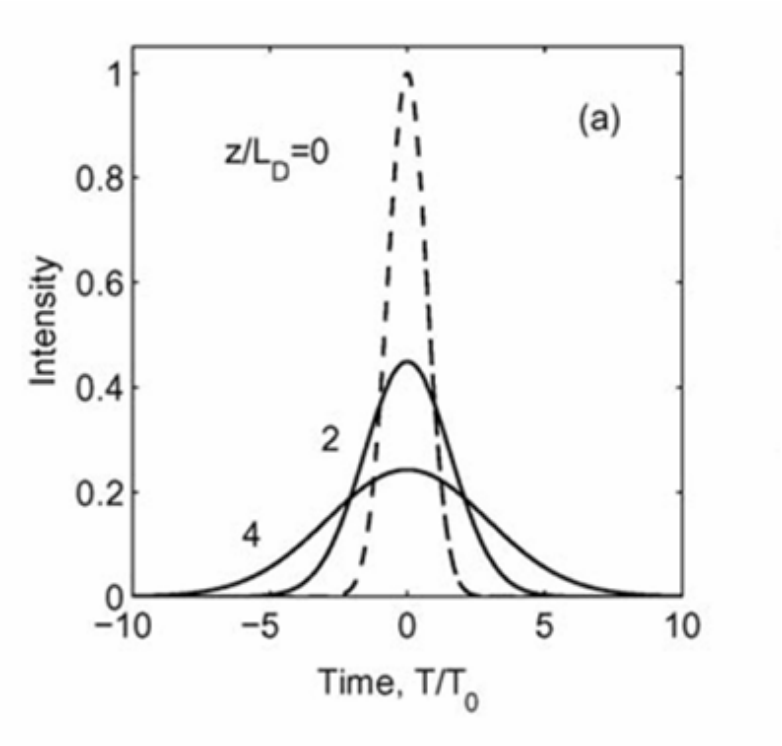

Fig. 2.3.1 Pulse broadening after transmission (REF [2])

To see the influence of CD in optical multicarrier systems, it is possible to add fiber to the system discussed in section 2.2 and set the roll-off factor to 0 and 0.1. The BER values at different transmission distance are plotted in Fig. 2.3.2. In this calculation,

only CD is considered in the fiber, with the dispersion parameter D as 16×10^{-6} s/m^2 ($D = -2\pi c\beta^2/\lambda^2$, c is the speed of light in free space, λ is the wavelength).

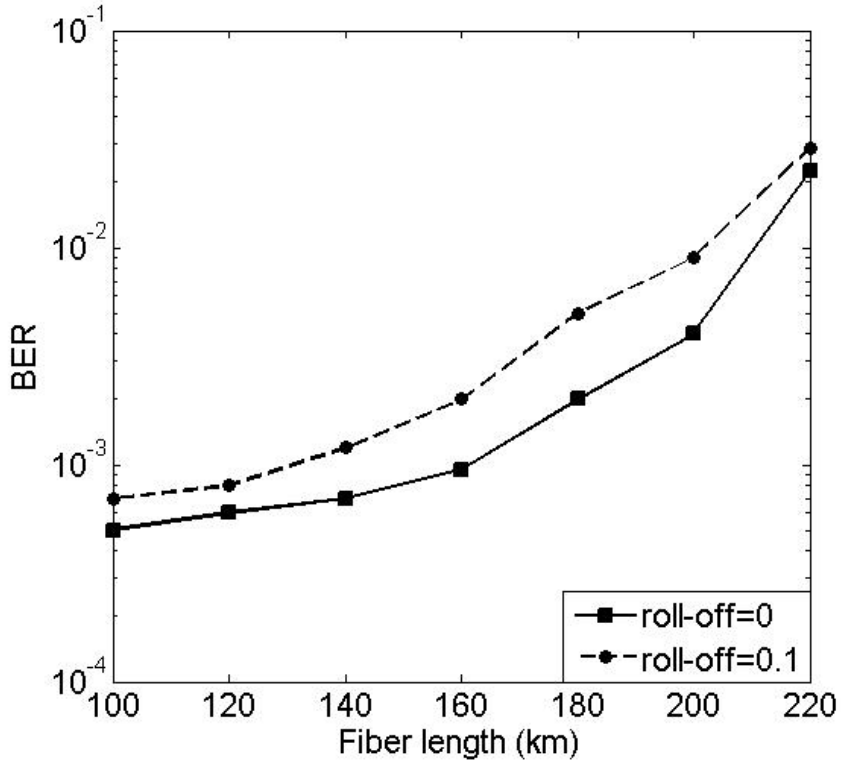

Fig. 2.3.2 Impact of CD in multicarrier system

The curves in Fig. 2.3.2 show that CD can significantly reduce system performance as transmission distance increases. When the distortion from CD becomes dominant, the advantage of low roll-off filters will be diminished. Therefore, in modern multicarrier systems, equalization algorithms are often used for dispersion compensation.

2.4 Impact of fiber nonlinearity

Kerr effect nonlinearity is introduced by the fact that the refractive index of an optical material is often a weak function of the optical power density:

$$n = n_0 + n_2 \frac{P}{A_{eff}} \tag{2.5.1}$$

Here, n_0 is the linear refractive index of the material, n_2 is the nonlinear index, P is the optical power, and A_{eff} is the effective cross-section area of the optical waveguide. P/A_{eff} represents optical power density. Kerr effect results in three major nonlinear distortions to the transmitted signal: self-phase modulation (SPM), cross-phase modulation (XPM), and four-wave mixing (FWM).

SPM adds a nonlinear phase shift to the optical field, which follows the time-dependent change of the optical power. The introduced frequency shift is the first order derivative of the phase change, and therefore it is introduced primarily at the leading edge and the falling edge of signal optical pulses. This frequency shift broadens the signal optical spectrum. Together with the chromatic dispersion, it introduces additional group delay mismatch between the leading and falling edges of signal pulses, and therefore creating waveform distortion.

In the discussion of SPM, only one wavelength channel is considered, and its optical phase is affected by its own intensity. If more than one wavelength channel travels in the same fiber, XPM and FWM will also be introduced by Kerr effect. XPM is similar to SPM in that both create a nonlinear phase shift to the signal, but XPM instead creates the shift through the optical power change of other channels. It also requires chromatic dispersion to convert this nonlinear phase shift into waveform intensity distortion. FWM can be understood through the simplest case in which two optical carriers co-propagate along an optical fiber. In this instance, the beating between the carriers modulates the refractive index of the fiber at the frequency difference between them. Subsequently, all the optical carriers, including the original two, will be phase-

modulated by this frequency, creating extra modulation sidebands. When there are only two optical carriers in the fiber, four modulation sidebands will be generated through the FWM process, hence the name “four-wave mixing”.

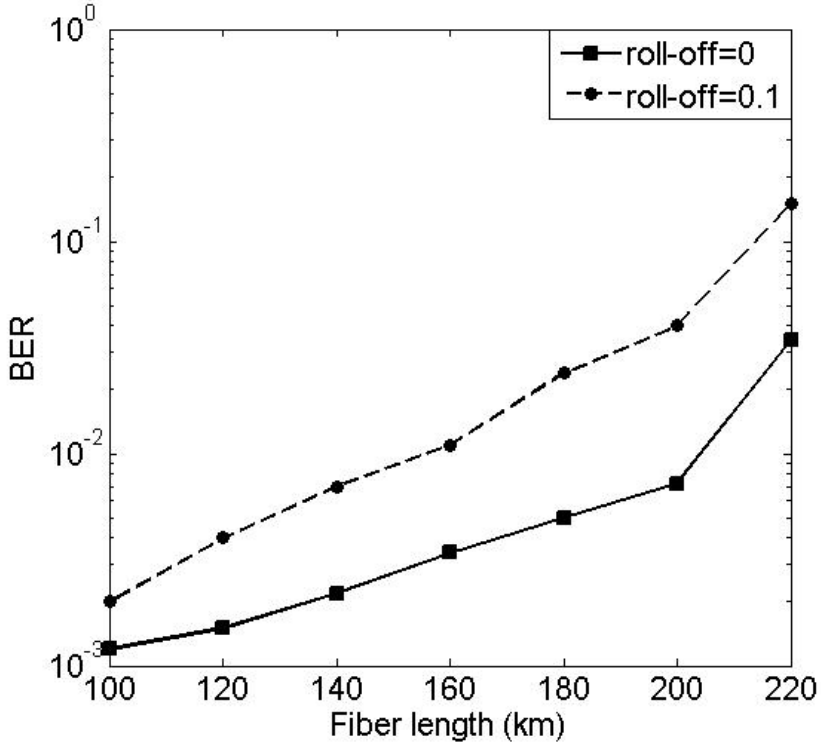

Fig. 2.4.1 Impact of nonlinearity in multicarrier system

Add the influence of fiber nonlinearity into the system in section 2.3 and set the nonlinearity index coefficient n_2 to $26e^{-21}$ m^2/W, input power to 0dBm for each subcarrier channel, the result is Fig. 2.4.1. In comparison with Fig. 2.4.1, nonlinearity impairments further decreases the system performance in Fig. 2.3.2. Furthermore, the system with higher roll-off filter has more degradation. Since the nonlinearity effect is unavoidable in

fiber-optic transmission, the designing of pulse shaping filter in multicarrier system has become a research area of high focus.

2.5 Conclusion

This chapter included an examination of the optical multicarrier system, with analytical equations providing an explicit understanding and illustration of the physical mechanism of the system. The influence of filter bandwidth on ideal system was demonstrated in section 2.1, which further confirmed the minimum frequency bandwidth requirement for a zero ISI and zero crosstalk multicarrier system. The investigation of the impacts of pulse shaping filter and fiber impairments provided a theoretical foundation for optical multicarrier system design.

3. FFT-based optical OFDM system

Through detailed investigation, multi-carrier systems have been shown potential in the improvement of the performance of long-distance optical fiber transmission. With the rapid progress of high-speed digital electronic circuits, including ADC and DAC in recent years, FFT-based OFDM for high-speed optical systems became possible. In addition to the increase of optical bandwidth efficiency compared to that in analog SCM systems, other digital signal processing techniques can be applied to reduced inter-symbol interference through equalization, as well as through pre- or post- digital compensations. As a well-studied digital modulation method, FFT-based OFDM has the capability to support various advanced electrical and optical modulation formats. FFT-based OFDM also is capable of utilizing various digital signal-processing algorithms [16] in order to achieve higher spectral efficiency and better system performance for high-speed optical transmission. FFT-based OFDM optical systems with both coherent-detection and direct-detection have been demonstrated with single sideband (SSB) optical spectrum to reduce the impact of fiber chromatic dispersion and make full use of the optical bandwidth. While coherent detection provides better spectral selectivity and receiver sensitivity, direct detection has a much simpler system configuration. This configuration avoided the requirement of an optical local oscillator and the associated stabilization and phase/polarization diversity apparatus.

It is commonly known that in an OFDM receiver with direct detection, signal in the optical domain are down-converted into RF domain through the mixing with the optical carrier in the photodiode. But in the same process, subcarrier channels within the same OFDM band may also mix with each other generate crosstalk between them. To

avoid this signal-signal beat interference (SSBI), a spectral guard-band between the optical carrier and the OFDM subcarriers has to be reserved with the same bandwidth as the OFDM signal [17]. This is commonly referred to as offset–SSB modulation.

Offset-SSB modulation not only reduces the bandwidth efficiency, but also wastes approximately 50% of the DAC and ADC capabilities in the transmitter and the receiver. Theoretically, this problem can be solved by encoding the information into the exponential envelope of the optical signal [18], which eliminates the nonlinear mixing among OFDM channels in the photo-detection process. Therefore, the guard-band between the optical carrier and the OFDM subcarriers is unnecessary. This compatible-SSB modulation has the least complexity in comparison with other techniques involving the removal of the guard-band [19, 20].

The implementation of optical SSB modulation is another important issue in the transmitter of an OFDM system. The most straightforward technique is to use a simple intensity modulator and a narrowband optical filter to select one from the two redundant optical sidebands. Other techniques involve the use of Hilbert transform in both the RF and the optical domains to suppress the unwanted optical sideband. Ideally, an optical IQ modulator can directly translate complex RF signals into optical domain [18], whereas a more traditional dual-drive MZM can also be used with appropriate digital signal processing to obtain real-valued electrical signals to drive the two modulator arms [21].

This chapter presents a theoretical and experimental systemic investigation of compatible-SSB modulation technique in long-distance FFT-based OFDM transmission. The system uses a traditional dual-drive MZM in the transmitter and direct detection in the receiver. The primary focus is on the simplicity of implementation while still

maintaining the desired transmission performance. The experimental setup utilizes a commercial optical transmitter initially designed for 10 Gb/s binary optical transmission with electrical-domain pre-compensation (eDCO) [22], which is equipped with two 22.2Gs/s DACs and a dual-drive MZM. Although an IQ modulator has been previously suggested for a compatible-SSB system [18], results from the present study indicate that a simple dual-drive MZM provides comparable performance for this particular modulation format. Furthermore, it is evident that system transmission performance can be improved by appropriate digital pre-compensation in the transmitter to correct the nonlinear transfer characteristics of the MZM. After performing a detailed analysis on the impact of the MZM bias variation and the optical modulation index, results indicate that high modulation index is preferred for noise limited systems. On the other hand, a lower modulation index is required for uncompensated long-distance systems with significantly large chromatic dispersion. The impact of nonlinear SPM has also been investigated in this system. Because compatible-SSB modulation eliminated the requirement of the guard-band between the carrier and the OFDM signal sideband, the overall optical bandwidth is 50% narrower than the offset-SSB modulated OFDM system of the same data rate. Consequently, the tolerance to nonlinear SPM is also improved.

3.1 Principle of operation

In general, an OFDM optical signal can be expressed by a summation of a central optical carrier and multiple subcarriers:

$$\tilde{x}(t) = A_0\left[1 + \sum_{k=0}^{N-1} \tilde{X}_k \exp\left(j2\pi k\Delta f t\right)\right] \cdot e^{j\omega_0 t} \qquad (3.1.1)$$

In this equation, ω_0 is the optical carrier frequency, A_0 is the optical carrier amplitude, N is the total number of subcarrier channels and Δf is the frequency spacing between

adjacent channels. $\widetilde{X}_k = A_k e^{j\theta_k}$ is the normalized complex QPSK/QAM data symbol on the k_{th} carrier with A_k and θ_k representing the magnitude and the phase, respectively. Therefore, the bandwidth of the OFDM sideband is $N \cdot \Delta f$.

At the optical receiver, the photo-detector performs square-law detection, and the photocurrent is proportional to the received optical power:

$$\widetilde{i}(t) = \eta |A_0|^2 \left| 1 + \sum_{k=0}^{N-1} \widetilde{X}_k \exp(j2\pi k \Delta f t) \right|^2 \qquad (3.1.2)$$

Here, η is the photo-detector responsivity. While the useful RF spectrum comes from the mixing between the optical carrier and the OFDM subcarriers whose amplitude is proportional to $\widetilde{X}_k$, mixing also happens among subcarrier channels producing crosstalk with the amplitude proportional to $\widetilde{X}_i \widetilde{X}_j$ (i, j = 1, 2 …. N). The frequency of this inter-mixing crosstalk spreads over the RF bandwidth between DC and $N \cdot \Delta f$. To avoid the contamination of the OFDM signal from this signal-signal beating interference, the OFDM signal subcarriers must be offset to higher frequencies in order to reserve a sufficient guard-band between the optical carrier and the signal sideband. Fig. 3.1.1 illustrates the optical and electrical spectra of the offset-SSB modulation for an OFDM system in which the 6GHz guard-band is equal to the OFDM signal sideband. After direct detection in a photodiode, the guard-band in the electrical domain is filled with signal-signal beat interference noise. The requirement of the guard-band obviously reduces the spectral efficiency by a factor of 2. Also, the DAC in the transmitter must have twice the

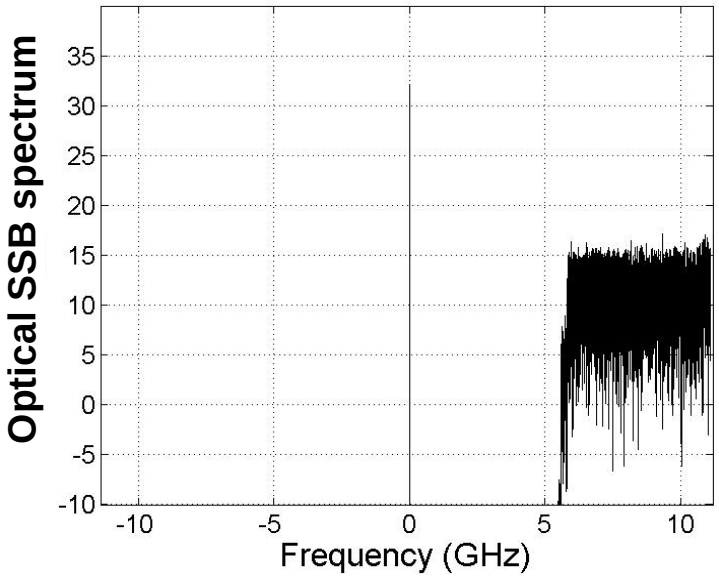

(a)

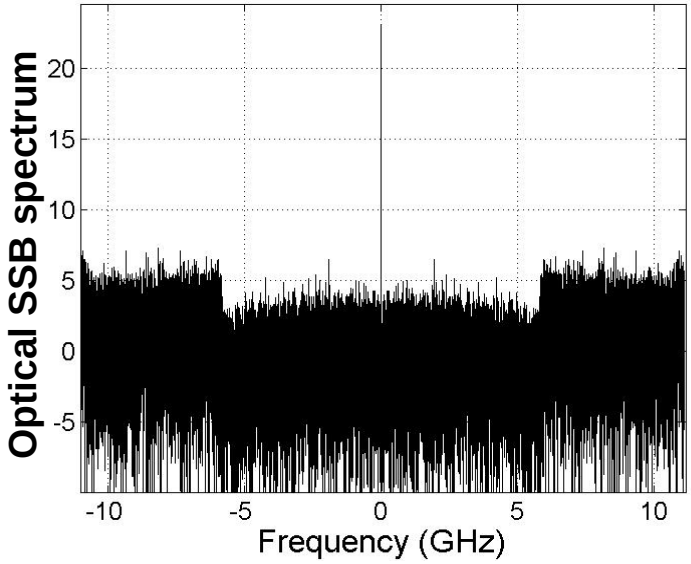

(b)

Fig. 3.1.1 Spectra of offset modulation (a) optical single-sideband spectrum, and (b) electrical double-sideband spectrum after square law detection

bandwidth of the OFDM signal, which often imposes the upper limit on the overall data rate the transmitter can support.

Compatible-SSB modulation encodes the OFDM data onto the exponential envelope of the optical field, which can be expressed as:

$$\tilde{x}(t) = A_0 \exp\left[\sum_{k=0}^{N-1} \tilde{X}_k \exp\left(j2\pi k\Delta f t\right)\right] \cdot e^{j\omega_0 t} \tag{3.1.3}$$

After the square-law detection in an optical receiver, the photocurrent is:

$$\tilde{i}(t) = \eta |A_0|^2 \exp\left\{2\sum_{k=0}^{N-1} \tilde{X}_k \exp\left(j2\pi k\Delta f t\right)\right\} \tag{3.1.4}$$

This avoided the nonlinear mixing among the OFDM subcarriers in the detection process as illustrated by Fig. 3.1.2. By applying a square root operation and a nature log operation, the original OFDM signal can be digitally recovered. Therefore, with compatible-SSB modulation and direct detection, a guard-band is not needed, and the OFDM signal can occupy the entire DAC bandwidth starting from almost DC.

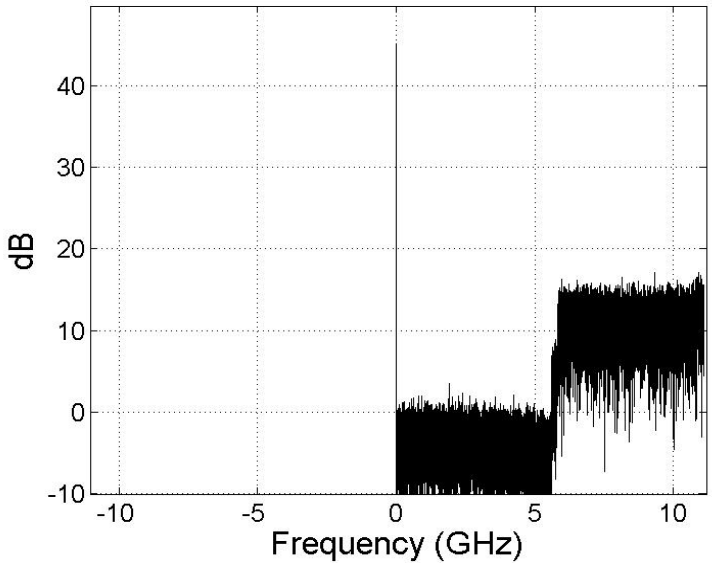

(a)

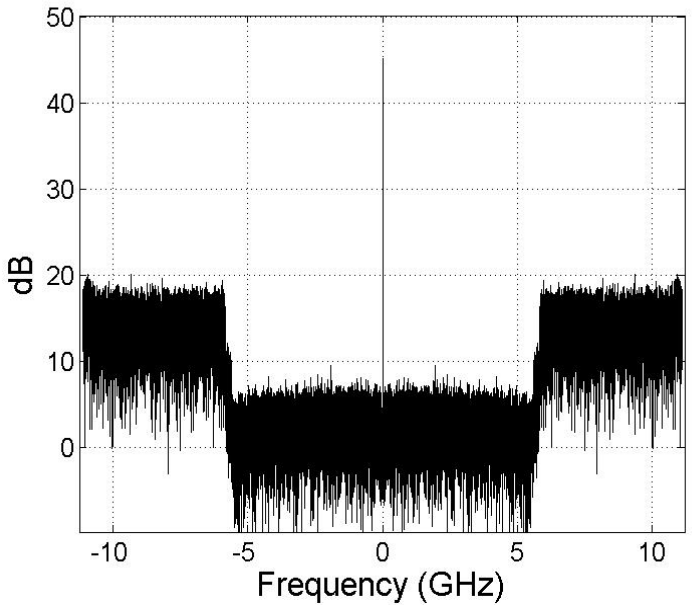

(b)

Fig. 3.1.2 Spectra of compatible-SSB modulation (a) optical single-sideband spectrum, and (b) electrical double-sideband spectrum after square law detection

The optical signal of compatible-SSB modulation can be generated through an ideal I/Q modulator, which directly translates the complex electrical waveform into optical domain [18]. However, since the OFDM signal is encoded as an exponential term as indicated in Eq. (3.1.3), the negative part of the optical field envelope cannot be explored. From that point of view, one should also be able to use a simple dual-drive MZM for the same functionality, while more cost effective and less complexity.

In order to derive the voltage waveforms to drive the dual-electrode MZM, it is assumed that the OFDM signal in the electrical domain is $\sigma(t) = \sum_{k=0}^{N-1} \tilde{X}_k \exp(j2\pi k\Delta f t)$. To convert $\sigma(t)$ into single sideband, another waveform must be created:

$m(t) = \sigma(t) + jH[\sigma(t)]$, where $H[\ ]$ denotes Hilbert transform. For compatible-SSB optical modulation, this single-sideband electrical signal is carried as an exponential term in the optical signal, which is:

$$n(t) = \exp[m(t)] = A(t)e^{j\Phi(t)} \tag{3.1.5}$$

The amplitude and phase of this optical signal is related to the original OFDM signal by both [18]

$$A(t) = \exp[\sigma(t)] \tag{3.1.6}$$

and

$$\Phi(t) = H[\sigma(t)] = H\{\ln[A(t)]\} \tag{3.1.7}$$

For an ideally linearized modulator with two balanced electrodes, the intensity modulation is proportional to the differential phase between the two arms, while the phase modulation is proportional to the common-mode phase of the two arms. Therefore, the optical signal required for compatible-SSB transmitter can be obtained through the following equation:

$$\frac{\varphi_1(t) - \varphi_2(t)}{2} \exp\left[j \frac{\varphi_1(t) + \varphi_2(t)}{2} \right] = A(t)e^{j\Phi(t)} \tag{3.1.8}$$

The optical phases φ_1 and φ_2 of the two modulator arms should be [19]:

$$\varphi_1(t) = \Phi(t) + A(t) \tag{3.1.9a}$$
$$\varphi_2(t) = \Phi(t) - A(t) \tag{3.1.9b}$$

For practical dual-drive MZM biased at the quadrature point, the transfer function between the CW input optical field E_i and output optical field $E_0(t)$ is not perfectly linear:

$$E_0(t) = 2E_i \sin\left[\Delta\varphi(t) + \frac{\pi}{4} \right] \exp j\left[\varphi_0(t) - \frac{\pi}{4} \right] \tag{3.1.10}$$

In this equation, $\varphi_0(t) = \pi[v_1(t) + v_2(t)]/2V_\pi$, $\Delta\varphi(t) = \pi[v_1(t) - v_2(t)]/2V_\pi$ are the common-mode and differential phase delay of the two MZM arms, respectively. $v_1(t)$ and $v_2(t)$ are electrical signal voltage applied on the two electrodes, and V_π is the voltage for a π phase shift in the MZM power transfer function.

To take this nonlinear intensity transfer characteristic into account, the required electrical signals on the two MZM electrodes should be written as:

$$v_1(t) = \frac{V_\pi}{\pi}\left\{\Phi(t) + \sin^{-1}\left(A(t)\right)\right\} \qquad (3.1.11a)$$

$$v_2(t) = \frac{V_\pi}{\pi}\left\{\Phi(t) - \sin^{-1}\left(A(t)\right) + \pi/2\right\} \qquad (3.1.11b)$$

Unlike the use of an ideal I/Q modulator where the complex RF spectrum is linearly translated into the optical domain [18], in a practical system using a dual-drive MZM, both modulation index and the accuracy of bias setting are important parameters affecting system transmission performance. A small modulation index can ensure the linear operation and avoid the clipping from the MZM. But, the signal sideband will have much lower power than that of the carrier if the modulation index is too small. Therefore, the system will be vulnerable to optical noise. On the other hand, a high modulation index will explore the nonlinear transfer function of the MZM, and clipping will occur at the peak intensity of the OFDM signal. The interaction between these nonlinear modulation effects and the chromatic dispersion in the transmission fiber will further distort the waveform and introduce transmission performance degradation. Thus, the optimal MZM modulation index usually depends on the fiber characteristics and the transmission distance of the system.

For a noise-limited system, higher modulation index can help to reduce the carrier-to-signal power ratio and therefore improve the system performance. Yet, if the system is limited by the chromatic dispersion, the modulation index cannot be too high. If this is the case, the sideband suppression ratio of the signal will deteriorate and high-order harmonics will increase in the spectrum. Fig. 3.1.3 shows two examples of optical spectra with low and high optical modulation indices. Obviously, when the modulation index is increased from 10% to 40%, the power in the OFDM sideband increases by 6dB. However, at the same time, frequency components at high-order harmonics, as well as in the image sideband, are increased dramatically due to the nonlinear transfer function and clipping of the MZM. Therefore, the system will become vulnerable to chromatic dispersion in the system. Throughout the analysis, the modulation index is defined as the RMS voltage of the OFDM signal divided by the V_π of the modulator.

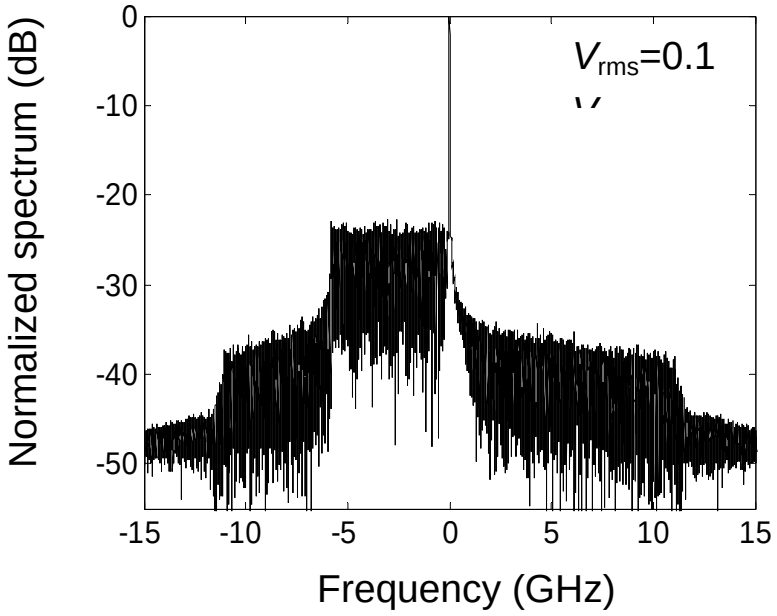

(a)

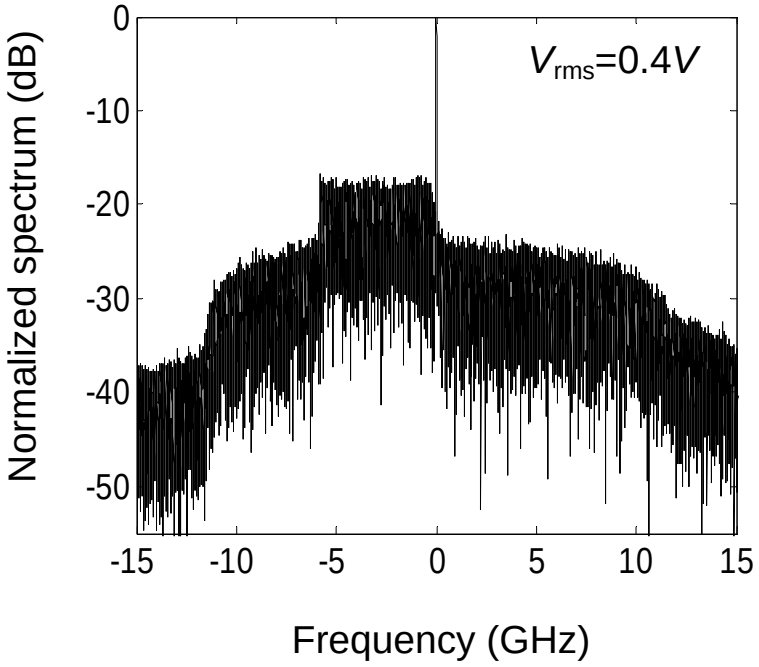

(b)

Fig. 3.1.3 Optical spectra of compatible-SSB OFDM signal with small modulation index (a) and large modulation index (b)

3.2 Experimental setup

In order to experimentally investigate the compatible-SSB modulated OFDM system for long-distance fiber-optic transmission, a transmission test-bed using an optical re-circulating loop has been established. Fig. 3.2.1 shows the block diagram of the experimental setup. The OFDM signal is generated by an offline program in MATLAB. An 11.1 Gb/s serial data is mapped onto QAM-4 format, and then loaded onto 64 subcarriers by serial-to-parallel conversion. We have used N = 256 block in the IFFT operation so that the minimum sampling rate is 4 bits per period. The OFDM subcarriers occupy inputs 65 – 128 while the complex conjugate of the OFDM subcarriers are loaded

into inputs 129 – 192 in a reverse sequence. This data mapping insures that the time-domain signal has real values after the IFFT operation. Inputs 1 – 64 and 192 – 256 are padded with zeros to fill up the entire 256 IFFT block. Two training symbols are inserted at the beginning of the OFDM symbol for timing synchronization and digital equalization.

In the experimental configuration below, a commercial optical transmitter provided by Nortel is used, which was initially designed for 10 Gb/s binary optical transmission with electrical-domain pre-compensation (eDCO) [22, 23]. This eDCO card is equipped with two DACs with 22.2Gs/s sampling speed at 6-bits resolution and a 2^{15}-long memory, so that it functions as a 22.2 Gs/s dual-channel arbitrary waveform generator (AWG). The card is also imbedded with a tunable laser and a balanced duel-drive MZM. By loading the digitally-created OFDM data into the eDCO memory, the compatible-SSB optical signal is obtained.

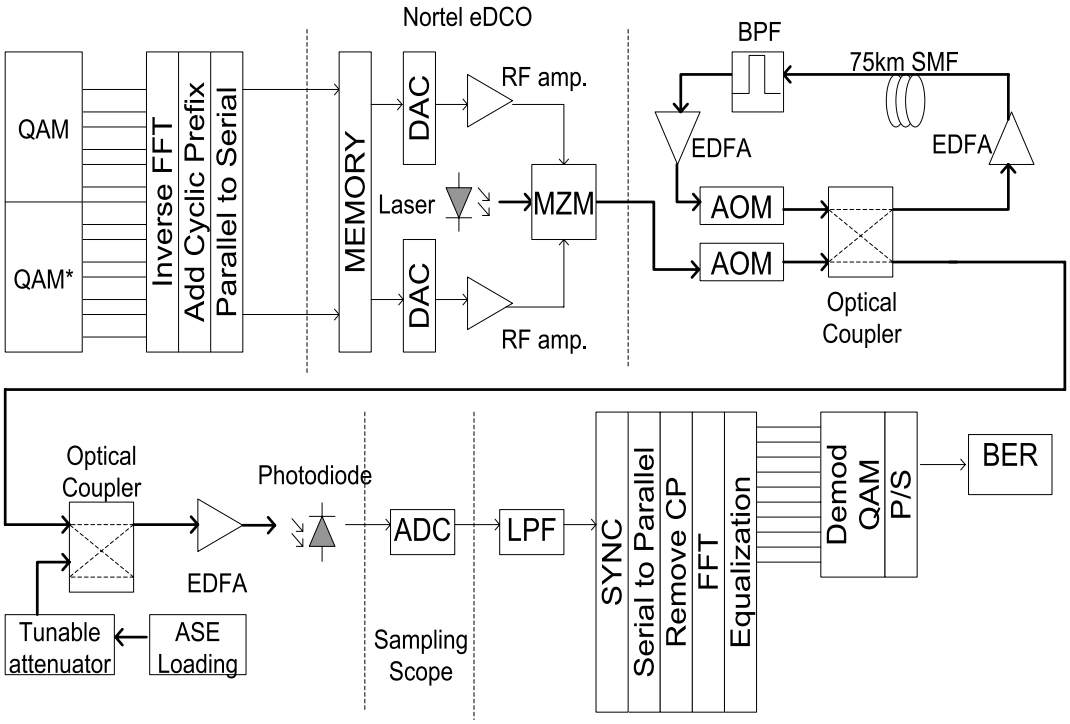

Fig. 3.2.1 Experimental configuration

To test the long-distance transmission performance, a fiber-optic re-circulating loop is used in the system. Each span of the loop consists of 75km uncompensated standard single-mode fiber (SMF), two in-line EDFAs, and a 1-nm bandwidth tunable optical filter to prevent saturation of in-line EDFA by the accumulated ASE noise. At the output of the re-circulating loop, another EDFA is used as a pre-amplifier to boost the signal optical power before it reaches the photodiode. The electrical signal output from the photodiode is sampled and recorded by a real-time oscilloscope (LeCroy 8600A), which has a 20 Gs/s sampling rate and 6 GHz analog bandwidth. Receiver signal-processing functions, including synchronization, cyclic prefix removal, FFT, and equalization are performed offline in a MATLAB program. In order to evaluate the required optical signal to noise ratio (R-OSNR) for different system configurations and settings, noise loading is used in the experiment, in which a controllable amount of ASE noise generated by an EDFA without input is added to the optical signal at the receiver by an optical coupler.

It is worthwhile to note that with QAM-4 data format using compatible-SSB modulation, the 11.1 Gb/s data signal only occupied approximately 5.5GHz. While this eDCO transmitter card is capable of delivering 22.2 Gb/s data rate, the system capacity described here is primarily limited by the real-time oscilloscope at the receiver, which only has 6GHz analog bandwidth.

3.3 Results and discussion

Based on the operation principle described in section 3.1 and the system configuration discussed in section 3.2, it is also possible to compile a numerical simulation tool to investigate the properties of optical OFDM systems using compatible-

SSB modulation. The transmitter model uses the same parameters as those in the experiment, with 6-bits DAC at the sampling rate of 22.2Gs/s. The fiber transmission model uses a split-step Fourier analysis, which includes chromatic dispersion and Kerr effect nonlinearity in the fiber. The comparison between measured results and those from numerical simulations provide help to better understand mechanisms of various system degradation effects, as well as ways to optimize the system.

a. MZM bias setting and nonlinear equalization

As discussed in the previous section, a practical MZM has nonlinear transfer characteristics. Driving waveforms given by Eq. (3.1.9) derived from the linear approximation of the MZM transfer function [19] may introduce waveform distortions. As a result of the digital implementation of the transmitter, this nonlinear transfer function can be pre-compensated by using the driving waveforms defined by Eq. (1.1.11). Fig. 3.3.1 shows the measured BER versus OSNR characteristics for a back-to-back OFDM system. In the experiment, digital signal was pre-clipped such that the peak amplitude of the OFDM waveform was 4.62 times its root-mean-square (*rms*) value. This value was chosen based on the theoretical analysis provided in [18]. Less clipping would result in high DC level in the signal and this high CSPR, whereas stronger clipping would cause intolerable signal bit errors even before transmission. Without nonlinear pre-compensation, the MZM operates in linear regime only when the modulation index is small enough. Nonlinear pre-compensation relaxes this restriction to some extent and allows the use of higher modulation indices. Without applying the nonlinear pre-compensation, the required OSNR to achieve a BER of 10^{-3} is approximately 22dB and optimum modulation index is $0.2V_{\pi}$. We choose 10^{-3} for the acceptable BER level

because a forward error correct (FEC) [24] is able to further reduce the BER from 10^{-3} to 10^{-15}. In our experimental, BER = 10^{-3} is the pre-FEC value. With nonlinear pre-compensation, a higher modulation index of $0.3V_{\pi}$ can be used for the optimum system performance. Subsequently, the required OSNR to achieve a BER of 10^{-3} is improved by 4dB to approximately 18dB. The two constellation diagrams in Fig. 3.3.1 were examples measured at 20dB OSNR level, with and without the nonlinear pre-equalization.

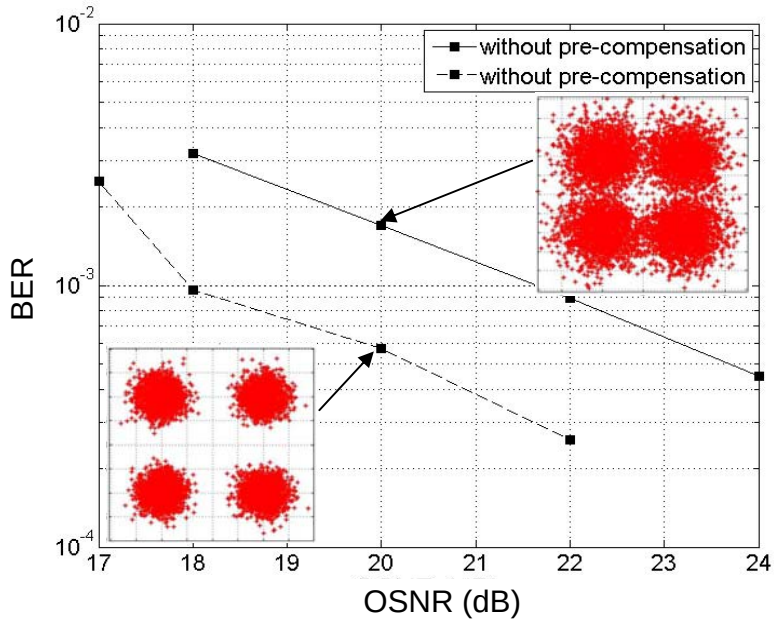

Fig. 3.3.1 BER versus signal OSNR in a back-to-back system with and without nonlinear pre-compensation of MZM transfer function

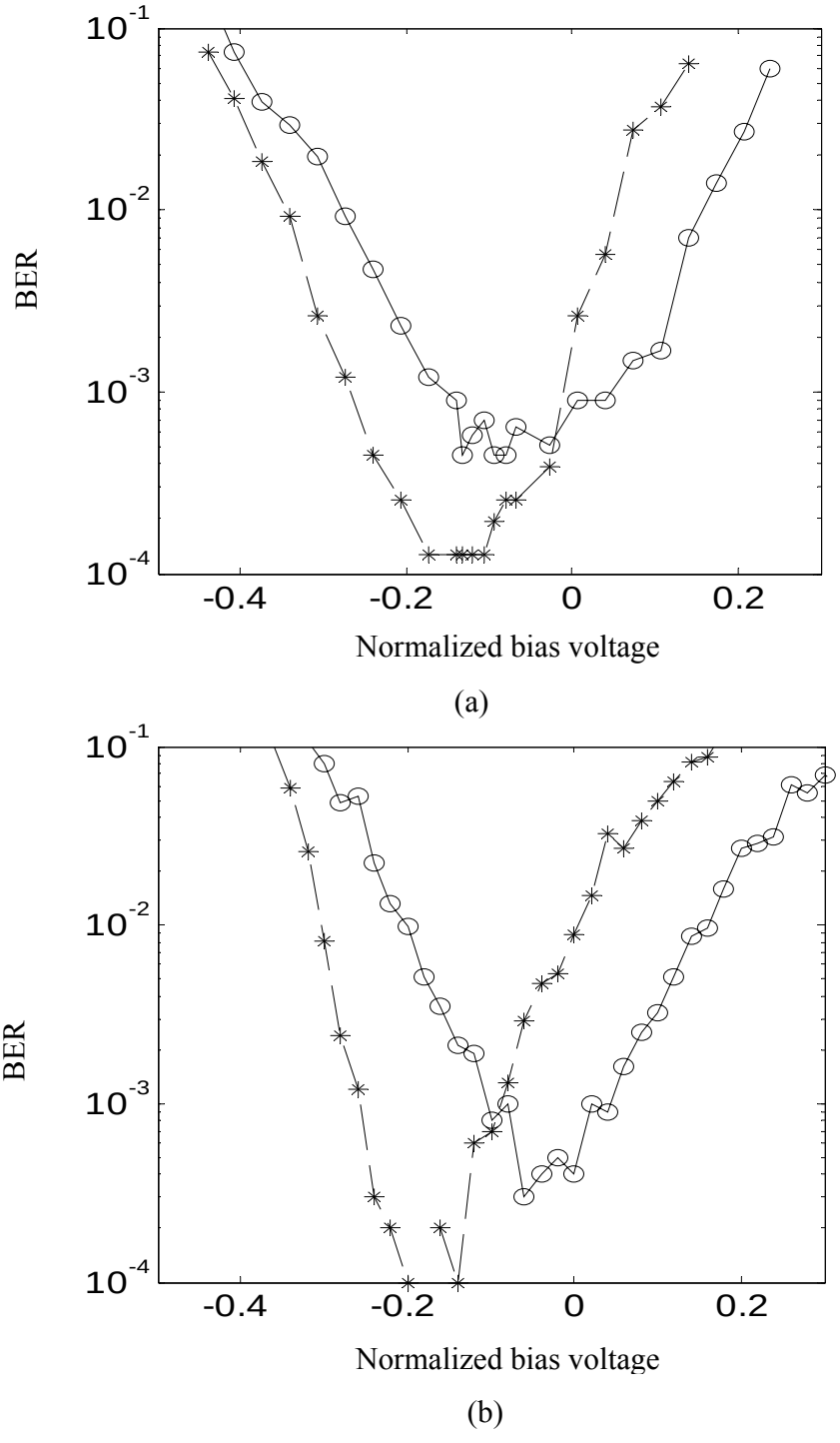

Fig. 3.3.2 BER versus normalized bias voltage variation for back-to-back (stars) and over three fiber spans (open circles). (a) measured and (b) numerical simulation

For a practical electro-optic modulator based on a dual-drive Mach-Zehnder interferometer, proper DC bias and the correction of nonlinear transfer function are two important issues to optimize the system performance.

In a dual-drive MZM, the generation of optical single-sideband modulation requires the bias level to be at the quadrature point [25, 26]. The system performance sensitivity to the level of MZM biasing is an important parameter in practical system implementation, which determines whether a precise feedback control is required. Fig. 3.3.2 (a) shows the measured BER versus the normalized MZM bias voltage variation for back-to-back (stars) and over a 3-span (open circles) OFDM systems. In the experiment, digital signal was pre-clipped by 6dB. For the back-to-back measurement, the modulation index on the MZM was about $0.35V_{\pi}$ and the signal OSNR was 20dB, In the measurement of the 3-span system, the modulation index was $0.22V_{\pi}$, and the OSNR was about 24dB.

Fig. 3.3.2 (b) shows the results of numerical simulation for the same systems, but in order to obtain the comparable BER levels within the experiments, the OSNR had to be 14dB for the back-to-back system and 20dB for the 3-span system. Both the measured and the simulated BER curves indicate that the optimum bias level of the MZM changes for approximately 10% between the back-to-back system and the system with three spans of standard SMF. This is because in back-to back experiments, chromatic dispersion is negligible, and the deterioration of sideband suppression ratio caused by moving the bias away from the quadrature point does not significantly degrade transmission performance. This allows the bias to be set at a lower transmission point so that the power in the carrier can be reduced. Thus, of the carrier-to-signal ratio is reduced. On the other hand, for a

long-distance transmission over fiber with significant chromatic dispersion, optical sideband suppression ratio must be high enough to avoid the crosstalk between the two sidebands at the receiver. In this case, the bias has to be set very close to the quadrature point. In both cases, the normalized bias voltage variation has to be kept within < ±5% for negligible BER degradation.

b. Impact of MZM modulation index

In addition to the bias level and the pre-equalization of MZM nonlinear transfer function, modulation index is another important parameter critical to the system transmission performance. Fig. 3.3.3 (a) shows the measured BER as the function of the MZM modulation index in a re-circulating loop experiment. It is worth noting that for a back-to-back system not involving optical fiber, the optimum modulation index is around 35%. When transmission fiber is introduced with significant chromatic dispersion, the optimum modulation index becomes much smaller, at about 13%. This reduced optimum modulation index in long distance systems is primarily due to the requirement of high sideband suppression ratio of SSB modulation. Although the carrier-to-signal ratio can be improved to some extent, the rise of the unwanted optical sideband as illustrated in Fig. 3.1.3 reduces the system tolerance to chromatic dispersion at a high modulation index. The result of numerical simulation shown in Fig. 3.3.3 (b) qualitatively agrees with the measurements and thus verifies the observation in the experiments.

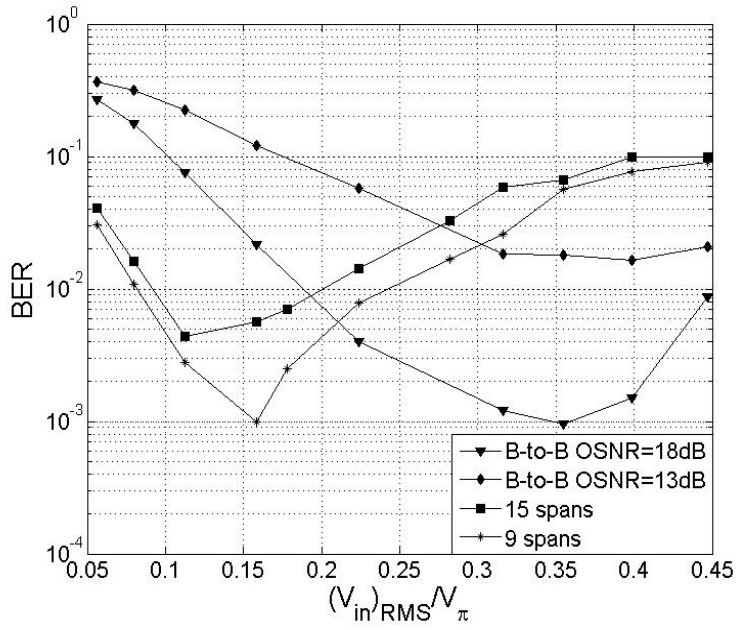

(a)

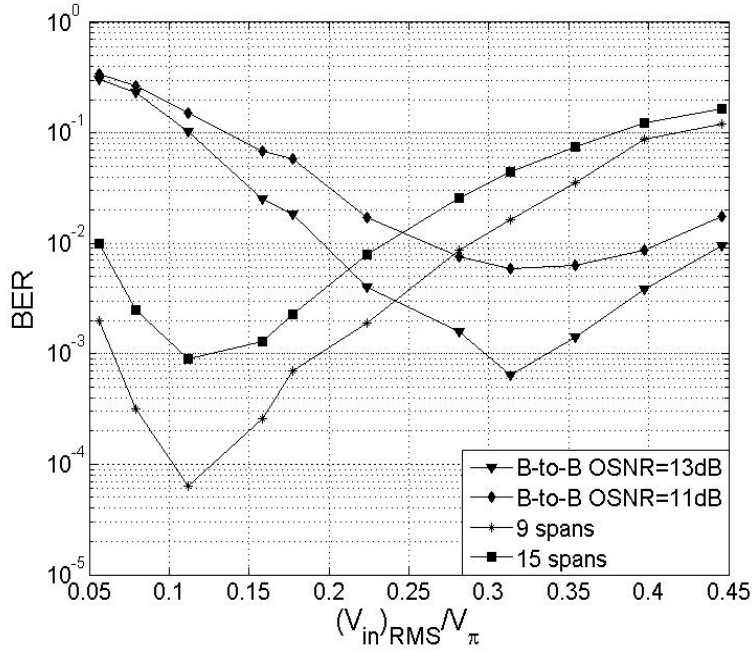

(b)

Fig. 3.3.3 BER versus MZM modulation index: (a) experiment; (b) simulation.

Fig. 3.3.4 illustrates the optimum modulation index as the function of the number of uncompensated fiber spans (75km standard SMF per span) obtained by more systematic numerical simulations. The OSNR level at the receiver was kept at 17dB in the simulation. The optimal modulation index reduces significantly over the first five spans, which is roughly equivalent to the dispersion length of the signal with 5GHz bandwidth over standard SMF. A further decrease of the modulation index will not bring additional improvement on the sideband suppression ratio in the SSB modulation, while only deteriorating (increasing) the carrier-to-noise ratio. A tradeoff has to be made between minimizing the dispersion-induced crosstalk and maximizing the power in the OFDM sideband.

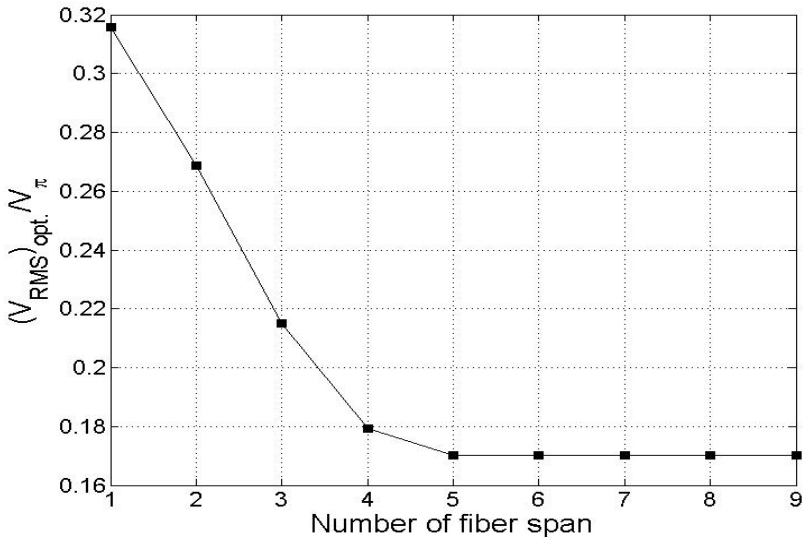

Fig. 3.3.4 Simulated optimum modulation index as the function of fiber length

c. Required OSNR

For long-distance optical transmission over amplified fiber spans, one of the most important parameters is the required OSNR to achieve the pre-FEC BER of 10^{-3}. Fig. 3.3.5 shows measured and simulated BER versus OSNR characteristics of the 11.1 Gb/s compatible-SSB system for back-to-back, as well as over different numbers of uncompensated fiber spans. The measurement was performed using an optical re-circulating loop setup as described in section 3.2. The roundtrip optical loss in each loop is approximately 28dB, which includes 16dB loss for 75km standard SMF, and losses from optical coupler (3dB), band-pass optical filter (2dB) and an acousto-optic switch (7dB). Optical noise loading was used before the receiver to measure the BER as the function of signal OSNR.

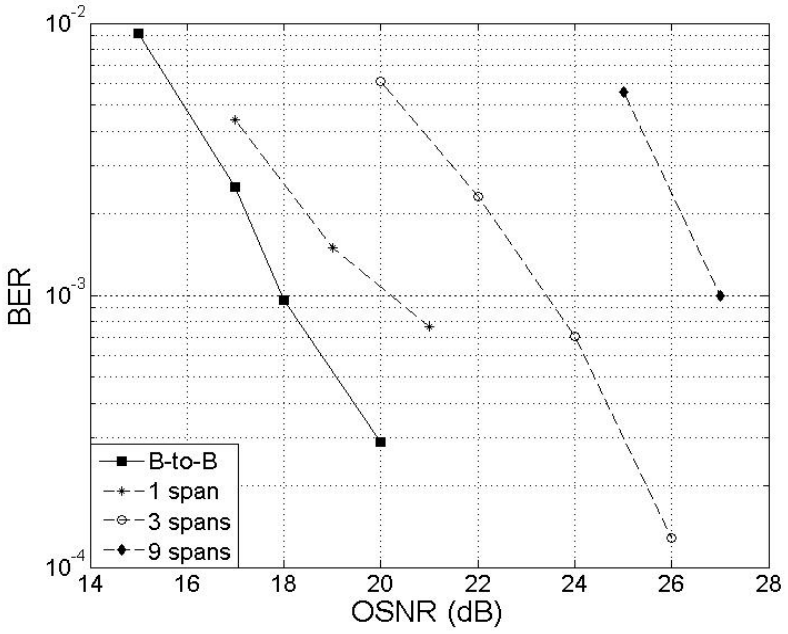

(a)

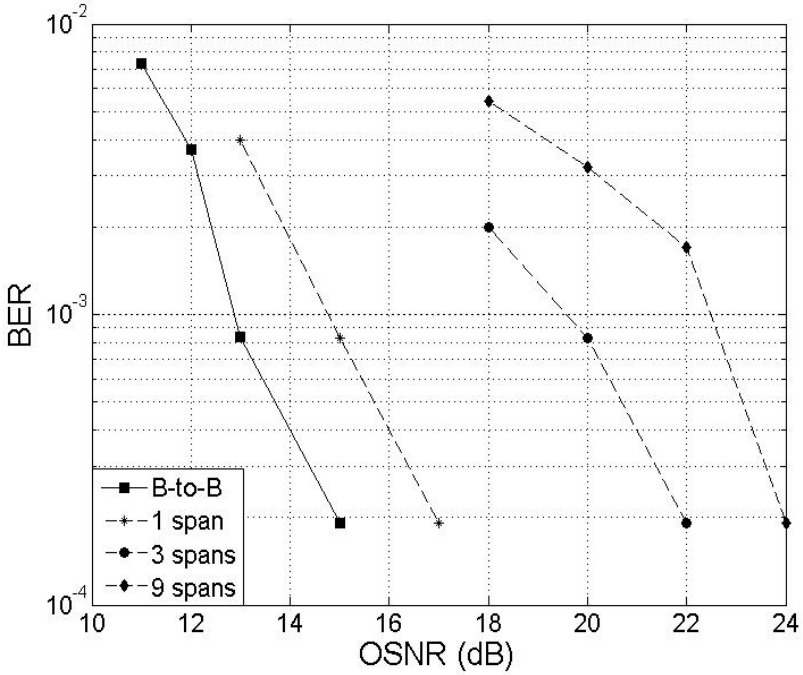

(b)

Fig. 3.3.5 BER versus OSNR for different transmission distances: (a) measured; (b) numerical simulation.

Fig. 3.3.6 summarizes the required OSNR (R-OSNR) for BER = 10^{-3} as a function of the system fiber length. There is an approximate 5 dB difference between the measured R-OSNR and the results of numerical simulation using the same parameters. This discrepancy can be attributed to time jitter in the receiver clock (oscilloscope clock is free-running), as well as the multipath optical and RF interferences along the system which create ripples in the transfer functions. There is an approximately 9dB OSNR penalty after 675km transmission over the fiber compared to back-to-back. This is partially attributed to the high modulation index used for the short distance transmission, which must be reduced for long distances. The maximum transmission distance here is

primarily limited by the achievable OSNR of 27dB after 9 fiber spans in the re-circulating loop. A longer transmission distance may be possible in a real multi-span optical system in which there is no extra insertion loss in each span as in the re-circulating loop system. In this instance, the OSNR level can be higher.

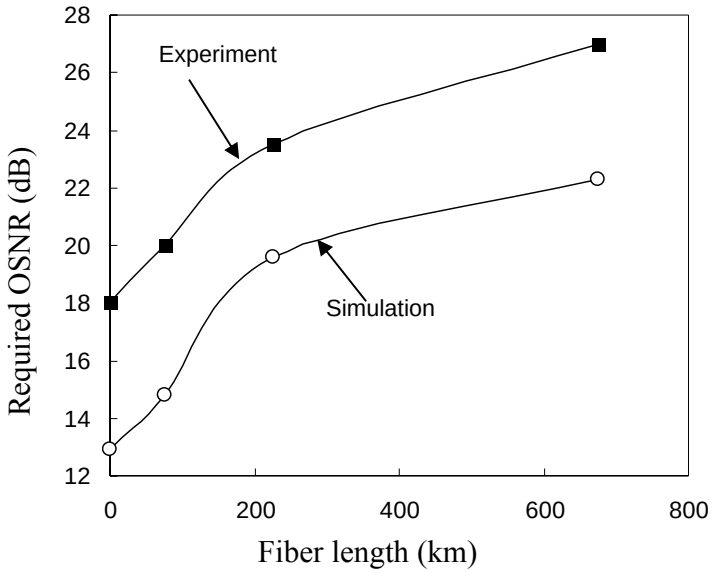

Fig. 3.3.6 Required OSNR versus fiber length.

d. Impact of self-phase modulation

A general concern in OFDM modulation format is the high pick-to-average ratio for the signal. Therefore, transmission systems using OFDM might be vulnerable to fiber nonlinear effects, such as self-phase modulation (SPM) [27]. Although it is an important parameter, the sensitivity to SPM has not yet been investigated for the OFDM system based on compatible-SSB modulation.

The present SPM measurement was performed in the same re-circulating loop setup previously described in section 3.2. The launched optical power into the transmission fiber was varied by changing the saturation level of the in-line EDFA in the loop through the pump power adjustment. Because the optical loss is fully compensated by the EDFA gain in the re-circulating loop, the launched power into the transmission fiber is expected to be the same for every span. Fig. 3.3.7 shows the BER measured after 9 spans of fiber transmission as the function of the launched optical power. Throughout the measurement, the receiver OSNR was kept at about 27dB. The results shown in Fig. 3.3.7 indicate that BER is not sensitive to the launched optical power when its level is lower than 4.5dBm. Rapid BER degradation is observed when the power level is beyond 5dBm. A numerical simulation was also performed based on the experimental system configuration and used a split-step Fourier method. The parameters used in the simulation were: fiber length of each span L = 75 km; fiber attenuation parameter α = 0.21 dB/km; nonlinear refractive index n_2 = 2.35 m^2/W; fiber core effective area A_{eff} = 80μm^2; and fiber dispersion coefficient D = 16 ps/nm·km at the signal wavelength of λ = 1547nm. The result from numerical simulation, also shown in Fig. 3.3.7, agrees reasonably well with the experiment.

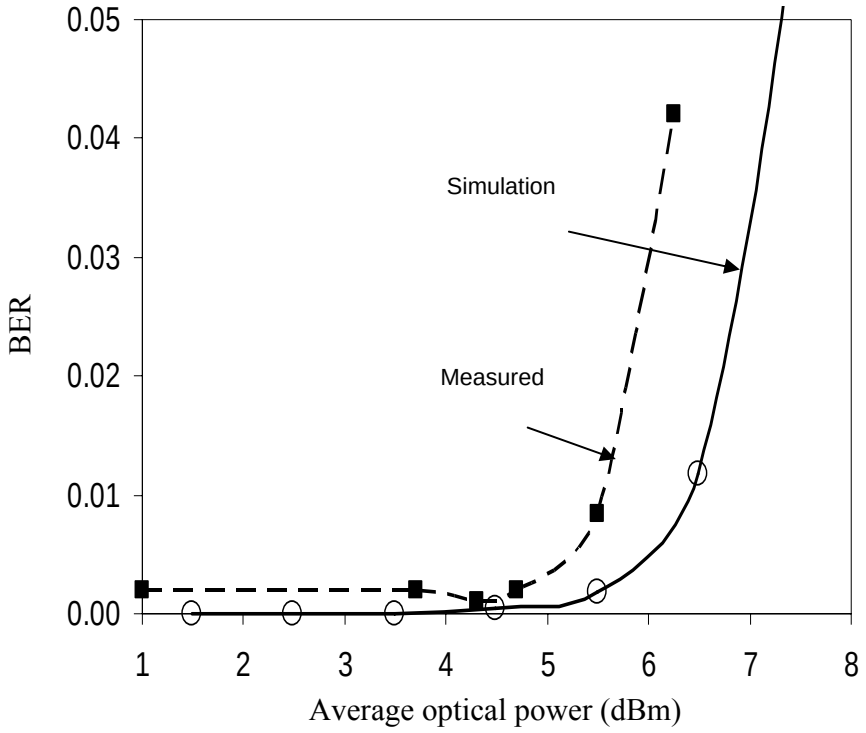

Fig. 3.3.7 BER versus launch power for OFDM after 675km fiber transmission

SPM performance in OFDM system with direct detection has been previously measured using standard offset-SSB modulation at the data rate of 11.1 Gb/s [27]. The system performance was found to degrade by SPM significantly when the launched optical power approached 0dBm. Fig. 3.3.7 indicates that for the same data rate, an OFDM using compatible-SSB modulation is much less sensitive to the impact of SPM. The reason is mainly due to the reduced optical spectral bandwidth of compatible-SSB modulation. For 11.1 Gb/s data rate, standard offset-SSB modulation requires the modulation bandwidth of approximately 11.5 GHz because of the required guard-band between the carrier and the OFDM sideband. Since this guard band is not necessary in

compatible-SSB format, its optical bandwidth is only half in comparison to the offset-SSB modulation.

It is well known that SPM-induced optical frequency chirp is proportional to the time derivative of the signal power [26]. This nonlinear frequency chirp is converted into an intensity crosstalk through chromatic dispersion in the transmission fiber. The impact of this extra intensity crosstalk in the system performance is proportional to the optical bandwidth of the signal. Therefore, part of the SPM tolerance improvement should be attributed to the signal bandwidth change from 11.5GHz (for offset-SSB modulation) to 5.75GHz (for compatible-SSB modulation). Another reason for the decreased sensitivity to SPM on compatible-SSB modulated system is the relatively small modulation index and the high carrier-to-signal ratio.

It is also worth noting that although the system using compatible-SSB modulation is less sensitive to the effect of SPM, other nonlinear effects, such as cross-phase modulation and four-wave mixing, may set the upper power limit in WDM optical systems using this modulation format due to inter-channel crosstalk. This, however, is beyond the scope of the present investigation.

3.4 Conclusion

This chapter performed a systemic investigation of a compatible-SSB modulated OFDM system for long-distance optical transmission. The simple system configuration used direct-detection. With the elimination of the guard-band requirement, this modulation format is attractive for low-cost implementation. Furthermore, this chapter experimentally demonstrated a compatible-SSB modulated OFDM system with 11.1 Gb/s data rate based on a standard dual-drive MZM in the transmitter, as well as an optical

transmission over 675km uncompensated standard SMF in an optical re-circulating loop. Various issues in system performance optimization have been investigated, which included digital pre-compensation of the MZM nonlinearity transfer function, optimum bias level and modulation index and their dependence on system transmission distance. The impact of nonlinear SPM in the transmission performance was also measured, which demonstrated the improved SPM tolerance of compatible-SSB modulated OFDM system compared to its offset-SSB counterpart at the same data rate. The results of the numerical simulation based on split-step Fourier method agree reasonably well with the experiments, which helped to understand the physical mechanisms behind the measured results.

4. DSCM-based optical OFDM system

High speed bandwidth scalable transmission systems are under consideration as a means of addressing flexible capacity requirements of next generation optical networks. Wavelength routed transparent network architectures can reduce the need for electrical regeneration, and thus, reduce network cost. For optical switching and grooming on shorter timescales, several approaches have been proposed in recent years, namely, optical packet switching (OPS) [28], optical virtual concatenation (OVC) [15], and waveband switching [29]. The enabling technologies such as fast optical switches and optical buffers are still in gestation. The spectrum-sliced elastic optical path network (SLICE) is a demonstrated alternative network architecture [30] with improved bandwidth granularity in comparison to present WDM-based and wavelength-routed optical path networks. As one of the most important enabling technologies, bandwidth-variable transponders have recently gained considerable attention [31]. OFDM is a promising candidate, as it provides variable bandwidth allocation by selecting the number of assigned subcarriers according to traffic volume and granularity requirement, yet eliminating the requirement for a spectral guard-band between adjacent subcarrier channels.

Originating from wireless communication, in a FFT-based OFDM system as previously described in chapter 3, the data stream is first mapped into a 2-D array in the row-by-row manner. Oppositely, an IFFT is performed such that each column of the data array becomes a subcarrier channel. In this way, a data symbol is usually partitioned into different subcarriers [17]. In the corresponding OFDM receiver, an FFT process is used to convert the 2-D data array back into frequency domain, and the original digital signal

is reconstructed through parallel to serial conversion. In addition to the extra computational complexity due to IFFT and FFT, in this process it is not practical to select a subset of subcarriers without detecting the entire OFDM frame. In addition, the FFT-based OFDM requires pilot subcarriers and temporal guard interval for carrier recovery and synchronization [17], which increases the frame overhead. The combined overhead resulting from the guard interval and pilot subcarriers in FFT-based OFDM is typically 25% of total bits [32]. This reduces the bandwidth efficiency of FFT-based OFDM.

Wavelength-domain OFDM systems as described in [33] and [34] applies the orthogonality principle to multi-wavelength systems so that the spectral guard band between WDM channels is not required. A wavelength-domain OFDM system uses mutually frequency-locked optical subcarriers created by a multicarrier comb generator. Further, an array of electro-optic modulators is used to encode data signals onto these optical carriers. In this scheme, channel spacing is determined by the multicarrier generator, and data rate on each wavelength channel cannot be dynamically changed without sacrificing optical bandwidth efficiency. This reduces the flexibility in bandwidth allocation, as well as data rate granularity in the optical network.

In this chapter, an investigation of the performance of a DSCM-based OFDM system with flexible bandwidth assignment in the transmitter and dynamic channel selectivity at the receiver is presented. In a DSCM-based OFDM system, subcarrier channels are digitally generated and linearly up-converted to an optical carrier by an electro-optic IQ modulator. This allows a higher degree of flexibility in bandwidth allocation and scalability in data rate granularity while maintaining high bandwidth efficiency. The receiver with coherent detection has the flexibility to dynamically select

different number of subcarrier channels in the detection without the need to change system configuration. The bandwidth requirement in the receiver should be reduced if only a subset of subcarrier channels is to be detected instead of the entire OFDM frame. Here, an experimental demonstration of a DSCM-based OFDM system with 10 subcarrier channels using with both ASK modulation and QPSK modulation based on the commercially available transmitter card originally designed for 10 Gb/s binary optical transmission with electrical-domain pre-compensation (eDCO) is presented. This is the same transmitter card as used in the OFDM experiment in Chapter 3, but the dual-drive intensity modulator is replaced by an IQ modulator for complex optical field modulation. The impact of inter-channel crosstalk and tolerance to bit misalignment are also discussed. Numerical simulations are then performed to understand and illustrate various mechanisms which help to determine system transmission performance.

4.1 Principle of operation

Wavelength-domain OFDM systems have been studied as the bandwidth variable transponder for SLICE [34]. In that system, mutually frequency-locked optical carriers were generated through a comb generator [11]. These carriers were optically demultiplexed so that each could be modulated by an independent electro-optic modulator before recombined and launched into a transmission fiber. The clock of the data signal driving each modulator is synchronized to satisfy the orthogonality condition of OFDM. Practically, 10Gb/s, 40Gb/s and 100Gb/s data rates carried by each optical carrier have been demonstrated, and the aggregated data rate can reach terabits per second in such a wavelength-domain OFDM system [10]. However, from a network application point of view, a finer channel data rate granularity is desired to improve

network flexibility and reduce blocking probability [31]. Realistically, it is not efficient to generate optical frequency combs with extremely narrow channel spacing (e.g., 1GHz). Also, it is not efficient for the use of a large number of electro-optic modulators with each only operating at a low data rate.

In order to improve data rate granularity and simplify the transmitter implementation, a DSCM modulation format can be used in which subcarriers are generated digitally in the electronics domain. Since all subcarrier channels share the same wideband electro-optic modulator, bandwidth allocation and data rate granularity can be digitally adjusted without changing transmitter optical configuration. In comparison to subcarrier generation which uses optical techniques, digital signal processing (DSP) in the electrical domain can provide better reliability and flexibility. Technological advances in high-speed digital-to-analog converts (DAC) and modulation formats with high spectrum efficiency in recent years have made the DSCM transmitter practical. It is also straightforward to combine DSCM technique with wavelength-domain OFDM [33, 34] to provide both high data rate throughput and flexible data rate granularity.

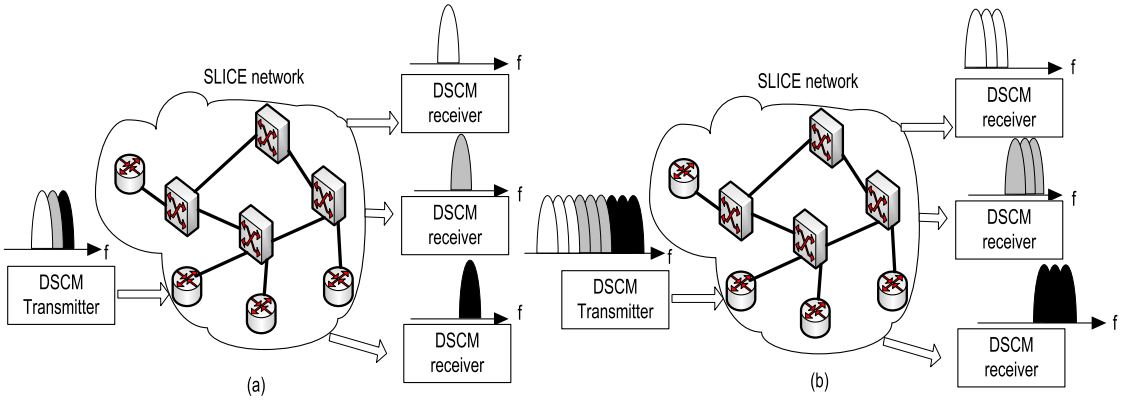

Fig. 4.1.1 SLICE transponder using DCSM

As illustrated in Fig. 4.1.1 (a), the lowest data rate that can be assigned to each end user is that assigned on each subcarrier. Whereas, multiple subcarriers may also be dedicated to an end user if higher data rate is required in SLICE (Fig. 4.1.1 (b)). In the wavelength-domain OFDM system proposed in [34], each subcarrier channel requires a standard receiver. The implementation may become expensive as the number of subcarriers increases although the data rate per channel may be low. Further, the structure is not flexible for dynamic bandwidth allocation. In the DSCM system through the use of coherent detection, DSP in the receiver allows the flexible selection of any subcarrier channels within the receiver bandwidth. Thus, these subcarriers do not have to be adjacent to each other. This will be described in detail in section 4.3.

4.2 Experimental setup

In order to experimentally investigate the DSCM-based OFDM system, a test-bed was assembled, which is schematically shown in Fig. 4.2.1. Parallel data streams are digitally modulated onto different subcarriers in a DSP, with the in-phase and quadrature components converted from a digital to analog format by an arbitrary waveform generator composed of two 22.2GS/s, 6-bits DACs. The analog voltage waveforms are amplified to drive an optical IQ modulator. The overall analog bandwidth of the transmitter is approximately 10GHz. At the output of the modulator, an erbium-doped fiber amplifier (EDFA) is used to boost the optical signal power to approximately 1dBm before it is launched into 75km standard single mode fiber for transmission. For these experiments, the same (100 KHz linewidth) laser was used as both the light source in the transmitter and the local oscillator in the coherent receiver. Local oscillator tuning with respect to the transmitted frequency was accomplished with a sinusoid modulation of a

Mach-Zehnder intensity modulator biased at the minimum transmission point. In this way, the optical carrier was suppressed and two narrow sidebands were generated in the optical spectrum at the modulation frequency as shown in inset (b) of Fig. 4.2.1. An FBG optical filter with a 3dB bandwidth of 0.08nm was used to reject one of the two sidebands (insertion (c) in Fig. 4.2.1). In the coherent intradyne receiver, the local oscillator is combined with the received optical signal in a 2x2 fiber-optic 90 degree hybrid so that the in-phase and the quadrature components from the received optical signal can be independently recovered after photodetection. The RF bandwidths are 32GHz for the photodiodes and 37GHz for the RF pre-amplifiers. The electrical signals are then sampled and recorded by a real-time oscilloscope (LeCroy 8600A), which has a 20GS/s ADC sampling rate and approximately 6 GHz of analog bandwidth. Receiver signal processing functions, including synchronization, subcarrier separation and carrier recovery, are then performed offline in a MATLAB program.

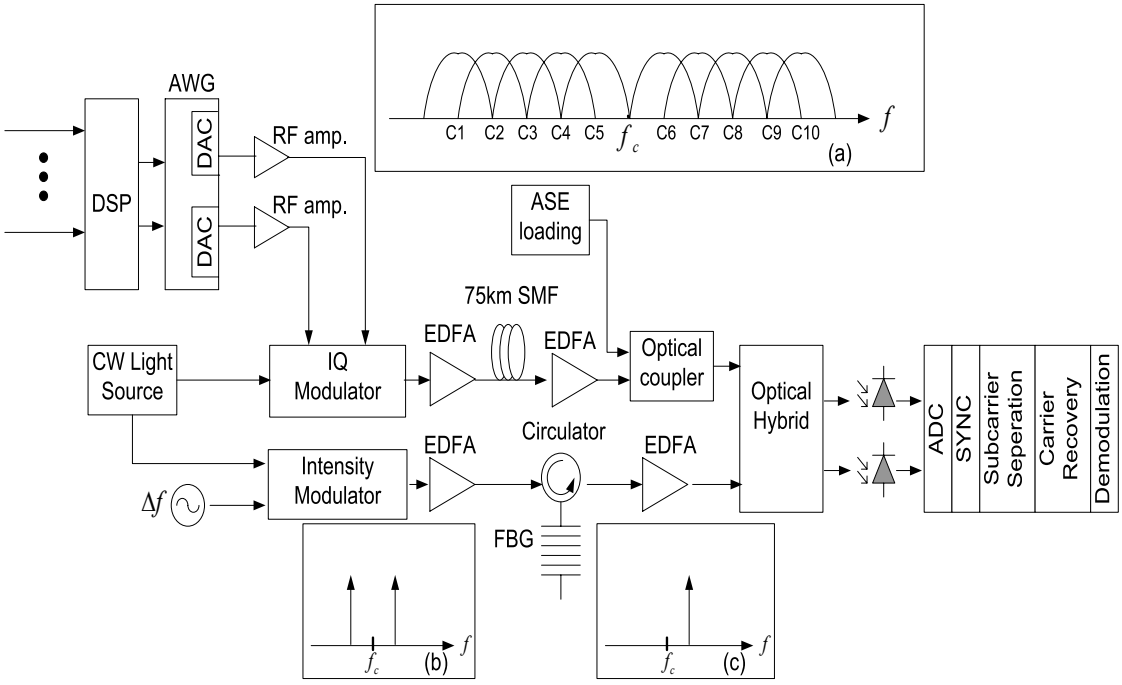

Fig. 4.2.1 System setup block diagram.

To measure the system transmission performance, an adjustable amount of ASE noise is added to the optical signal before the coherent receiver and the required optical signal to noise ratio (R-OSNR) to achieve the target bit error rate (BER) is evaluated. In fact, in an optical system with multiple subcarriers, the signal optical power is divided into subcarrier channels, and therefore the performance is determined primarily by the required optical carrier to noise ratio (R-OCNR). R-OCNR is defined as the power ratio between signal power of each subcarrier and the optical noise within 0.1nm resolution bandwidth.

For the data mapping in DSP, the first step is to generate ten parallel data streams, with each consisting of digitally modulated symbols. Each data stream is directly

uploaded onto a subcarrier frequency and multiplexed with other subcarriers to form a composite OFDM signal. The two parallel voltage waveforms used to drive the two arms of the IQ modulator can be derived based on [33]:

$$S_I(t) = \sum_{k=1}^{m} \{Q_{kL}(t) - Q_{kU}(t)\} \cos\left(2\pi \frac{\Delta f \cdot k}{2}\right) + \sum_{k=1}^{m} \{I_{kU}(t) - I_{kL}(t)\} \sin\left(2\pi \frac{\Delta f \cdot k}{2}\right) \quad (4.2.1)$$

$$S_Q(t) = \sum_{k=1}^{m} \{I_{kL}(t) + I_{kU}(t)\} \cos\left(2\pi \frac{\Delta f \cdot k}{2}\right) + \sum_{k=1}^{m} \{Q_{kU}(t) + Q_{kL}(t)\} \sin\left(2\pi \frac{\Delta f \cdot k}{2}\right) \quad (4.2.2)$$

Here, I_{KU} and Q_{KU} are in-phase and quadrature components of the k_{th} subcarrier in the upper side frequency band of the optical carrier (e.g. C6, C7, C8, C9 and C10 in inset (a) of Fig. 4.2.1). Similarly, I_{KL} and Q_{KL} are in-phase and quadrature components of the k_{th} subcarrier in the lower side frequency band of the optical carrier (e.g. C1, C2, C3, C4 and C5 in inset (a) of Fig. 4.2.1). Further, Δf represents the bandwidth of each subcarrier. In the experiment, QPSK modulation was applied with 2.22Gb/s data rate and ASK modulation with 1.11Gb/s data rate on each subcarrier. A total of 10 subcarrier channels were used, with 5 on each side of the optical carrier and the subcarrier channel spacing was 1.11GHz. The optical bandwidth efficiency was approximately 2bits/s/Hz for QPSK and 1bit/s/Hz for ASK.

In the receiver, the off-line signal processing included inter-channel crosstalk rejection, carrier recovery and time synchronization. To prepare the data for signal recovery, data of both the *I* and the *Q* channels downloaded from the oscilloscope were re-sampled to 20 samples per bit by interpolation, DC component was removed and the amplitude was re-normalized. The inter-channel crosstalk rejection was done by digital integration through a finite-impulse-response (FIR) filter with 19 taps with 50 picosecond delay time for each tap. Time synchronization was performed by pilot bits. After

synchronization, data was sliced to one sample per bit. Carrier recovery was accomplished with Viterbi-and-Viterbi phase estimation (VVPE) [35], in which samples went through an M^{th} power operation (M is the modulation level, with M = 4 for the QPSK system) to remove the modulation. The average phase estimation was obtained from an 11-tap FIR filter, and finally the phase of the samples was corrected according to the unwrapped phase estimation.

4.3 Results and discussion

a. DSCM-based OFDM optical spectra

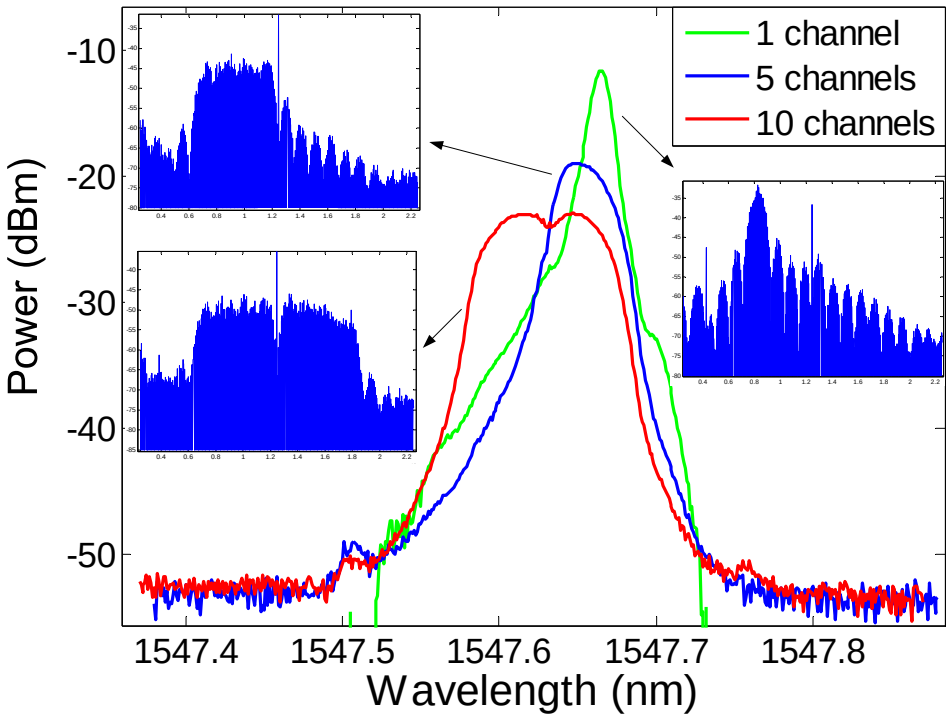

Fig. 4.3.1 Optical spectra of QPSK modulation systems measured by an optical spectrum analyzer. The insets are corresponding spectra measured by coherent detection.

One of the advantages of coherent detection is the better utilization of optical bandwidth in comparison to direct detection. In the optical transmitter, an IQ modulator allows independent data signals to be loaded onto the upper and the lower optical sidebands without interaction. The IQ modulator consists of a Mach-Zehnder interferometer with an intensity modulator in each arm, and a phase shifter between the two arms. In order to suppress the optical carrier, both of the intensity modulators should be biased at the minimum power transmission point. The phase shifter has to be biased at the quadrature point to allow the in-phase and the quadrature components to be mapped into the upper and the lower optical sidebands. Fig. 4.3.1 shows the measured optical spectra using an optical spectrum analyzer with a 0.01nm resolution bandwidth. The insets in Fig. 4.3.1 show the corresponding electrical spectra measured by a coherent heterodyne detection and an RF spectrum analyzer to provide a better spectral resolution. Fig. 4.3.1 indicates that when data is loaded onto subcarrier channels on one side of the optical carrier, the power leaked into the opposite sideband of the carrier ranges approximately from -15dB to -20dB. This single sideband (SSB) power suppression ratio determines the level of crosstalk between the two optical sidebands when both are loaded with data. Note that crosstalk between channels on the opposite sides of the optical carrier due to the non-ideal SSB power suppression has different nature compared to that between mutually orthogonal subcarrier channels. The impact of this crosstalk as illustrated in insets (a) and (b) in Fig. 4.3.1 cannot be removed by integration over 1-symbol period because the power leaked from the opposite sideband has the same spectral component as the signal channel. Precise bias control is essential both for optical carrier suppression and for minimizing of the crosstalk between two optical sidebands.

b. ASK modulation

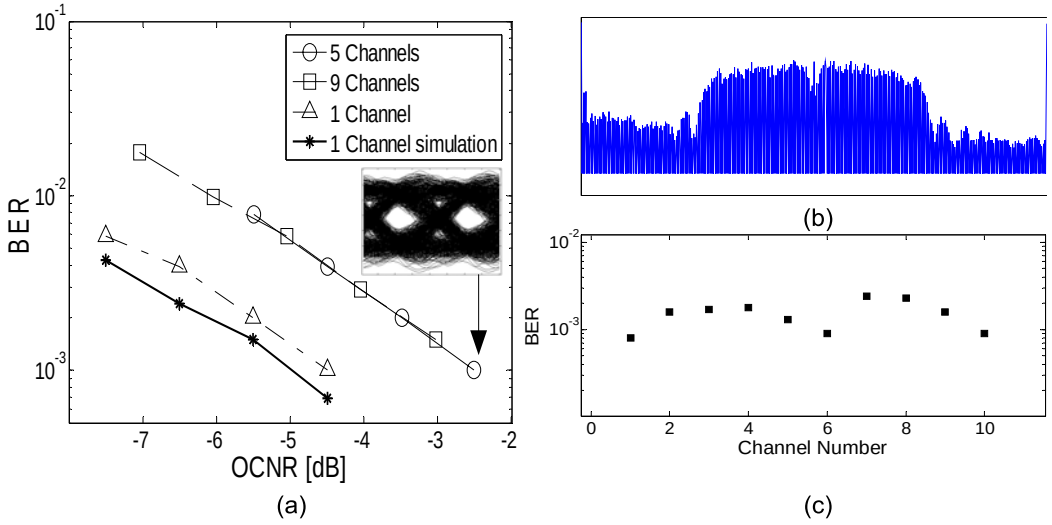

Fig. 4.3.2 (a): Measured and calculated BER as a function of OCNR in an ASK system over 75km SMF. (b): optical spectrum of the system with 10 subcarrier channels, and (c): calculated BER of all 10 channels.

ASK is the simplest modulation format in which optical phase information is not utilized. Fig. 4.3.2 (a) shows the measured BER of the 4.44GHz subcarrier channel as a function of OCNR for the systems with a single subcarrier channel (C9 in inset (a) of Fig. 4.2.1), five subcarrier channels on the upper side of the optical carrier (C6, C7, C8, C9 and C10 in inset (a) of Fig. 4.2.1), and nine subcarrier channels. If only one subcarrier channel exists at 4.44GHz, the required OCNR to achieve the BER of 10^{-3} is approximately 4.7dB. When the number of subcarrier channels increase, the integration over a bit period does not completely remove the inter-channel crosstalk, introducing degradation of the R-OCNR. In general, major contributions of crosstalk come from

adjacent subcarrier channels. As shown in Fig. 4.3.2 (a), a 5-channel system introduces approximately 2dB OCNR degradation in comparison to the single channel system. Yet, further increasing the number of channels from five to nine does not create additional R-OCNR degradation. Results of numerical simulation are also shown in Fig. 4.3.2 (a). Here, a single channel system agrees reasonably well with the measured results. Numerical simulations indicate that when all the transfer functions are ideal, inter-channel crosstalk can be made negligible through post signal processing. The 2dB extra OCNR degradation in multi-channel experimental is attributed to optical reflections and un-equalized non-uniformity transfer function within the passband. Fig. 4.3.2 (b) shows the measured heterodyne spectrum of optical signal with ten subcarrier channels. The BER for all subcarrier channels at -3dB OCNR was also calculated, with the results presented in Fig. 4.3.2 (c). These results indicate that there is no significant performance fluctuation among subcarrier channels.

Frequency spacing between adjacent subcarrier channels is an important parameter in DSCM system. Theoretical orthogonality requires the channel spacing to be equal to the symbol rate on each subcarrier channel. Fig. 4.3.3 shows the measured BER as a function of channel spacing normalized by the data rate in a system with five subcarrier channels, where the OCNR was -4.5dB. The results indicate that local minima of BER happen when the normalized channel spacing is an integer. The residual crosstalk still exists in the present experiment, even at a normalized channel spacing of one (when compared to the case of very large channel spacing). This crosstalk is attributed to the existence of noise and the limited sampling points per period, which may have impacted the accuracy of integration to minimize the crosstalk.

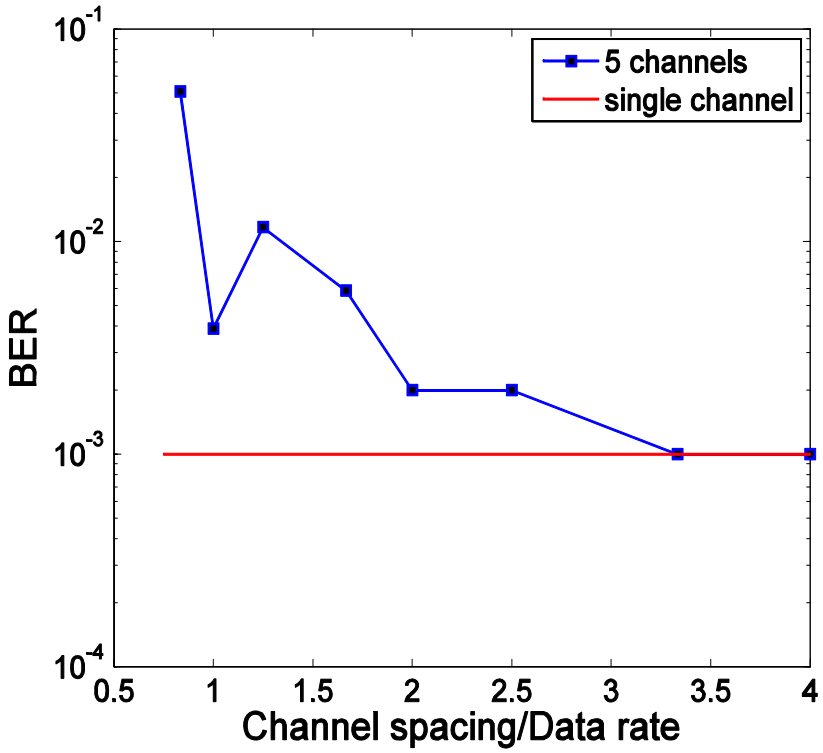

Fig. 4.3.3 Measured BER vs. normalized channel spacing in a ASK system.

c. QPSK modulation

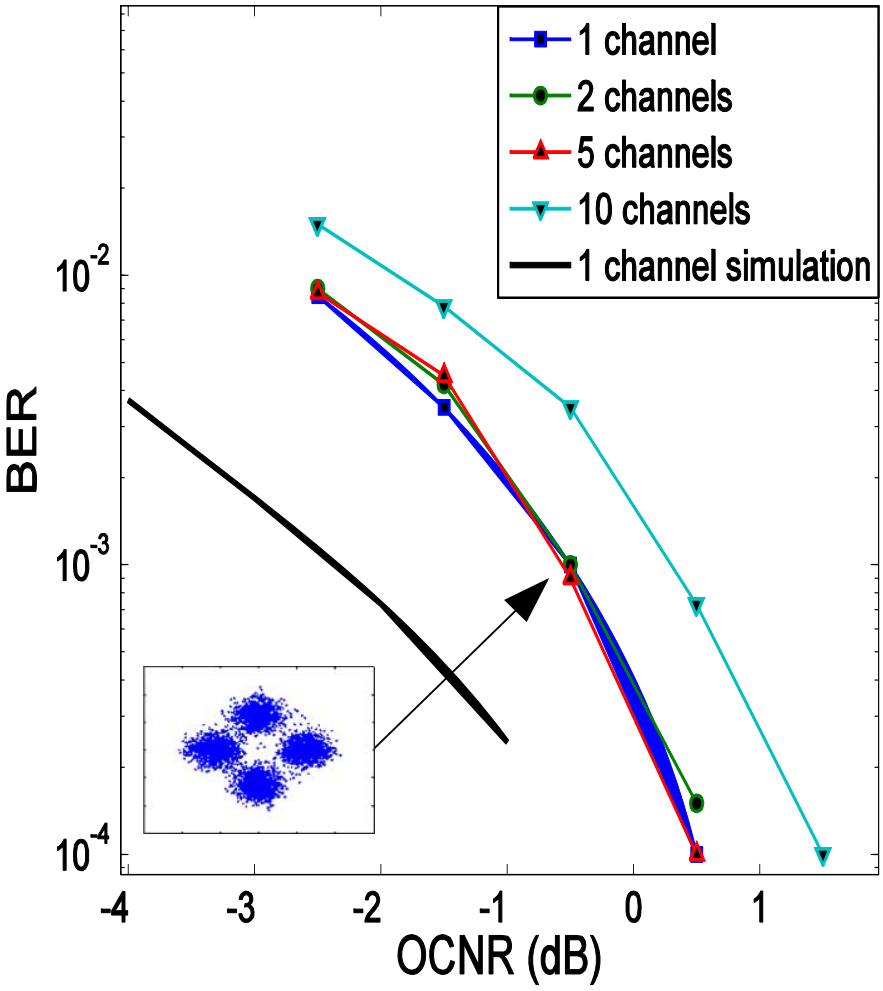

(a)

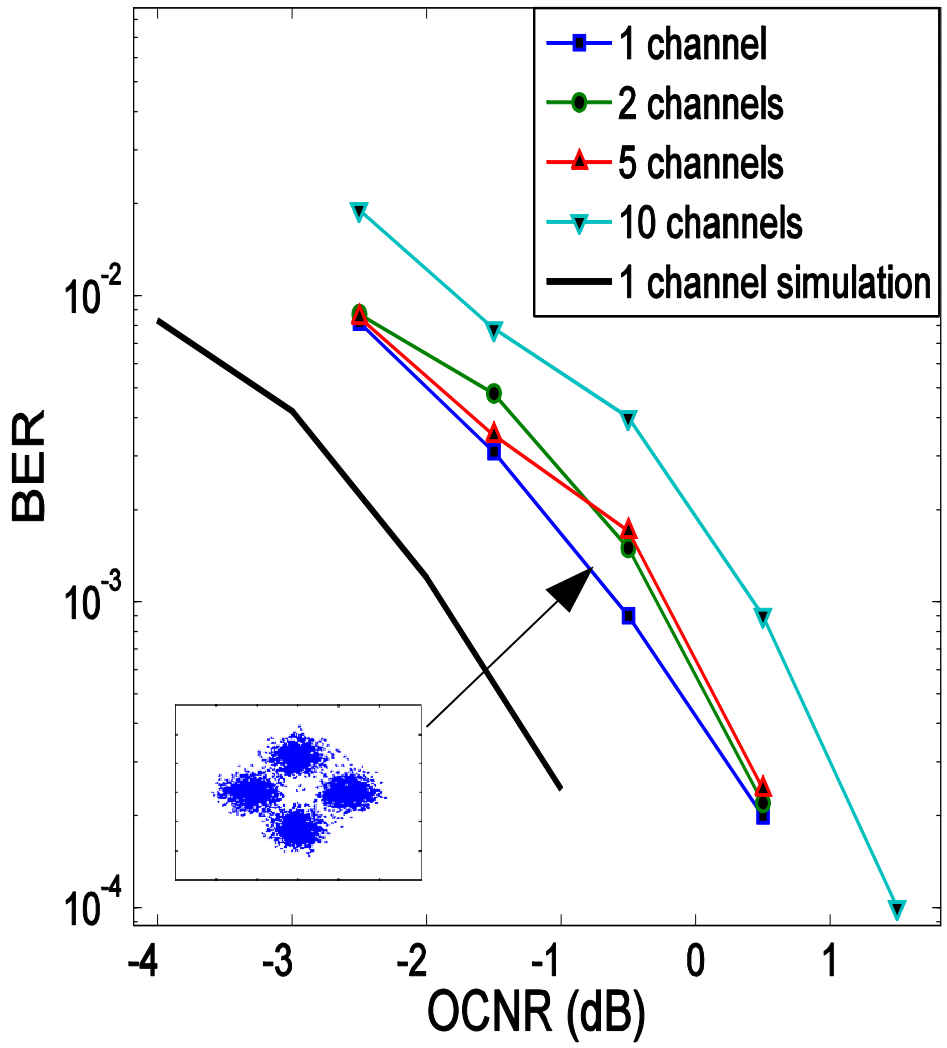

(b)

Fig. 4.3.4 Measured BER vs. OCNR in QPSK system: (a) back-to-back; (b) after 75km SMF.

The major advantage of ASK modulation discussed in the last section is its simplicity. However, the bandwidth efficiency for binary ASK modulation cannot exceed 1 bit/s/Hz. Thanks to the flexibility of DSP and IQ modulation in the transmitter, as well

as digital phase recovery in the coherent receiver, multi-level modulation can be used. This utilizes both amplitude and phase information of the optical signal. In this section, a discussion of a DSCM-based OFDM system with QPSK modulation in each subcarrier is presented. For this experiment, each subcarrier channel has 1.11GHz spectral bandwidth, but carries a 2.22Gb/s data rate, resulting in a 2 bits/s/Hz spectral efficiency.

Fig. 4.3.4 shows the measured BER vs. OCNR with different number of channels. There is a negligible increase in OCNR penalty when the number of subcarrier channels increases from one to five. Note that in these measurements, all the five subcarrier channels are located on the upper sideband with respect to the center optical carrier. When the other five subcarrier channels on the lower sideband of the spectrum are added to make the total channel count 10, there is an approximately 1 dB OCNR penalty introduced. This can be partly attributed to the imperfect sideband suppression in the single-sideband modulation process. Compare Fig. 4.3.4 (b) with Fig. 4.3.4 (a), there is negligible OCNR degradation introduced by a 75km transmission fiber. Results of numerical simulation are also shown in Fig. 4.3.4. Here, a single channel system predicted an approximately 1.5dB lower R-OCNR compared to the experiment for the BER of 10^{-3}. This discrepancy is attributed to the phase recovery algorithm used in the post processing. In the simulation the linewidth of the laser was 100 kHz, the fiber dispersion was $D = 16\times10^{-6}$ s/m^2, nonlinear index was $n_2 = 2.6\times10^{-20}$ m^2 /W, and the attenuation was $\alpha = 0.2$dB/km. The sampling rate of DAC and ADC were both 22.2GS/s, and other components were considered ideal with infinite bandwidths. A 1nm optical filter was used in front of the photodetector and a 6GHz electrical filter after the photodetector to simulate the bandwidth limit of the oscilloscope in the experiment. For a

single channel system, simulation predicted an approximately 1.5dB lower R-OCNR compared to the experiment for the BER of 10^{-3}. We attribute this discrepancy to the distortion introduced by pass band ripple in RF amplifiers, multiple reflections in the RF and optical paths, as well as time jitter in the ADC process. For an ideal system only considering local oscillator-ASE beat noise in the coherent detection, an oversimplified analytical solution can be obtained as $OSNR = Q^2 B_e/(2B_0)$ which provides the ultimate OSNR requirement for the QPSK system. For the optical bandwidth B_0 = 12.5GHz (0.1nm) used to measure OSNR and electrical bandwidth B_e = 1.11GHz (for 2.22GHz QPSK data rate), the required OSNR for Q = 3.08 (BER ≈ 10^{-3}) should be -3.75dB.

In a multi-carrier system, channel orthogonality is determined by the ratio between the symbol rate and the channel spacing. Ideally in an OFDM system with rectangular data pulses, digital integration over one symbol period is able to remove the inter-channel crosstalk. However, if the bandwidth of the system is not much wider than that of a subcarrier, crosstalk cancelation may not be complete, depending on the actual shape of the pulses. Practically in high data rate wavelength-domain OFDM, the component bandwidth may only be comparable to the symbol rate per subcarrier, and the residual inter-channel crosstalk may be significant.

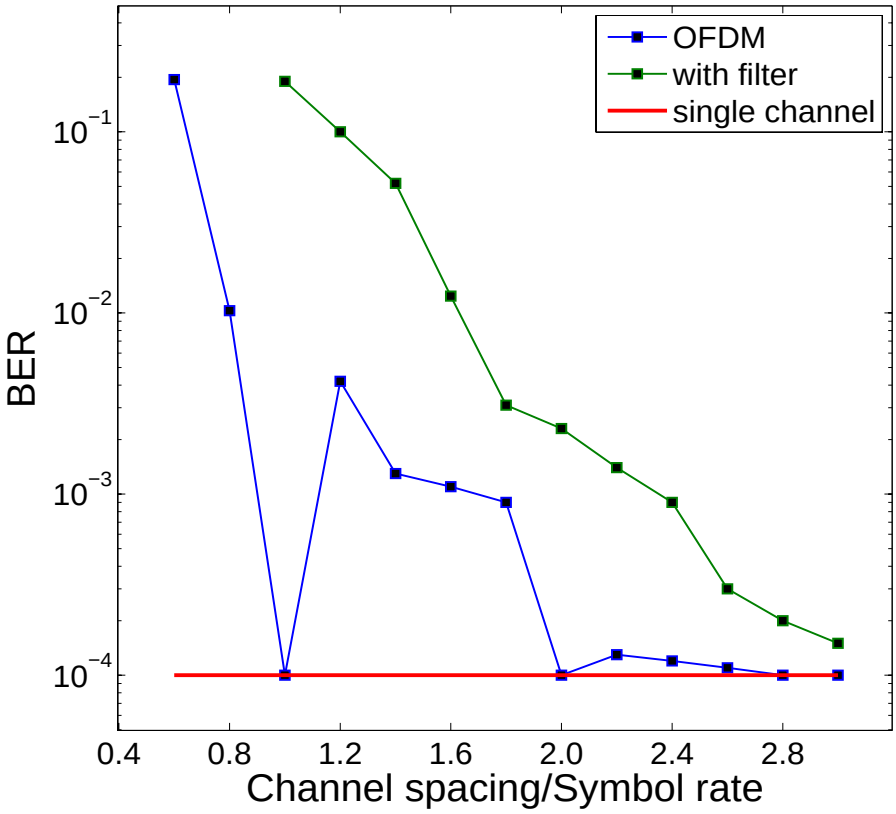

Fig. 4.3.5 Measured BER vs. normalized channel spacing in QPSK system.

To demonstrate the orthogonality between adjacent subcarrier channels and the cancellation of inter-channel crosstalk through signal processing, Fig. 4.3.5 shows the measured BER as a function of normalized channel spacing between adjacent subcarrier channels. In this experiment, two subcarrier channels were transmitted over 75km standard single-mode fiber (SMF), and the BER was measured with 1dB OCNR at the receiver. In this DSCM system, the receiver bandwidth is approximately 6GHz, which is much wider than that of each subcarrier channel, and therefore BER degradation can be eliminated through digital integration when the channel spacing is integer multiple of the

symbol rate. On the other hand, if a simple 5th order Bessel filter is used with 1.1GHz (3dB) electrical bandwidth, the crosstalk monotonically increases with the decrease of the channel spacing, and the crosstalk can be significant when the normalized channel spacing is lower than 2.5. This is similar to the performance observed in an analog SCM optical system [25].

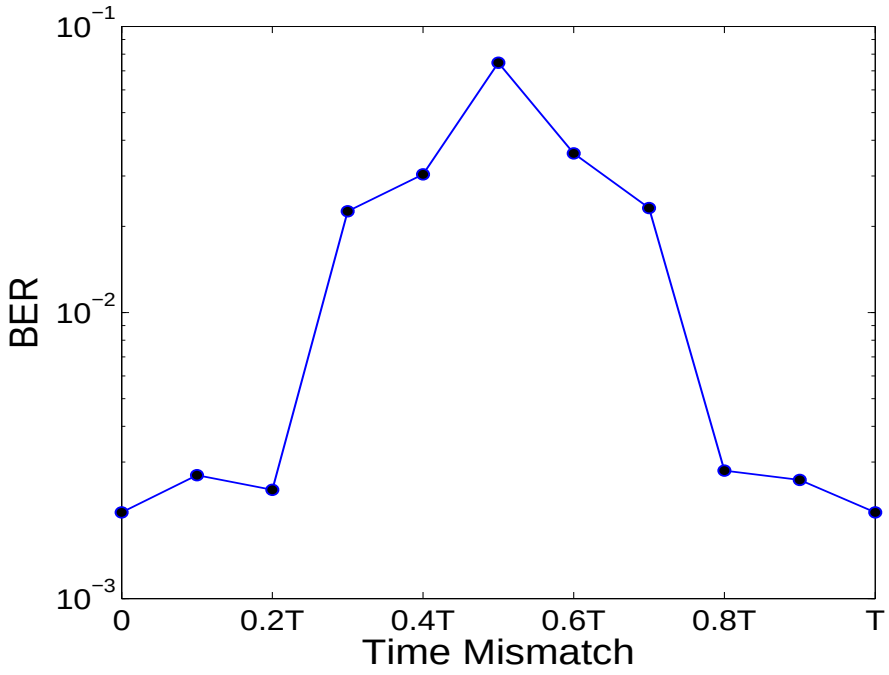

Fig. 4.3.6 Measured BER vs. time mismatch.

It is important to note that crosstalk cancellation based on orthogonality and digital integration in the receiver requires time synchronization between digital symbols carried by adjacent SCM channels. Although phase synchronization between subcarriers may not affect system performance, misalignment between symbols carried by these channels may result in incomplete cancellation of the crosstalk. Time mismatch tolerance

is an important performance measure of DSCM-OFDM systems, especially if adjacent subcarrier channels originate from different optical transmitters in a distributed optical network. Fig. 4.3.6 shows the measured BER as the function of the normalized time misalignment, where T stands for the symbol period. Since the largest crosstalk comes from adjacent channels, ch-8 and ch-9 (as indicated in inset (a) of Fig. 4.2.1) were used in this measurement, in which signal was transmitted over 75km SMF and the receiver OCNR was 1dB. Fig. 4.3.6 indicates that the DSCM-QPSK system can tolerate the time mismatch of up to ±20% of symbol period without significant BER degradation. In a dynamic optical network, bit walk-off between adjacent subcarrier channels caused by fiber chromatic dispersion may change with the fiber length between the transmitter and the receiver. In our experiment with 1.11 Gbaud/s symbol rate on each subcarrier, the corresponding time misalignment tolerance is about ±200ps, equivalent to the differential delay of approximately 1500km of standard single mode fiber when the subcarrier channel spacing is 1.11GHz. For systems with longer fibers, digital compensation in the receiver can be applied to minimize the differential delay between channels.

d. Flexible data rate

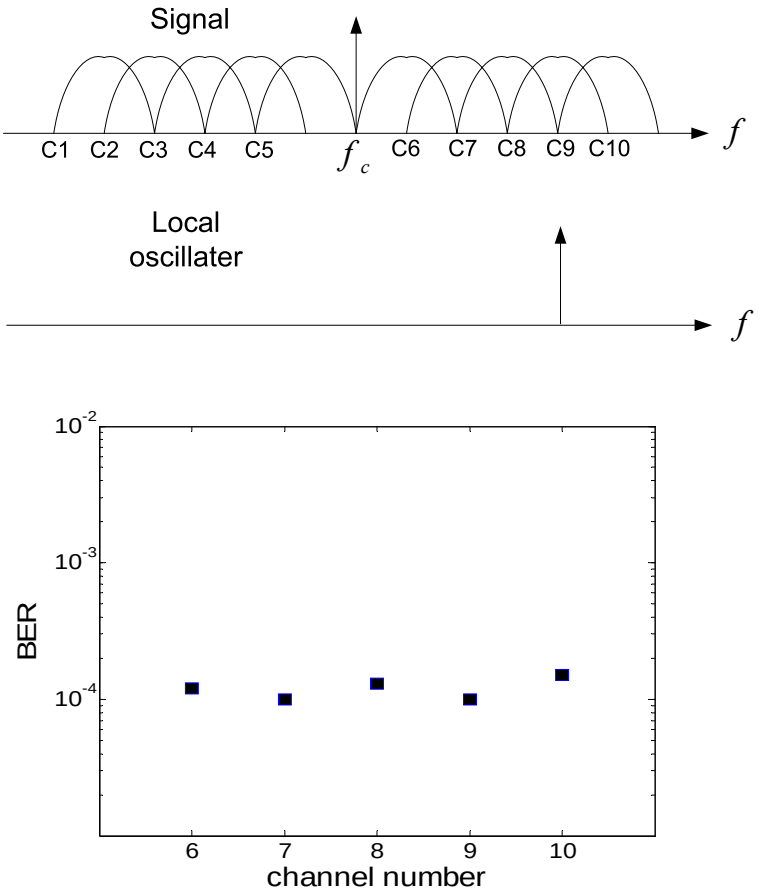

(a)

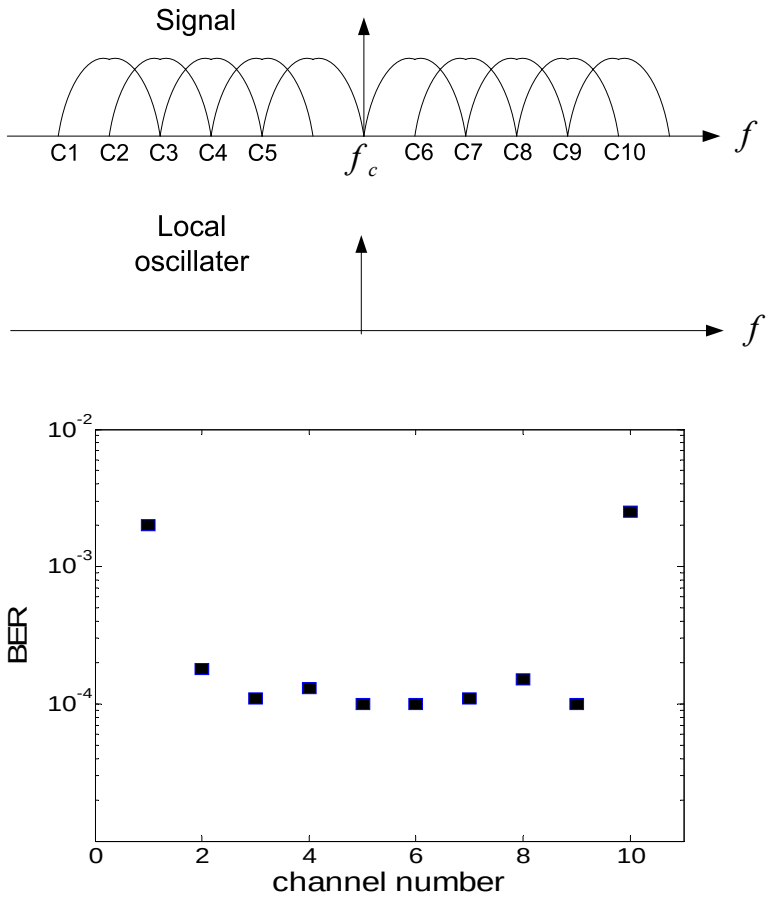

(b)

Fig. 4.3.7 BER measured as a function of the channel index for (a) when the local oscillator was tuned to channel 9, and (b) when the local oscillator was tuned to the center optical carrier.

As discussed in section 4.1, when a higher data rate is required by an end user, multiple subcarriers can be delivered to the same end user without changing the network architecture. The end user then tunes the local oscillator to one of the subcarrier frequencies in the OFDM spectrum, and coherent IQ detection translates the optical spectrum to the electrical domain with the selected subcarrier channel in the center. Next,

a selected number of neighboring subcarrier channels within the receiver bandwidth can be detected and recovered by digital heterodyne detection in the receiver DSP. In order to test this scheme, the BER of selected channels in a ten channel QPSK system at 1.5 dB OCNR was measured. In Fig. 4.3.7 (a), the wavelength of the local oscillator is set at subcarrier channel C9, and the BERs of five adjacent channels are measured, indicating no significant performance variation among channels. The local oscillator wavelength was also set to the center of the signal optical carrier, as shown in Fig. 4.3.7 (b), in an attempt to detect all the ten subcarrier channels. The results show reasonably uniform BER performance except for the two outmost channels C1 and C10. The increased BER in these two channels is due to the bandwidth limit of the real-time oscilloscope, which is 6GHz. Additionally, potions of the spectra of these two channels are already outside of this receiver bandwidth.

e. Fiber nonlinearity

In addition to linear degradation effects discussed above, OCNR penalty caused by fiber nonlinearity is another important parameter to be investigated in optical transport systems. Fig.7 shows the calculated OCNR penalty as the function of the optical power launched to the fiber. The simulation parameters are the same as those used to obtain Fig. 4. The simulation exams a QPSK modulated DSCM system with a fixed 20Gb/s total data rate, but partitioned into different number of subcarrier channels. The total length of standard single mode fiber was 450km divided into 6 amplified spans. If the system only has two subcarrier channels (10Gb/s per channel), there is minimum impact due to four wave mixing (FWM) and therefore OCNR penalty is relatively small. Increasing the number of subcarrier channels moderately increases the penalty due to fiber nonlinearity. But this

degradation ceases to increase when the number of channels is high enough (at the same time the data rate per channel becomes low). There is no significant increase from 6 to 10 subcarrier channels as shown in Fig.7. Therefore, from nonlinearity point of view, there is no limitation on the number of subcarrier channels that can be used in the DCSM implementation.

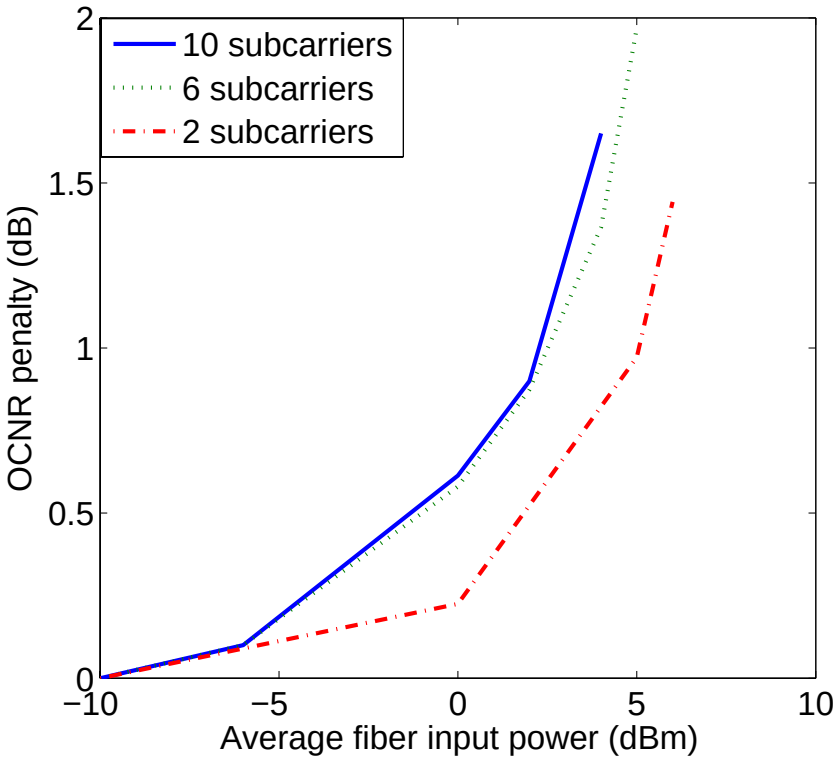

Fig. 4.3.8 OCNR penalty as a function of average fiber input power

4.4 Conclusion

In this chapter presented a DSCM-based OFDM optical system, which provides scalable bandwidth allocation. In a DSCM-based OFDM, because subcarrier channels are digitally generated in electrical domain, high degree flexibility in data rate granularity

and dynamic provisioning of subcarrier channels in both data rate and power levels are allowed. Transmission performance with both ASK modulation and QPSK modulation using coherent detection were investigated in detail. One or multiple subcarrier channels from the optical spectrum can be recovered either individually or as a group as desired on the sub-wavelength level. Orthogonality and cancelation of crosstalk rely on the precise setting of channel spacing and the temporal synchronization of data bits between subcarrier channels. Furthermore, clock synchronization has to be within ±20% of the symbol period to avoid significant crosstalk between subcarrier channels.

5. Nyquist-WDM system

In chapter 3 and chapter 4, two OFDM systems were discussed: an FFT-based OFDM system, and a DCSM-based OFDM system. In these two systems, not only were the modulation formats different, but they also utilized different detection methods. However, both of these two systems require bit time synchronization between adjacent subcarrier channels. This requirement is essential for the elimination of crosstalk between subcarrier channels, but it imposes a restriction in many optical network applications where symbol bits of subcarrier channels may not be mutually synchronized. Nyquist-WDM discussed in this chapter can potentially solve this problem.

From application point of view, the benefit of coherent detection was obvious because a coherent receiver is much more flexible in channel selecting and dynamic bandwidth allocation. Also considering its compatibility with advanced multilevel and phase modulation formats, coherent detection has showed its importance in the next generation fiber-optic transmission. Therefore in this chapter, coherent detection will be used with Nyquist-WDM system.

5.1 Principle of operation

OFDM has been extensively studied in the last few years [10, 36]. In this research, the frequency spacing between adjacent subcarrier channels is equal to the data symbol rate and therefore, no spectral guard-band between them is required. This research is in line with the discussion of two OFDM systems in chapters 3 and 4. If the electrical bandwidth in the receiver is much wider than the symbol rate on each subcarrier, the crosstalk between the two can be removed by digital integration over a symbol period. Since the channel orthogonality of OFDM relies on the ideally rectangular signal

waveforms, crosstalk may become significant if the receiver bandwidth is not wide enough. OFDM systems also require time synchronization between data symbols carried by adjacent subcarrier channels. Another high spectral efficiency multicarrier system, known as Nyquist-WDM [37], uses Nyquist spectral shaping to eliminate spectral overlap between adjacent channels without introducing ISI within each channel. Unlike OFDM, Nyquist-WDM does not rely on orthogonality between channels and therefore, symbol synchronization is not required. Furthermore, data rates of subcarrier channels do not have to be uniform; this flexibility may be beneficial in optical networks with mixed data rates. Performance comparisons between OFDM and Nyquist-WDM have been reported primarily through numerical simulations [37, 38]. Experimental comparisons require fairly precise control of filter transfer functions for spectral shaping, which is not easily realizable in the optical domain. This chapter will describe an experimental comparison between the performances of OFDM and Nyquist-WDM. In this work, optical subcarrier channels were generated using digital electronics, allowing strong control over the implemented spectral shaping filters.

5.2 Experimental setup

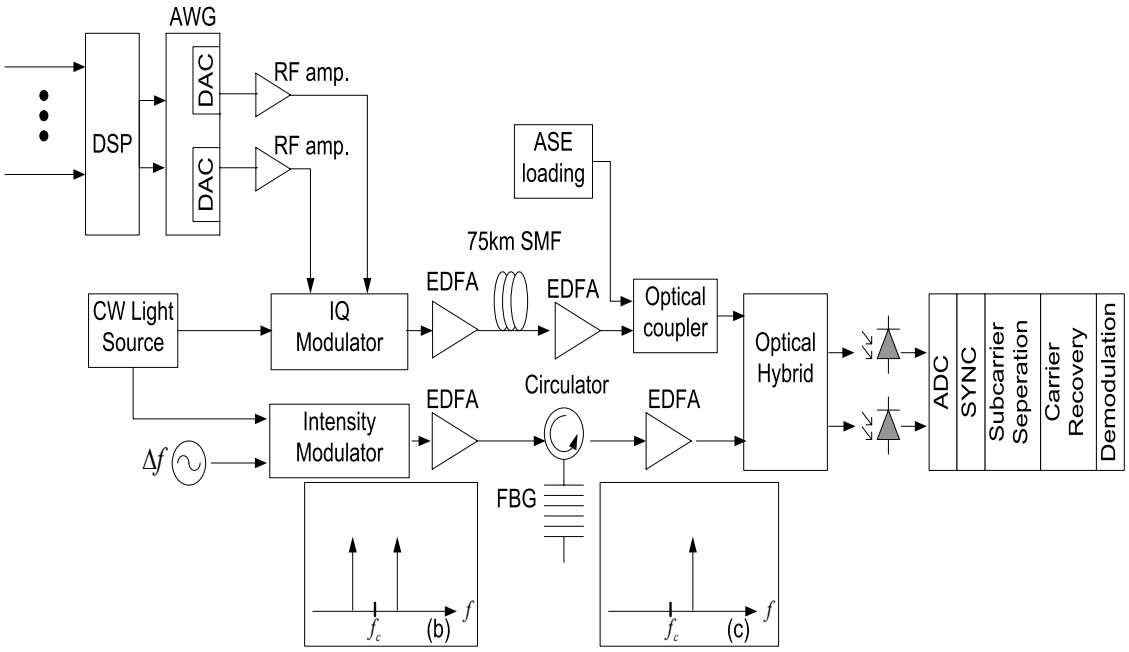

Fig. 5.2.1 Block diagram of experimental system

Fig. 5.2.1 shows the block diagram of the experimental test-bed. Parallel data streams are digitally modulated onto different subcarriers in a DSP. It is then possible for the in-phase and quadrature components to be converted from digital to analog format by an arbitrary waveform generator composed of two 22.2GS/s, 6-bits DACs. Both OFDM and Nyquist-WDM multiplexing formats can be realized through the arbitrary waveform generator. Frequency spacing between subcarrier channels, as well as the spectral shapes, can be easily defined and modified. The analog voltage waveforms are amplified to drive an optical IQ modulator. The overall analog bandwidth of the transmitter is approximately 10GHz. At the output of the modulator, an erbium-doped fiber amplifier (EDFA) is used to boost the optical signal power to approximately 1dBm before it is

launched into 75km standard single mode fiber (SMF) for transmission. For these experiments the same (100 KHz linewidth) laser was used as both the light source in the transmitter and the local oscillator in the coherent receiver. Local oscillator tuning with respect to the transmitted frequency was accomplished with a sinusoid modulation of a Mach-Zehnder intensity modulator biased at the minimum transmission point. In this way, the optical carrier was suppressed and two narrow sidebands were generated in the optical spectrum at the modulation frequency as shown in inset (b) of Fig. 5.2.1.

An FBG optical filter with a 3dB bandwidth of 0.08nm was used to reject one of the two sidebands (insertion (c) in Fig. 5.2.1) [12]. In the coherent intradyne receiver, the local oscillator is combined with the received optical signal in a 2x2 fiber-optic 90º hybrid so that the in-phase and the quadrature components from the received optical signal can be independently recovered after photodetection. In the receiver, the photodiodes have 32GHz RF bandwidth and the following RF pre-amplifiers have 37GHz bandwidth. The electrical signals are then sampled and recorded by a real-time oscilloscope (LeCroy 8600A), which has a 20GS/s ADC sampling rate and an approximate 6 GHz analog bandwidth. Receiver signal processing functions, including synchronization, subcarrier separation and carrier recovery, are performed offline in a MATLAB program. In order to evaluate transmission performance in terms of the BER and the required OSNR, optical noise loading is used at the receiver with an adjustable optical noise source.

5.3 Results and discussion

Fig. 5.3.1 shows the measured BER versus optical carrier to noise ratio (OCNR) for the system using Nyquist-WDM multiplexing format. In this system, each subcarrier

channel carries 2.22Gb/s QPSK data. The spectrum was pre-shaped by a Nyquist filter with the -6dB bandwidth of 1GHz and a roll-off rate of 0.1. An ideal brick-wall filter with 1GHz bandwidth is used after photodetector at the receiver for channel selection. The frequency spacing between adjacent subcarrier channels is 1.11GHz, so that the bandwidth efficiency is 2bits/Hz. There is also approximately 10% spectral overlap between adjacent subcarrier channels, which introduces noticeable crosstalk when multiple subcarrier channels are used. This crosstalk can be removed if frequency spacing between subcarrier channels is increased to 1.22 GHz so that there are no spectral overlaps, but only with 10% reduced bandwidth efficiency. In this system, because multiple subcarrier channels are generated through the same electro-optic modulator, intermodulation may be introduced through the nonlinear transfer function of the modulator, especially when the modulation index is high. Therefore, moderate OCNR degradation is observed when the number of subcarrier channel is high.

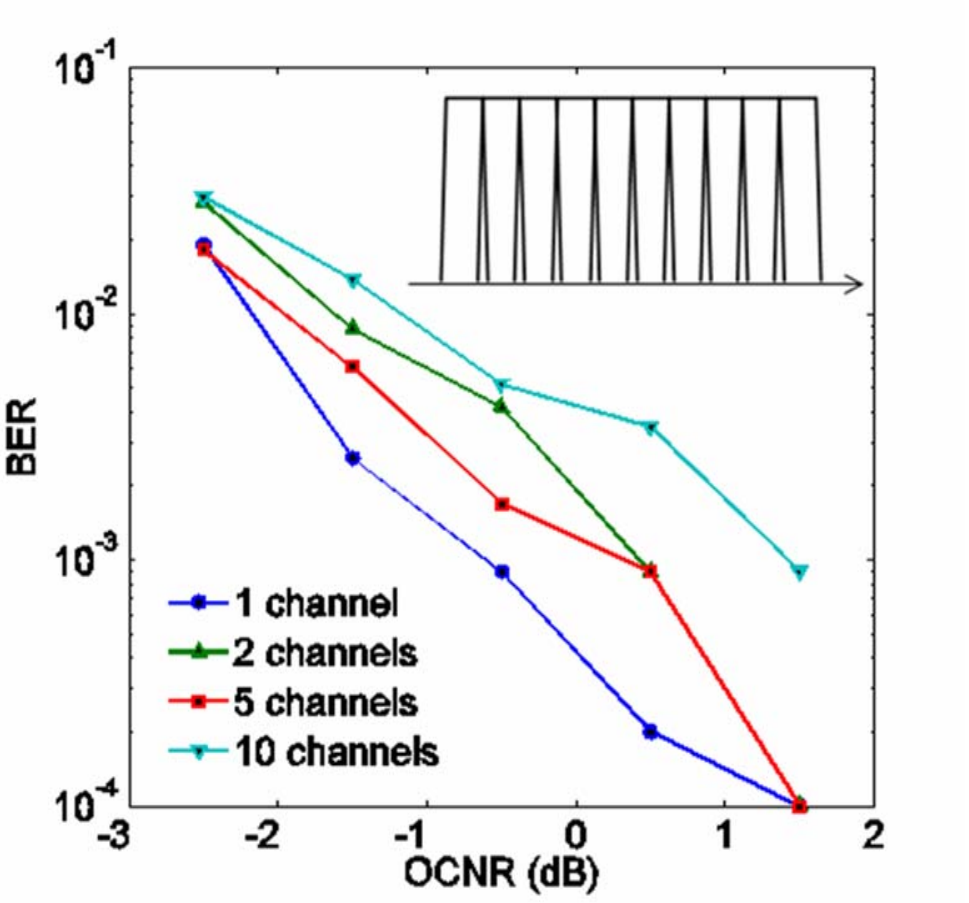

Fig. 5.3.1 Measured BER vs. OCNR for Nyquist-WDM

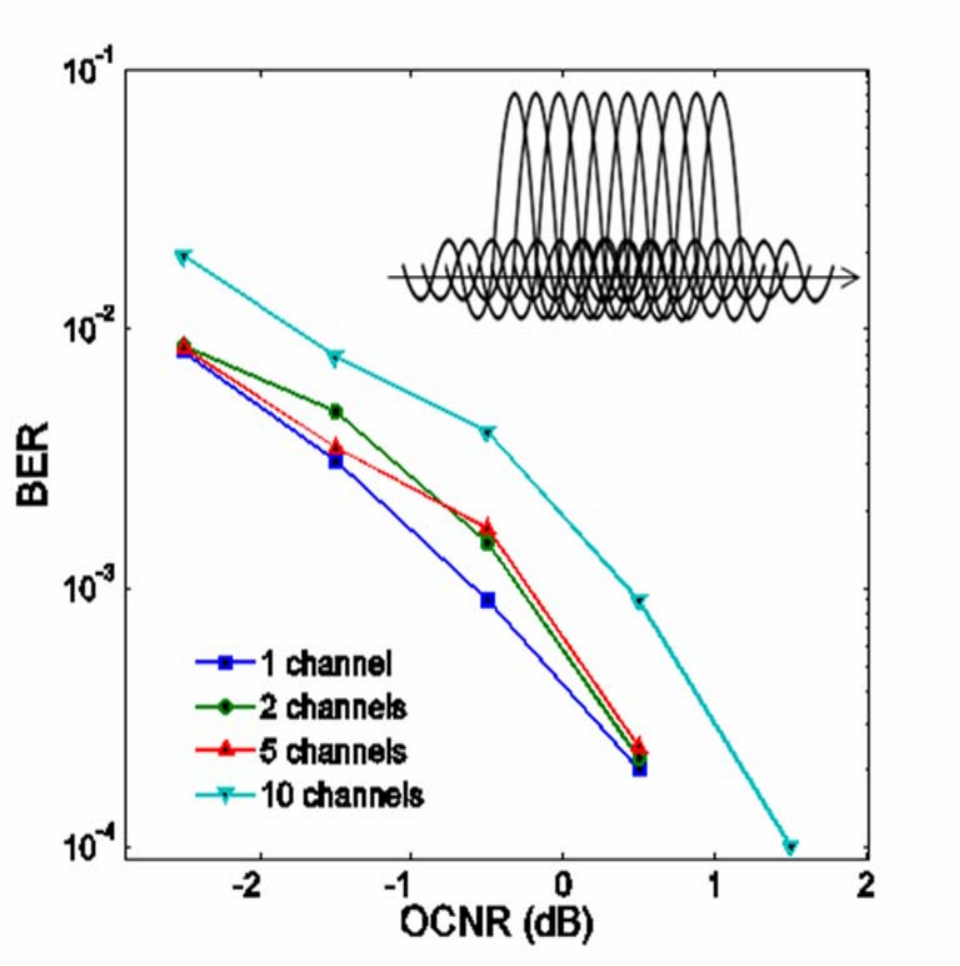

Fig. 5.3.2 Measured BER vs. OCNR for CO-OFDM

The same experimental setup can also be configured to OFDM format. Fig. 5.3.2 shows the measured BER versus OCNR characteristics of the coherent OFDM similar to that discussed in Chapter 4, also with 2.22 Gb/s QPSK data on each subcarrier channel with 1.11 GHz channel spacing. In this case, the receiver electrical bandwidth is 6GHz, and a digital integration is performed over a symbol period to minimize inter-channel crosstalk. Fig. 5.3.1 and Fig. 5.3.2 show comparable system performances of the two multiplexing formats for the same data rate and subcarrier channel spacing.

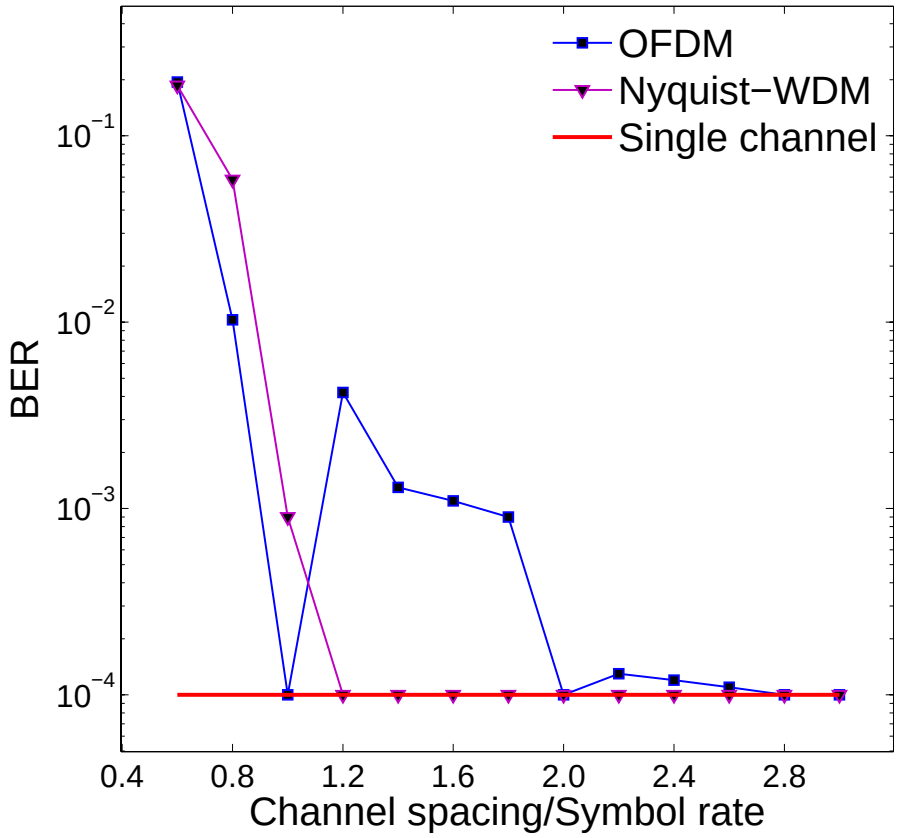

Fig. 5.3.3 Measured BER vs. normalized channel spacing

For multi-carrier systems, frequency spacing between adjacent carriers is an important parameter determining bandwidth efficiency and the level of crosstalk. Fig. 5.3.3 shows the measured BER as a function of normalized channel spacing between adjacent subcarriers. In this experiment, two subcarrier channels each carrying 2.22 Gb/s QPSK data were transmitted over 75km SMF. The BER was then measured with 1dB OCNR at the receiver. For the OFDM system, the crosstalk can be minimized through digital integration over one symbol period, only when the channel spacing is an integer multiple of the symbol rat. Whereas for the Nyquist-WDM system using an ideal Nyquist

filter with 1.11 GHz bandwidth and 0.1 roll-off rate, the crosstalk can be eliminated when the normalized channel spacing is larger than 1.1 since there is no spectral overlap.

While an OFDM system requires symbol time synchronization between data carried by adjacent channels, Nyquist-WDM does not require this synchronization. Fig. 5.3.4 shows the measured BER versus symbol time mismatch between two adjacent subcarrier channels using the same parameters as in Fig. 5.3.4, except for fixed channel spacing at the symbol rate. For OFDM, BER degradation becomes significant when the time mismatch is beyond ±20% of symbol period, while for Nyquist-WDM, BER is independent of the relative symbol phase between channels. This could be a distinct advantage for the application in distributed optical networks where channel synchronization may not be maintained.

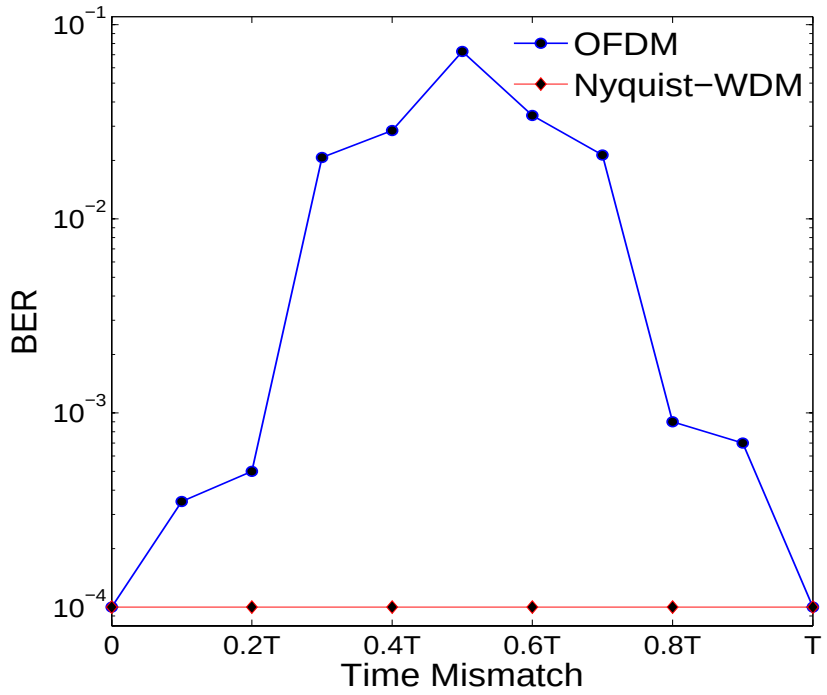

Fig. 5.3.4 Measured BER vs. normalized symbol time mismatch

5.4 Conclusion

This chapter experimentally compared the performances of Nyquist-WDM and DSCM-based OFDM. Results indicate that these two multiplexing schemes have comparable required-OCNR, as well as the ability to cancel crosstalk. However, the Nyquist-WDM system requires less electrical bandwidth at the receiver. Further, it does not require symbol time synchronization between adjacent channels. This property is useful in dynamic multi-carrier optical networks and supports subcarrier channels with mixed data rates.

6. Conclusion and future work

Since the advent of the "Information Age" the capacity of communication systems has been boosted dramatically. High capacity inevitably requires wide bandwidth, and therefore, the previously unlimited bandwidth in optical fiber is challenged. One of the requirements for the next generation optical transmission system is high spectral efficiency. Specifically, spectral efficiency of 1 baud/s/Hz will be a key feature of the next generation fiber-optic transmission systems.

The goal of this dissertation is to systemically investigate the performance of optical multicarrier systems and develop practical design guidelines according to the required system functions. In order to compare different designs, a theoretical and experimental investigation was performed of the following systems: an FFT-based OFDM system with direct detection, a DSCM-based OFDM system with coherent detection and a Nyquist-WDM system with coherent detection. From the three optical multicarrier systems demonstrated in this dissertation, results indicated the following conclusions:

- FFT-based OFDM scheme is suitable for long distance, point-to-point and relatively stable transmission. It has extremely low data rate on each subcarrier channel, which can be highly tolerable to fiber transmission impairments. But as for dynamic networks with frequent channel add/drop, the frame based multiplexing scheme may not be the best choice.
- In DSCM-based OFDM, relatively small number of subcarrier channels are modulated separately and multiplexed in digital domain. The receiver has the flexibility to dynamically select different number of subcarrier channels in the

detection without the need to change system configuration. The bandwidth requirement in the receiver can be reduced if only a subset of subcarrier channels is to be detected instead of the entire OFDM frame. Since the data rate on each subcarrier is higher than FFT-based OFDM, digital compensation will be needed when the transmission distance is long. And channels still need to be time synchronized for the crosstalk cancellation in DSCM-based OFDM.

- Nyquist-WDM system uses pulse shaping filter to limit the spectrum of the modulated signal to achieving high spectral efficiency, so there is no spectral overlap between adjacent channels, thus time synchronization is not required. The impact of pulse shaping filters on multilevel modulation formats still needs future investigation.

- Both MZM and IQ modulator can be used in optical multicarrier systems. While an IQ modulator is able to provide access to all 4 quadrants of the I-Q plane and flexible control of signal optical phase, a MZM only provides access to two quadrants in the I-Q plane (real part of the symbol has to be positive). IQ modulator is more appropriate for applications in the modern optical systems involving complex modulation. However, it is structurally more complex, high cost, and requiring more complicated bias controls and stabilization procedure.

- Coherent detection is compatible for multilevel modulation formats. With coherent detection, the receiver can easily select different number of subcarrier channels in the detection. As the price of tunable laser goes down, the phase noise reduces, and the improvements on carrier recovery algorithm, coherent detection will be widely adopted in the next generation fiber-optic transmission.

We have systematically investigated optical multicarrier systems for next generation fiber-optic transmission systems. However, there is still plenty of room for improvements. Several possible future improvement ideas are listed as follows:

- The compatibility between high spectral efficiency multicarrier system and multilevel modulation formats still need to be investigated. Some work has been done in OFDM systems, but for Nyquist-WDM system, modulation formats with more than 2bits per symbol has not been sufficiently studied.
- The performance of optical multicarrier system in long-haul transmission still needs to be tested.
- The work in this dissertation is concentrated in the point-to-point transmission. The application of optical multicarrier systems in network environment will need more research on switches and routers, the closely spaced subcarriers will place more requirements on the cross connect functionalities.

References

[1] R. Hui and M. O'Sullivan, *Fiber Optic Measurement Techniques*: Elsevier Academic Press, 2009.

[2] G. P. Agrawal, *FIBER-OPTIC COMMUNICATION SYSTEMS*: John Wiley & Sons, Inc., New York., 2002.

[3] X. Zhou, J. Yu, M.-F. Huang, Y. Shao, T. Wang, L. Nelson, P. Magill, M. Birk, P. I. Borel, D. W. Peckham, and R. Lingle, "64-Tb/s (640×107-Gb/s) PDM-36QAM transmission over 320km using both pre- and post-transmission digital equalization " presented at the (OFC/NFOEC) 2010.

[4] G. Bosco, A. Carena, V. Curri, P. Poggiolini, and F. Forghieri, "Performance Limites of Nyquist-WDM and CO-OFDM in High-Speed PM-QPSK Systems," *IEEE Photon. Technol. Lett.,* vol. 22, pp. 1129-1131, AUGUST 1, 2010 2010.

[5] G. Gavioli, E. Torrengo, G. Bosco, A. Carena, V. Curri, V. Miot, P. Poggiolini, M. Belmonte, F. Forghieri, C. Muzio, S. Piciaccia, A. Brinciotti, A. L. Porta, C. Lezzi, S. Savory, and S. Abrate, "Investigation of the impact of ultra-narrow carrier spacing on the transmission of a 10-carrier 1Tb/s superchannel " presented at the OSA/OFC/NFOEC, 2010.

[6] J. Zhao and A. Ellis, "Electronic Impairment Mitigation in Optically Multiplexed Multicarrier Systems " *Journal of Lightwave Technology,* vol. 29, pp. 278-290, FABRUARY 1 2011.

[7] A. Goldsmith, *Wireless Communication*: Cambridge Univerisity Press, 2005.

[8] "Fiber Types in Gigabit Optical Communications," Cisco Systems, Inc.2008.

[9] H. Nyquist, "Certain topics in telegraph transmission theory (Reprinted from Transactions of the A. I. E. E., February, pg 617-644, 1928)," *Proceedings of the Ieee,* vol. 90, pp. 280-305, Feb 2002.

[10] W. Shieh, H. Bao, and Y. Tang, "Coherent optical OFDM: theory and design," *Optics Express,* vol. 16, pp. 841-859, 2008.

[11] Y. R. Ma, Q. Yang, Y. Tang, S. M. Chen, and W. Shieh, "1-Tb/s single-channel coherent optical OFDM transmission over 600-km SSMF fiber with subwavelength bandwidth access," *Optics Express,* vol. 17, pp. 9421-9427, May 2009.

[12] Y. Y. Zhang, M. O'Sullivan, and R. Q. Hui, "Digital subcarrier multiplexing for flexible spectral allocation in optical transport network," *Optics Express,* vol. 19, pp. 21880-21889, Oct 2011.

[13] F. C. G. Gunning, S. K. Ibrahim, P. Frascella, P. Gunning, and A. D. Ellis, "High Symbol Rate OFDM Transmission Technologies," presented at the OSA/OFC/NFOFC, 2010.

[14] R. Hui, "High-speed optical transmission using sub-carrier multiplexing," in *IASTED*, Banff, Canada, July 2002, pp. 707-712.

[15] M. Tomizawa, J. Yamawaku, Y. Takigawa, M. Koga, Y. Miyamoto, T. Morioka, and K. Hagimoto, "Terabit LAN with optical virtual concatenation for Grid applications with super-computers," in *Optical Fiber Communication Conference (OFC)*, Anaheim, California, 2005, p. OThG6.

[16] P. J. Winzer and R. J. Essiambre, "Advanced optical modulation formats," *Proceedings of the Ieee,* vol. 94, pp. 952-985, May 2006.

[17] A. J. Lowery and J. Armstrong, "Orthogonal-frequency-division multiplexing for dispersion compensation of long-haul optical systems," *Optics Express,* vol. 14, pp. 2079-2084, Mar 2006.

[18] M. Schuster, S. Randel, C. A. Bunge, S. C. J. Lee, F. Breyer, B. Spinnler, and K. Petermann, "Spectrally efficient compatible single-sideband modulation for OFDM transmission with direct detection," *Ieee Photonics Technology Letters,* vol. 20, pp. 670-672, 2008.

[19] W. R. Peng, X. X. Wu, K. M. Feng, V. R. Arbab, B. Shamee, J. Y. Yang, L. C. Christen, A. E. Willner, and S. E. Chi, "Spectrally efficient direct-detected OFDM transmission employing an iterative estimation and cancellation technique," *Optics Express,* vol. 17, pp. 9099-9111, 2009.

[20] B. J. C. Schmidt, A. J. Lowery, and L. B. Du, "Low Sample Rate Transmitter for Direct-Detection Optical OFDM," presented at the Optical Fiber Communication Conference (OFC) San Diego, CA, 2009.

[21] Z. B. Xu, M. O'Sullivan, and R. Q. Hui, "OFDM system implementation using compatible SSB modulation with a dual-electrode MZM," *Optics Letters,* vol. 35, pp. 1221-1223, 2010.

[22] J. McNicol, M. O'Sullivan, K. Roberts, A. Comeau, D. McGhan, and L. Strawczynski, "Electrical Domain Compensation of Optical Dispersion," presented at the Optical Fiber Communication Conference (OFC), Anaheim, CA, 2005.

[23] K. Roberts, C. Li, L. Strawczynski, M. O'Sullivan, and I. Hardcastle, "Electronic pre-compensation of optical nonlinearity," *Ieee Photonics Technology Letters,* vol. 18, pp. 403-405, 2006.

[24] J. George Cyril Clark and J. B. Cain, *Error-Correction Coding for Digital Communication*: New York: Plenum Press, 1981.

[25] R. Q. Hui, B. Y. Zhu, R. X. Huang, C. T. Allen, K. R. Demarest, and D. Richards, "Subcarrier multiplexing for high-speed optical transmission," *Journal of Lightwave Technology,* vol. 20, pp. 417-427, Mar 2002.

[26] R. Hui and M. O'Sullivan, *Fiber Optic Measurement Techniques*: Academic Press, 2009.

[27] Y. Benlachtar, G. Gavioli, V. Mikhailov, and R. I. Killey, "Experimental investigation of SPM in long-haul direct-detection OFDM systems," *Optics Express,* vol. 16, pp. 15477-15482, 2008.

[28] S. J. Ben Yoo, "Optical packet and burst switching technologies for the future photonic Internet," *Journal of Lightwave Technology,* vol. 24, pp. 4468-4492, 2006.

[29] X. J. Cao, V. Anand, and C. M. Qiao, "Waveband switching in optical networks," *Ieee Communications Magazine,* vol. 41, pp. 105-112, 2003.

[30] M. Jinno, H. Takara, B. Kozicki, Y. Tsukishima, Y. Sone, and S. Matsuoka, "Spectrum-Efficient and Scalable Elastic Optical Path Network: Architecture, Benefits, and Enabling Technologies," *Ieee Communications Magazine,* vol. 47, pp. 66-73, Nov 2009.

[31] K. Christodoulopoulos, I. Tomkos, and E. A. Varvarigos, "Elastic Bandwidth Allocation in Flexible OFDM-Based Optical Networks," *Journal of Lightwave Technology,* vol. 29, pp. 1354-1366, 2011.

[32] A. F. Molisch, *Wireless Communications*: Willey, 2011.

[33] T. Kobayashi, A. Sano, E. Yamada, E. Yoshida, and Y. Miyamoto, "Over 100 Gb/s Electro-Optically Multiplexed OFDM for High-Capacity Optical Transport Network," *Journal of Lightwave Technology,* vol. 27, pp. 3714-3720, 2009.

[34] B. Kozicki, H. Takara, Y. Tsukishima, T. Yoshimatsu, K. Yonenaga, and M. Jinno, "Experimental demonstration of spectrum-sliced elastic optical path network (SLICE)," *Optics Express,* vol. 18, pp. 22105-22118, Oct 2010.

[35] A. J. Viterbi and A. M. Viterbi, "NON-LINEAR ESTIMATION OF PSK-MODULATED CARRIER PHASE WITH APPLICATION TO BURST DIGITAL TRANSMISSION," *Ieee Transactions on Information Theory,* vol. 29, pp. 543-551, 1983.

[36] S. Chandrasekhar and X. Liu, "Experimental investigation on the performance of closely spaced multi-carrier PDM-QPSK with digital coherent detection," *Optics Express,* vol. 17, pp. 21350-21361, Nov 2009.

[37] G. Bosco, A. Carena, V. Curri, P. Poggiolini, and F. Forghieri, "Performance Limits of Nyquist-WDM and CO-OFDM in High-Speed PM-QPSK Systems," *Ieee Photonics Technology Letters,* vol. 22, pp. 1129-1131, Aug 2010.

[38] J. Zhao and A. Ellis, "Offset-QAM based coherent WDM for spectral efficiency enhencement," *Optics Express,* vol. 19, pp. 14617-14631, 2011.